(12)

NOSC

NOSC TR 174

NOSC TR 174

Technical Report 174

COVERT COMMUNICATIONS BETWEEN PATROL AIRCRAFT IN RENDEZVOUS

Millimetre-wave and electro-optical technologies compared with uhf Link 4 for P-3 to P-3 hand-over in a maritime environment

LB Stotts, RT Kihm, RL Mather,
ME Hyde, GC Mooradian

8 November 1977

Final Report: Research
Prepared for
NOSC Fleet Readiness Office

NAVAL OCEAN SYSTEMS CENTER
SAN DIEGO, CALIFORNIA 92152

NAVAL OCEAN SYSTEMS CENTER, SAN DIEGO, CA 92152

AN ACTIVITY OF THE NAVAL MATERIAL COMMAND

RR GAVAZZI, CAPT, USN
Commander

HL BLOOD
Technical Director

ADMINISTRATIVE INFORMATION

The work reported upon in this document was performed by members of the EO and Millimeter Wave Communications Branch and the Microwave and MM Wave Antennas and Systems Branch for the Fleet Readiness Office under NOSC Project Number W040725. This document was approved for publication on 8 November 1977.

The authors thank WA Andrew, JR Beauchane, and RP McManus, all of the Fleet Readiness Office, for their initiation, interest, and support of this work.

Released by
WE Richards, Head
Communications Research and
Technology Division

CR Otey
Tactical Sensors and EW
Division

Under authority of
RO Eastman, Head
Communications Systems and
Technology Department

METRIC EQUIVALENTS

To convert from torrs (mm Hg, 0°C) to pascals (Pa), multiply by 133.

To convert from angstroms to metres, multiply by 10^{-10}.

To convert from degrees (°) to radians, multiply by 0.0175.

To convert from feet to metres, multiply by 0.305.

UNCLASSIFIED

SECURITY CLASSIFICATION OF THIS PAGE *(When Data Entered)*

(17) NOSC/TR-174

REPORT DOCUMENTATION PAGE

READ INSTRUCTIONS BEFORE COMPLETING FORM

1. REPORT NUMBER: NOSC Technical Report 174 (TR 174)

2. GOVT ACCESSION NO.

3. RECIPIENT'S CATALOG NUMBER

(9)

4. TITLE (and Subtitle)

(6) COVERT COMMUNICATIONS BETWEEN PATROL AIRCRAFT IN RENDEZVOUS: Millimetre-wave and electro-optical technologies compared with uhf Link 4 for P-3 to P-3 hand-over in a maritime environment

5. TYPE OF REPORT & PERIOD COVERED: Final report

6. PERFORMING ORG. REPORT NUMBER

7. AUTHOR(s)

(10) LB/Stotts, RT/Kihm, RL/Mather, ME/Hyde, GC/Mooradian

8. CONTRACT OR GRANT NUMBER(s)

9. PERFORMING ORGANIZATION NAME AND ADDRESS

Naval Ocean Systems Center
San Diego, California 92152

10. PROGRAM ELEMENT, PROJECT, TASK AREA & WORK UNIT NUMBERS

NOSC Project W040725

11. CONTROLLING OFFICE NAME AND ADDRESS

NOSC Fleet Readiness Office
San Diego, California 92152

(11) 12. REPORT DATE: 8 Nov[illegible]77

13. NUMBER OF PAGES: 118 Pp.

(12) 14. MONITORING AGENCY NAME & ADDRESS *(if different from Controlling Office)*

15. SECURITY CLASS. *(of this report)*: Unclassified

15a. DECLASSIFICATION/DOWNGRADING SCHEDULE

16. DISTRIBUTION STATEMENT *(of this Report)*

Approved for public release; distribution is unlimited

DDC RECEIVED MAR 3 1978 F

17. DISTRIBUTION STATEMENT *(of the abstract entered in Block 20, if different from Report)*

18. SUPPLEMENTARY NOTES

19. KEY WORDS *(Continue on reverse side if necessary and identify by block number)*

Covert operations – intelligence hand-over
Surveillance – surface/subsurface
Telecommunication – millimetre-wave and electro-optical

20. ABSTRACT *(Continue on reverse side if necessary and identify by block number)*

In response to the fleet operational requirement for covert hand-over between two P-3 patrol aircraft engaged in maritime surface/subsurface surveillance, trade-offs were addressed between two separate communication systems designed for such service – the first based on millimetre-wave technology, the other on electro-optical technology. Under the most ideal interception conditions, millimetre-wave and electro-optical technologies give comparable performance levels and both restrict communication to significantly lower maximum detectable range than do present uhf communication techniques.

DD FORM 1 JAN 73 1473 EDITION OF 1 NOV 65 IS OBSOLETE
S/N 0102-LF-014-6601

UNCLASSIFIED

SECURITY CLASSIFICATION OF THIS PAGE *(When Data Entered)*

393 159

OBJECTIVE

In response to the fleet operational requirement for covert hand-over between two P-3 patrol aircraft engaged in surface/subsurface surveillance, address trade-offs between two separate communication systems designed for covert hand-over – the first based on millimetre-wave technology, the other on electro-optical technology.

RESULTS

Under the most ideal interception conditions, millimetre-wave and electro-optical systems give comparable performance levels, and both limit communications to a significantly shorter maximum detectable range (thus providing more covertness) than can be achieved by present uhf communication systems.

RECOMMENDATIONS

1. Integrate the analytical models developed in this study with the graphical comparison techniques described in appendix G; extend the total intercept/communication analysis to more detailed fleet operational scenarios.

2. Extend the above analysis to the total probability-of-intercept problem.

3. Investigate the feasibility of hybrid millimetre-wave/electro-optical communications for increased performance and atmospheric channel availability.

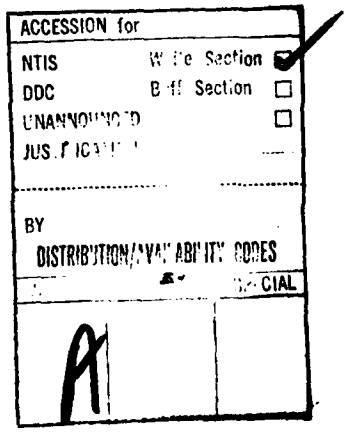

CONTENTS

1 INTRODUCTION

This study is in response to the fleet operations requirement, as described in MSG DTG 191429Z Jan 77, of covert hand-over between two P-3 patrol aircraft engaged in surface/subsurface surveillance. On close scrutiny of present P-3 "SWAP" procedures,* one is left with the impression that they are probably not the most efficient and effective ones available, given the present state of the art in electromagnetic technology. In particular, both millimetre and electro-optical technologies appear to have strong potential in meeting the above cited requirement with increased covertness over present P-3 communications techniques. The objective of this study is to address the trade-offs between two distinct communication systems designed to allow covert hand-over between aircraft, the first based on millimetre-wave technology, the other on electro-optical technology. The benchmark, for comparison, is an omnidirectional ultrahigh-frequency (uhf) communications system, Link 4. It is hoped that the results presented within the report will at least place in perspective the potential roles of millimetre and electro-optical technologies in Navy short-range covert communications.

The format of the report is as follows: Section 2 discusses the definition of covertness and the communications/interception criteria assumed for this study. Section 3 describes the present naval aircraft communication capability, uhf radio. Sections 4 and 5 discuss the proposed millimetre-wave and electro-optical communication systems, respectively, for P-3 to P-3 hand-over. Section 6 contains the comparison and summary portions of this study. All references are listed as section 7. The authors have presupposed the reader to be knowledgeable in the area of electromagnetic systems analysis. For those readers not familiar with this area, we have included introductory material on this subject in appendices A, B, and C. Appendix D contains the propagation model used in section 3; appendices E and F, the model used in section 4. Appendix G is a general discussion of the millimetre-wave and electro-optical P-3 to P-3 hand-over problem.

*The authors would like to thank LCDR WJ Tinston, of the Naval Ocean Systems Center, and LT R Krahe and Chief D Dionne of COMPATWINGPAC, Moffett Field, for their technical assistance concerning the P-3 aircraft and general P-3 SWAP procedures.

2 COVERT COMMUNICATION/INTERCEPTION CRITERIA

In general, a tactical communication system is designed to convey information only to an intended receiver (or receivers). Invariably, however, the radiated signals are not absolutely undetectable to an unfriendly interceptor. For this reason, a definition of system covertness must be introduced.[1-4] It is the intent of this section to do so. In particular, we will define in this section both the definition of covertness and the communications/interception criteria assumed for this study.

COVERTNESS

What is covertness? According to the American College Dictionary, it is a word describing the degree to which an entity is either "covered, sheltered, concealed, secret, or disguised." For our purposes, the terms covered or concealed seem most appropriate. In a covert communication system, the transmitted signal is somehow concealed from potential intercept receivers. The question then comes to mind, "How concealed is concealed?" The answer to that question is unfortunately not a concrete one, but rather is described by a probabilistic concept called the probability of intercept.

Crepeau[1] defined covert communications to be "the transfer of information by means which lower the probability of intercept so as to reduce or deny an unintended party information about the presence, location, and identity of the transmitting platforms." As this implies, the probability of intercept encompasses more than just a probability of detection and a false-alarm probability. What is usually required is the time coincidence of two or more activities, along with enough signal strength to overcome the system noise in the detection process. Such activities include the overlapping of the transmit/receive antenna patterns, tuning the receiver to the exact carrier/subcarrier frequencies, and synchronizing the transmit/receive turn-on/turn-off times. It is fairly apparent that the calculation of probability of intercept is rather a complex and subjective one. In addition, one would probably be hard put to keep this study unclassified while trying to include much of the above information.

The approach taken in this study to quantify system covertness is to sidestep the question of conditional probabilities and to base interception on the energy detectability of an intercept receiver. This implies the mandatory coincidence of antenna patterns, frequencies, and "on" times. It is reasoned that if an enemy is not in a position to detect the transmitted signal under his most "ideal" conditions, no amount of sophistication can be applied to allow interception at the same location under "nonideal" conditions. Thus, the act of interception depends solely on sufficient sensitivity by the receiver to respond to the intercepted transmitted signals. For the interested reader, a more elaborate discussion of covert communications and the probability of intercept can be found in references 1-4 or in appendix B.

---

[1] NRL Memorandum Report 2873, Fundamentals of Covert Communications, by PJ Crepeau, July 1974

[2] NOSC Technical Note NELC TN 2722, Detection of Covert Signals, by RA Dillard, 27 June 1974. (TNs are informal documents intended chiefly for internal use.)

[3] Naval Electronic Systems Command paper, Covert Communications Notes (on work performed by NOSC Tactical Command Control Division)

[4] BR Hatcher, Probability of Intercept and Intercept Time, Watson-Johnson Company Tech-note, vol 3 no 3, May/June 1976

COMMUNICATION SYSTEM CRITERIA

As was noted before, the problem which we are concerned with is the design of a low-intercept communication (Teletype, voice, data, etc) system for P-3 ASW aircraft in rendezvous. Implicitly coupled with this problem, however, is the need to keep the system both low in cost and free from exotic or unrealistic component designs. Otherwise, one might price himself out of the market either by the cost or fabrication complexity of a system in comparison with alternative solutions of the same problem.

For the purposes of this study, we will assume the following general operational criteria. (Figure 1 depicts the assumed communication/interception geometry and scenario.)

Maximum communication range between aircraft: 1.5 km

Transmitter altitudes: 0.03 km, 1.6 km, 3.2 km, and 6.4 km

Angular receiver position about transmitter: $(\theta_R, \varphi_R) = (90°, 180°), (120°, 180°), (135°, 180°), (150°, 180°), (165°, 180°), (180°, 180°), (165°, 0°), (150°, 0°), (135°, 0°), (120°, 0°)$ and $(90°, 0°)$

Communications Data Rate: 40 bits per second

Minimum signal-to-noise ratio for communications: 15 dB

Sun orientation: $(\theta_S, \varphi_S) = (45°, 0°)$

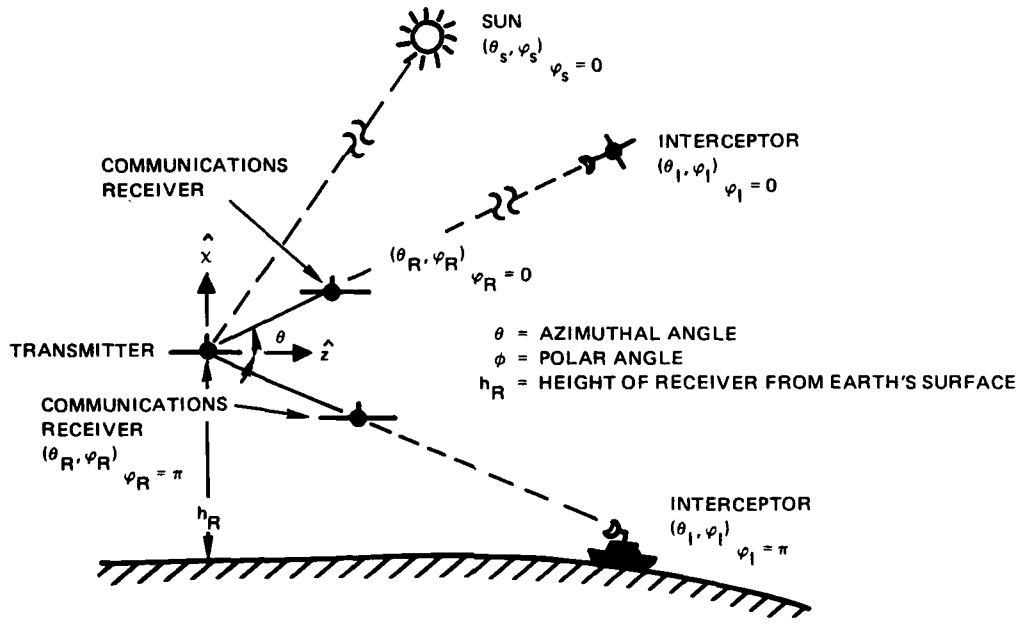

Figure 1. Typical communications/interception scenario and geometry. Transmitting P-3 aircraft assumed to be located at coordinate origin. (The figure is not drawn to scale.)

INTERCEPTION SYSTEM CRITERIA

The intercept receiver is assumed to be a highly directional radiometer "tuned" to exact carrier/subcarrier frequencies, synchronized to the transmit "on" time, and completely coincident with the maximum transmit antenna lobe. Because it is a radiometer, no

modulation can be recovered; only presence and location are achieved. The input transmit power is assumed to be fixed and is set to the worst-case sea-level value for communications.

Therefore, we will assume the following interception criteria.

Interceptor platform: ship-based, air-based, and satellite-based.

Intercept antenna

Millimetre-wave: 40 dB gain dish
Optical: 2-foot, 1.5° full field reflective telescope

Angular beamwidth: 1.5° full field (stabilized platform assumed)

Interceptor postdetection bandwidth: 5 Hz

Minimum signal-to-noise ratio for detection: 1 dB

Communication scenario: 1.5 km communications link operating on minimum signal-to-noise ratio of 15 dB

Angular intercept position about transmitter: Angular position of interceptor collinear with angular position of communication receiver

3 UHF COMMUNICATION/INTERCEPTION

The purpose of this section is to review and characterize the present P-3 short-range SWAP capability, Link 4.*,[5,6] The Link 4 system is composed of two uhf transceivers which cover 225 to 400 MHz in steps of 50 kHz and are capable of either clear voice, secure voice, or digital data transmission. They are solid state units and transmit carriers of 30 watts AM and 100 watts FM.

UHF PROPAGATION

The energy radiated from a transmitting antenna positioned a finite distance above the earth to a receiving antenna located more than a few wavelengths away may be divided into four distinct parts: a direct wave, a ground-reflected wave, a sky wave, and a ground wave. Since we are concerned only with the frequency range from 225 to 400 MHz, we will restrict our analysis to include only the direct and ground reflected waves.[7] Their joint sum is often referred to as the space wave.

The geometry of the space wave propagation is shown in figure 2. At the receiving antenna, interference will occur between the direct and reflected field components. The net result is a composite field described by the vector sum of the individual field components. The phase difference between the direct and reflected fields can be separated into two parts, the path length difference, s, and the phase shift for surface reflection, p. Following the treatment of Reed and Russel,[7] we define g(s) to be the ratio of the resultant field at the receiver to the free-space (direct) field. This function, g(s), is called the earth gain factor and is functionally dependent on several variables, including the reflection characteristic of the terrain, the angle of incidence, ψ, relative to the earth's surface, and the signal polarization. In general, g(s) is derived empirically and ranges in value from a minimum of 0.3 to a maximum of 1.9. Thus, the field at the receiver can be written as

*AF Wunsch, private communication

[5]CA Robinson, Jr, Computer Enhances P-3C Effectiveness, Aviation Week and Space Technology, p 34-35, 15 November 1976

[6]CA Robinson, Jr, S-3A Strengthens Carriers' ASW Role, Aviation Week and Space Technology, p 30-41, 22 November 1976

[7]HR Reed and CM Russel, UHF Propagation, Boston Technical Publishers, Lexington, Mass, 1964

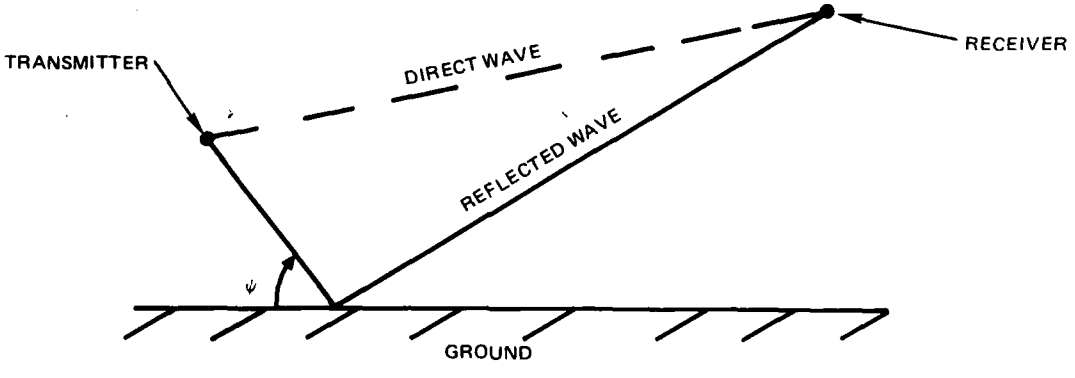

Figure 2. Uhf communication/interception geometry.

$$E_r = F_0 g(s) \text{ (in V/m)} , \quad (1)$$

where E_0 is the free-space field and E_r is the composite field at the receiver. It should be noted that we are ignoring field attenuation in this section. One finds that in the uhf band, the attenuation is on the order of 1.5×10^{-3} dB/km at sea level and decreases with altitude.[8] Thus, we expect that a free-space analysis is reasonably close to a similar clear-atmosphere analysis.

POWER AT THE RECEIVER

It can be shown (see appendix A) that the power density of an electromagnetic wave in free space is given by

$$S = E^2/Z \text{ (in W/m}^2) , \quad (2)$$

where

$E \equiv$ electric field strength in space (in V/m)

$Z \equiv$ free-space impedance (377 Ω).

The power absorbed by a receiving antenna is equal to

$$P_r = S A_{eff} = E^2 A_{eff}/Z \text{ (in W)} , \quad (3)$$

where A_{eff} is the effective cross-sectional area of the antenna. In terms of the antenna characteristics (see appendix A),

$$A_{eff} = \lambda^2 G/4\pi \text{ (in m}^2) , \quad (4)$$

where λ is the wavelength of the carrier frequency and G is the power gain relative to an isotropic antenna.

UHF RADIO NOISE

In the uhf portion of the radio spectrum there exist three distinct types of background noise: atmospheric, galactic, and man-made (see fig 3). The noise power generated by these sources, coupled with the internal noise of the receiver, limits the performance of any uhf receiver to some nonoptimum or nonideal level. From figure 3 (ref 8), it is apparent that the galactic noise level at 300 MHz is roughly comparable to the receiver noise level but is significantly higher than atmospheric noise. Man-made noise, on the other hand, can be seen to take on a range of values[7,8] depending only on the receiver's operational environment but exceeding any of the previously mentioned noise levels. Figure 3 provides values measured in both urban and suburban regions. The study which is the subject of this report, however, is concerned with operational scenarios in the maritime environment, where man-made noise sources at uhf are not found. Nevertheless, the platforms which house the receiver, even though specifically designed either for communications or for surveillance, can generate unexpected uhf RFI through their motors, fluorescent lights, etc. In general, measurements of uhf RFI in the 240–400 MHz range indicate that background ambient noise can

[8] ITT Handbook for Radio Engineers, chap 29, 1975

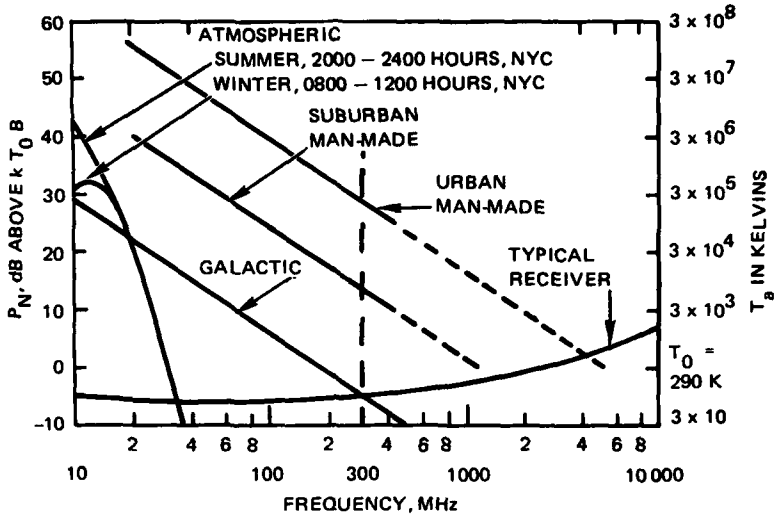

Figure 3. Median values of the average noise power produced by various sources, captured by a directional antenna.[8]

be typified as a thermal noise source at about 290 K.[9,10] This implies that the uhf intercept and communications receiver sensitivity calculations can consider internal receiver noise as the limiting factor in system performance. Thus, the equivalent noise power relative to the receiver input is given by

$$P_N \approx F_r \, k \, T_a \, B_{eff} \, , \tag{5}$$

where

$F_r \equiv$ receiver noise factor

$k \equiv$ Boltzmann's constant

$= 1.38 \times 10^{-23}$ J/K

$T_a = 290$ K

$= T_0$

$B_{eff} \equiv$ noise equivalent receiver bandwidth

$\approx (2 \, B_{rf} \, B_v)^{1/2}$

$B_{rf} \equiv$ predetection bandwidth

$B_v \equiv$ postdetection bandwidth.

For a Dicke radiometric receiver, (5) can be written as

[9]M Skolnik, Radar Handbook, McGraw-Hill, New York, chap 24, 1970
[10]NPS 620 L 76103, Shipboard RFI in UHF SATCOM, October 1976

$$P_N \approx F_r k T_0 \sqrt{\frac{B_{rf}}{\tau_v}} , \tag{6}$$

where

$$B_v = \frac{1}{2\tau_v}$$

$\tau_r \equiv$ postdetection integration time.

If we assume the receiver characteristics,

$$F_r = 2 \text{ dB}$$

$$B_{rf} = 1 \text{ MHz} ,$$

then

$$P_N \simeq 8.970 \times 10^{-18} \sqrt{\frac{B_v}{1 \text{ Hz}}} \text{ (in watts)} \tag{7a}$$

$$= 6.343 \times 10^{-18} \sqrt{\frac{1_s}{\tau_v}} \text{ (in watts)} . \tag{7b}$$

MINIMUM TRANSMITTER POWER

Section 2 showed that the minimum signal-to-noise power ratio for a 40 kilobit per second data link is 15 dB. We will utilize that value to determine the minimum amount of transmitter power required for communications.

In equation (1) we stated that the resultant field at the receiver from the joint sum of the direct and ground-reflected electromagnetic fields is given by

$$E_r = E_0 g(s) . \tag{8}$$

Hence, the received power

$$P_r = P_0 g^2(s) . \tag{9}$$

Assume the predetection equivalent bandwidth to be equal to 300 kHz and the noise factor to be equal to 2 dB. Then the noise power at the receiver is given by

$$P_N \simeq 9.826 \times 10^{-16} \text{ (in W)} .$$

For a 15 dB signal-to-noise ratio, with g(s) = 0.3, the direct power at the receiver is given by

$$P_0 = P_r/g^2(s)$$

$$= 3.453 \times 10^{-13} \text{ W} .$$

The free-space transmission equation is

$$P_0 = \frac{P_T A_T A_R}{d^2 \lambda^2}, \tag{10}$$

where

$P_0 \equiv$ received power

$P_T \equiv$ transmitter power

$A_T \equiv$ effective area of the transmitter antenna

$A_R \equiv$ effective area of the receiver antenna

$d \equiv$ source-receiver separation

$\lambda \equiv$ wavelength of the carrier frequency.

Thus, for an isotropic antenna, $\lambda = 1.0$ m and $d = 1.5$ km,

$$P_T = \frac{P_0 \lambda^2}{(4\pi)^2 d^2}$$

$$= 1.227 \times 10^{-4} \text{ W} .$$

Thus, about 123 μW in transmitter power is required for communications at 1.5 km for a 15 dB SNR.

INTERCEPT RANGE

Let us define intercept range as the maximum distance away from the transmitter that the carrier can be detected. From section 2, we know that the minimum detectable signal-to-noise ratio is 1 dB, assuming a 5 Hz postdetection bandwidth. The direct and ground-reflected fields are assumed to experience constructive interference at the receiver.

With these assumptions and a thermal-noise-limited omnidirectional receiver, we write, as before,

$$P_0 = \frac{P_T A_T A_R}{d^2 \lambda^2}$$

$$= \frac{P_T \lambda^2}{(4\pi)^2 d^2} . \qquad (11)$$

The noise power at the interceptor

$$P_N \simeq 2.0 \times 10^{-17} \text{ W} ,$$

using (7a), ie $B_{RF} = 1$ MHz. Thus where SNR = 1 dB,

$$d_{max} = \sqrt{\frac{P_T \lambda^2}{(4\pi)^2 P_0}} = 3.33 \times 10^5 \text{ m} ,$$

where

$$P_0 = P_r / g^2(s), \; g(s) = 1.9 .$$

Under constructive interference,

$$d_{max} = 5.26 \times 10^4 \text{ m} .$$

Let us now turn our attention to the effect on the detection range if the interceptor uses a directive antenna.

Equation (10) showed that the received power is functionally dependent on antenna gain G through the effective area, A. The gain is defined as the ratio of the radiated power in a particular direction to the power radiated in the same direction by an isotropic radiator, assuming a constant input power. Therefore, it can be shown, by using the results of appendix A, that the received power, P_0, at the interceptor, captured by a directional antenna, is given by the relationship,

$$P_0 = \frac{P_T A_T}{d^2 \Omega_{INTCP}} , \tag{12}$$

where Ω_{INTCP} is the main-beam solid angle of the interceptor's antenna. Thus, the maximum detectable range

$$d_{max} = \left(\frac{P_T A_T}{\Omega_{INTCP} P_0} \right)^{1/2} . \tag{13}$$

Therefore, if $\Omega_{INTCP} = 5.383 \times 10^{-4}$ sr, ie 1.5° full-angle divergence, then

$$d_{max} \simeq 5.1 \times 10^7 \text{ m}$$

for $g(\theta) = 1.9$, and

$$d_{max} = 8.04 \times 10^6 \text{ m}$$

for $g(\theta) = 0.3$.

Table 1 summarizes these results.

Table 1. Detection range.

Source	Maximum detectable range, m: Omnidirectional antenna	Maximum detectable range, m: Directive antenna
Constructive interference between direct and reflected fields	5.26×10^4	8.04×10^6
Destructive interference between direct and reflected fields	3.33×10^4	5.1×10^7

4 MILLIMETRE-WAVE COMMUNICATION/INTERCEPTION

The purpose of this section is to define, describe and estimate the performance of a covert, short-range, millimetre-wave communication system.

COMMUNICATION SYSTEM DESIGN

By selecting the appropriate millimetre wavelength, one can take advantage of very strong atmospheric oxygen absorption to limit the maximum range of interception while allowing short-range communications. Figure 4 shows the atmospheric attenuation at sea level. A maximum occurs at 60.3 GHz. Very limited interception and communication ranges exist at this frequency, and the solid-state transmitting sources used at this frequency are IMPATT & Gunn diodes, which have output powers of about 50–100 mW. These two facts make the use of directive antennas (gain $\simeq$ 25 dB and bw $\simeq 5^\circ$) a necessity. As one moves either down to 55 GHz or up to 70 GHz, the antenna gain requirement for fixed transmitter power is relaxed somewhat (perhaps by 5–10 dB). However, by no means could omnidirectional antennas be employed. Of course, directive antennas are more desirable for covertness, since the transmitted signal is confined to a relatively small portion of space.

Several factors influence the choice of modulation: the type of diode, the data rate, and the simplicity of the circuit used. The IMPATT is most easily frequency modulated by bias variation, whereas the Gunn diode is more readily bias pulsed. Bias pulsing of the IMPATT is accompanied by unwanted FM, whereas the Gunn diode is relatively difficult to frequency modulate through bias variation. Both diodes can be externally frequency modulated by a varactor diode or externally pulsed by a PIN diode. For the sake of transceiver circuit simplicity, it is desirable to use the same diode for the local oscillator (receive mode) as for the transmitter (transmit mode). The Gunn diode has much less FM and AM noise than the IMPATT and is therefore better as the local oscillator. The noise characteristics are

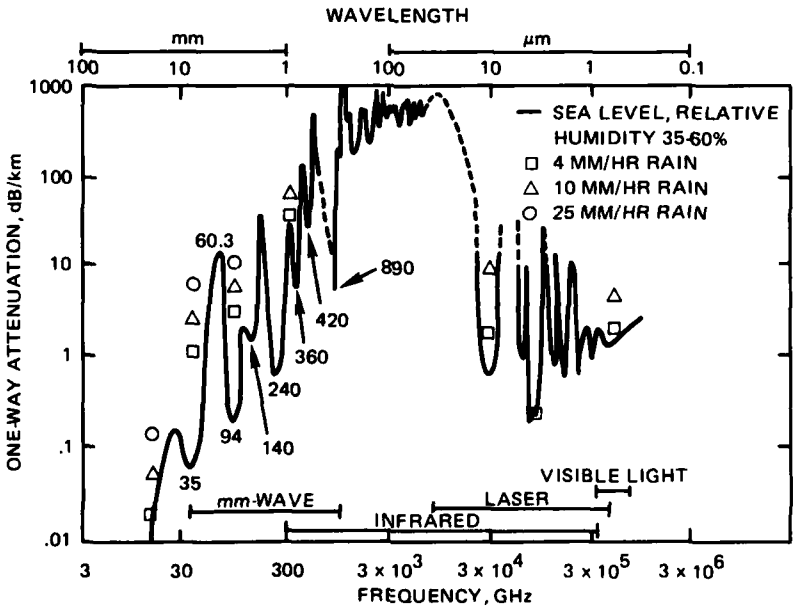

Figure 4. Atmospheric attenuation as a function of frequency.

important when a relatively low frequency IF (10.7 MHz) is used. Integrated circuit FM receivers operating at 10.7 MHz are very inexpensive and readily available. Using these would result in a low-cost transceiver. An FM system also allows the local oscillator to search and "track" the signal via an AFC loop. With all these considerations in mind, a reasonable choice is frequency shift keying (FSK). Correspondingly, the source choice is a varactor-tuned Gunn oscillator.

Figure 5 shows a possible Transceiver FM circuit. The source in the transmit mode is frequency modulated at voice or 40 kbit (data) rates with deviation of ± 100 kHz and produces about 100 mW. Thus the signal spectrum occupies a maximum bandwidth of about 280 kHz. The Gunn oscillator is cavity stabilized to 1 part in 10^4. This assures that the transmit frequency is close enough to its assigned value that the receiver LO can search and lock onto the signal before it reaches its electronic tuning limits. A circulator routes the transmitted signal to the antenna and routes the received signal to the balanced mixer.

In the receive mode, the varactor voltage is sawtooth swept until the signal is found. When the difference between f_S and f_{LO} is 10.7 MHz, the sawtooth is removed and the FM receiver discriminator output error voltage locks the LO to the signal and forces it to track. In addition, the FM receiver demodulates the signal, recovering either voice or data. The 10.7 MHz filter restricts the rf bandpass to about 250 kHz. This narrow bandwidth can be tolerated since the LO tracks the signal. Table 2 lists the pertinent electrical characteristics of the transceiver.

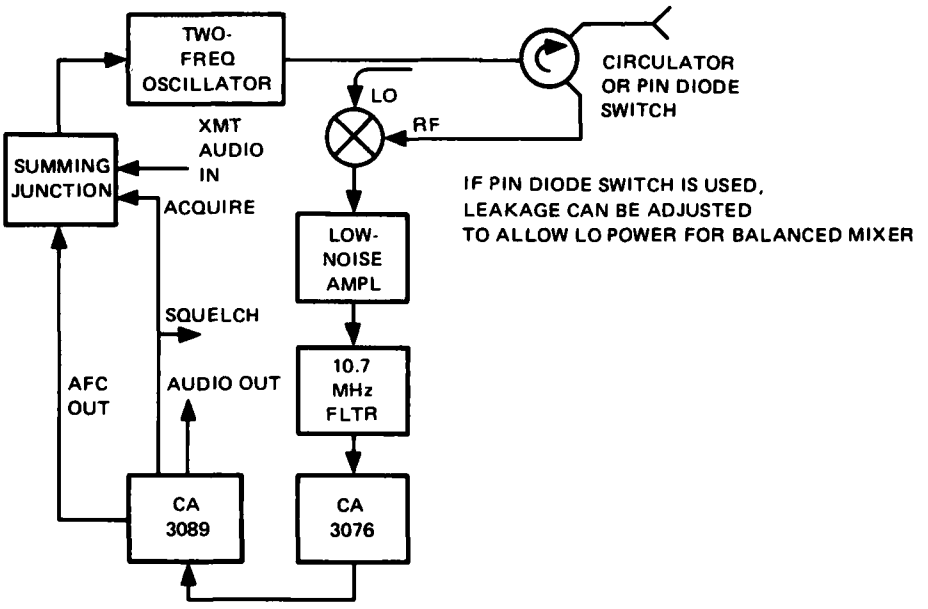

Figure 5. Possible transceiver FM circuit.

Table 2. Transceiver electrical characteristics.

Transceiver component	Characteristics
Transmitter	Varactor: tuned Gunn Oscillator $P_t \simeq 100$ mW Electronic tuning $\simeq \pm 100$ MHz Frequency $\simeq 60.36$ GHz Modulation: FM; deviation = ± 100 kHz
Receiver	Beam lead Schottky barrier balanced mixer $L_c \simeq 7$ dB Ant-mixer loss $\simeq 1$ dB Preamp NF $\simeq 2$ dB Overall NF $\simeq 10$ dB Rf bw = 250 kHz Base bw: 40 kHz data 5 kHz voice IF: 10.7 MHz

ATMOSPHERIC PROPAGATION CHARACTERISTICS

For a transmitter of power, P_T, and antenna gain, G_T, separated a distance, R, from a receiver having a sensitivity, P_S, and a receiving antenna gain, G_R, the expression relating all of the quantities is

$$P_R = P_T G_T e^{-\alpha R} A_R/4\pi R^2$$
$$= (S/N)P_S \ , \qquad (14a)$$

where

(S/N) = required signal-to-noise ratio at the receiver,

$A_R = G_R \lambda^2/4\pi$

$\lambda = 5$ mm

and

$e^{-\alpha R}$ = atmospheric propagation loss.

(14a) can be written as

$$R^2 e^{\alpha R} = (P_T/P_R) G_T G_R \lambda^2/(4\pi)^2 \ . \qquad (14b)$$

The right side of this equation is independent of range and depends solely upon the transmitter-receiver system parameters. We define a transmitter-receiver system performance

parameter $\Delta \equiv (P_T/P_R)\, G_T\, G_R\, \lambda^2/(4\pi)^2$. It is obvious that the larger Δ is, the greater the range. (15) gives Δ in dB when R is in km and λ in mm. For every value of Δ there corresponds a range R such that (14a) is satisfied. Hence Δ vs range curves can be plotted like those in figures 11 through 29. When the receiver is an interceptor, Δ becomes Δ_{intcp}. Rewriting, we have

$$\Delta \equiv 10 \log P_T + 10 \log G_T + 10 \log G_R - 10 \log P_R \qquad (15)$$

$$+ 20 \log \lambda - 142 \text{ dB}$$

$$= 20 \log R + (4.34\, \alpha R) \text{ dB} , \qquad (16)$$

where

Δ = detectable signal power in dBm

R is in km, λ is in mm, and

P_T and P_R are in dBm.

Of course the appropriate value of α must be used. Since propagation takes place from one altitude to the next, the behavior of α vs altitude, h, must be known. From experimental data[11] a plot of α vs h is obtained as shown in figure 6. Three frequencies of operation (60.3 GHz, 57.6 GHz, and 55.2 GHz) are shown. Figures 7 through 10 show the behavior of both attenuation and phase dispersion at four different altitudes and two different spectral linewidths.

[11] EE Reber, RL Mitchell, CJ Carter, Oxygen Absorption in the Earth's Atmosphere, The Microwave Journal, November 1969.

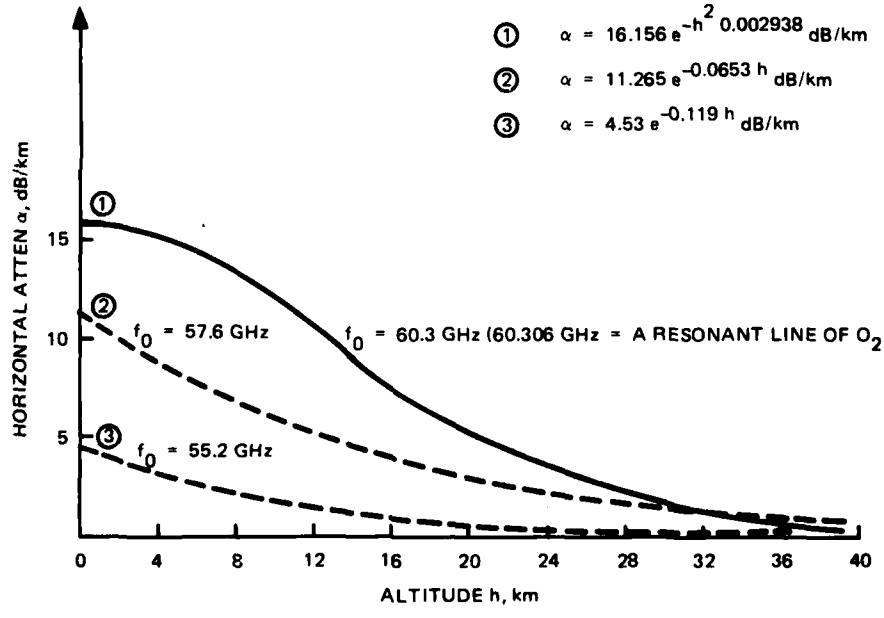

Figure 6. Horizontal attenuation vs altitude.

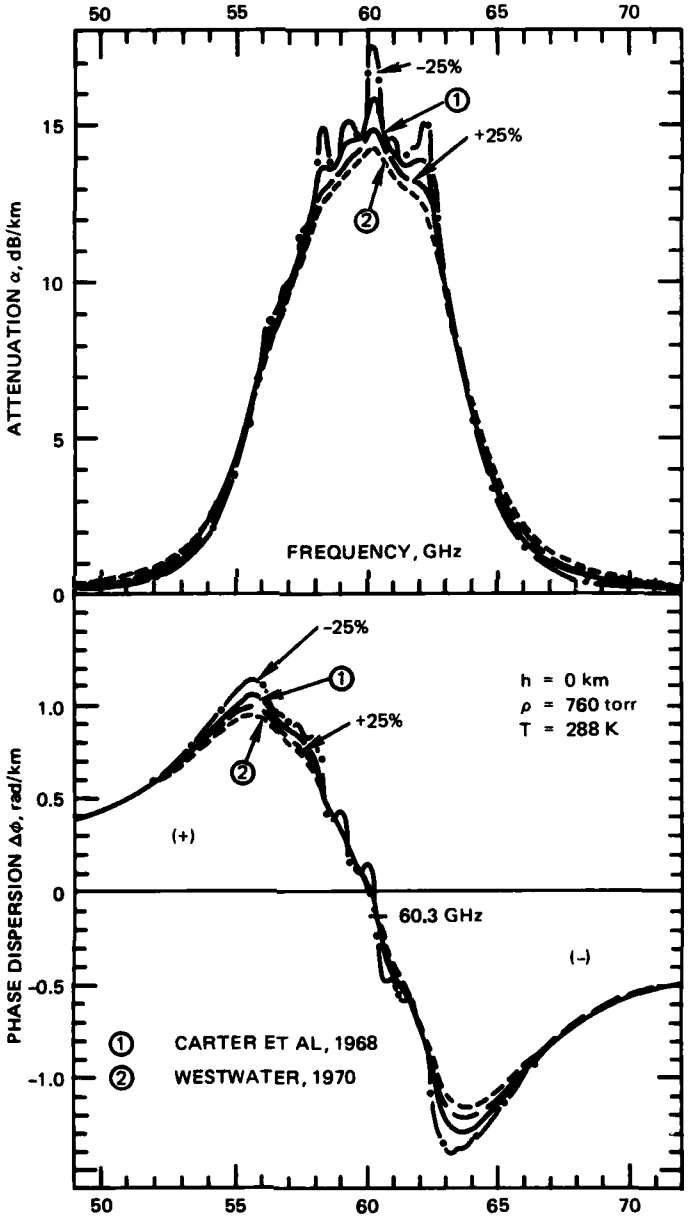

Figure 7. Horizontal (homogeneous) transmissivity at sea level, h = 0 km. Variations are shown due to different linewidth values: ① γ_i = 666 MHz ±25%, ② γ_i = 968 MHz.

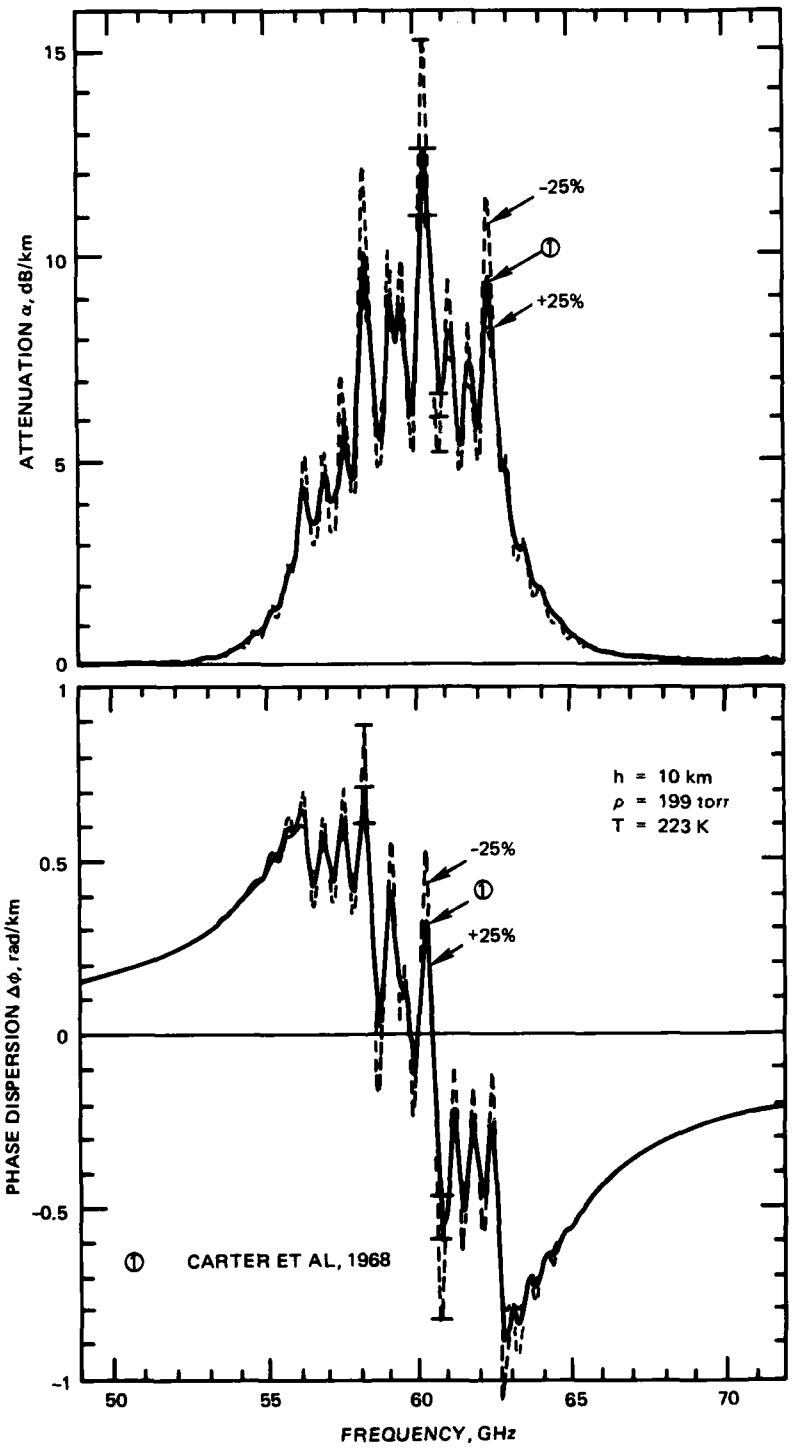

Figure 8. Horizontal (homogeneous) transmissivity at h = 10 km (US Std Atm 62). Variations are shown due to different line-width values: ① γ_i = 255 MHz ± 25%.

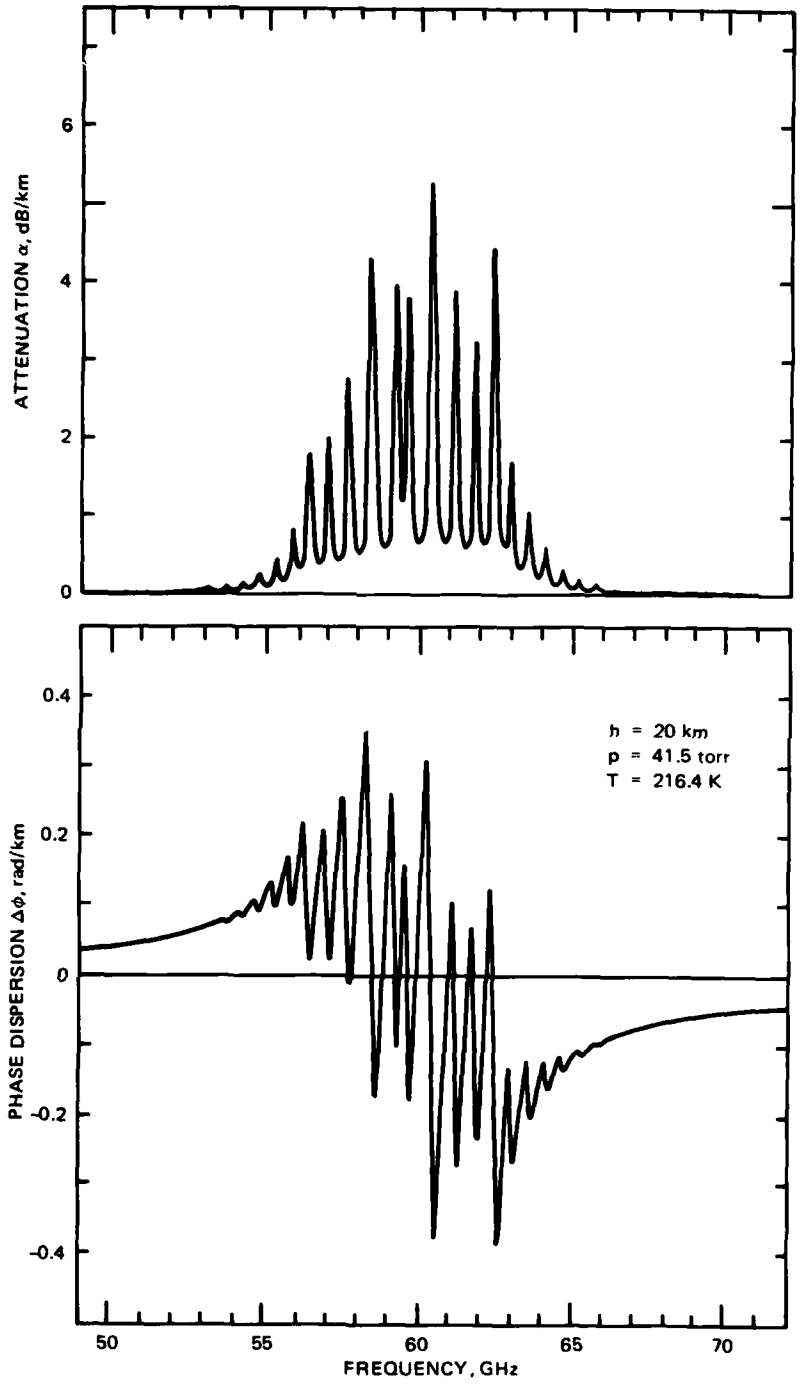

Figure 9. Horizontal (homogeneous) transmissivity at h = 20 km (US Std Atm 62). The linewidth values are, γ_i = 86.6 MHz.

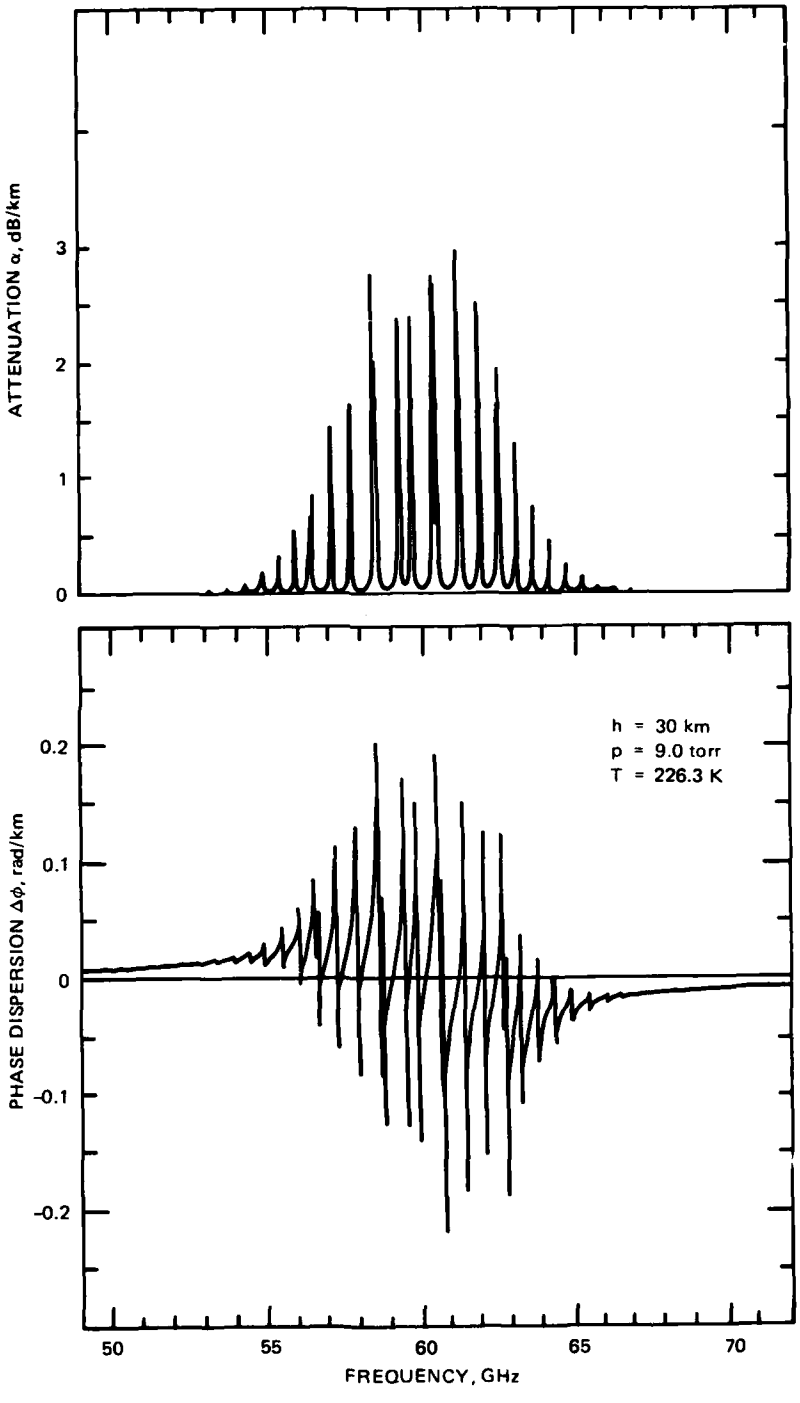

Figure 10. Horizontal (homogeneous) transmissivity at h = 30 km (US Std Atm 62). The linewidth values are, γ_i = 21.2 MHz.

For these figures γ represents the width of a resonance line possessing a Lorentzian shape. The value difference of γ at different altitudes is due to pressure broadening. T represents the atmospheric temperature and p is the barometric pressure. The reason for the atmospheric effect at these frequencies is the interaction of the millimetre-wave fields with the magnetic dipole moment of the oxygen molecule. Oxygen has approximately 44 resonant lines in the 50–70 GHz spectral region. At sea-level, pressure broadening produces a broad absorption peak. As altitude increases, the individual lines begin to appear with decreasing intensity as shown in the figures.[12] The expressions for α as a function of altitude, h, in figure 6 were obtained by curve fitting the data of Reber, et al.[11] These expressions are used in plotting Δ vs R, to produce the range curves in figures 11 through 29 (at the end of this section). Knowing the initial altitude and the local elevation angle, θ_o, one can determine the α (h) at each point along the slant range, R. From these range curves it is easily seen how much better the intercepting receiving system must be in order to detect the signal and at what maximum range this will occur. If an interceptor is beyond the maximum range, then detection is impossible.

The α used in the equation to generate the range curves is for clear weather. It is reasonable to treat the clear atmosphere as a spherically stratified medium. As altitude increases, the density of the atmosphere decreases. Because of this, the propagation path for a millimetre-wave signal transmitted from the earth's surface is not exactly straight, but bends slightly toward the denser part of the atmosphere. It can be shown that the angle of bending, Υ, (a refractive effect) is given by

$$\Upsilon = -\int_{n_2}^{n_1} \frac{\left[r^2 n_o^2 - r_o^2 n^2 \cos^2 \theta_o\right]^{1/2} dn}{n\, r_o\, n_o \cos \theta_o},$$

where

n = atmospheric index of refraction
$= n(h)$
r_o = Earth mean radius
$r = r_o + h$
h = altitude above Earth surface
n_o = atmosphere's index of refraction at transmitter
θ_o = local elevation angle at transmitter

Liebe gives the index of refraction as

$$n = 1 + \frac{103P + P_w \left(95.5 + \frac{5 \times 10^5}{T}\right)}{10^6\, T} + \sum_i S_i F_i ,$$

where

P = atmospheric pressure

[12] US Dept of Commerce Office of Telecommunications Report OT 73-10, Molecular Attenuation and Phase Dispersion Between 40 and 140 GHz for Path Models from Different Altitudes, by HJ Liebe and WM Welch, May 1973.

P_w = partial pressure of water

T = temperature, K

S = individual O_2 line strengths, in Hz/torr

F = line shape functions, in 1/Hz

For a detailed discussion of the O_2 line effects on propagation, see Liebe.[12]

At the Earth's surface, where $n \simeq 1.0003$ (neglecting the oxygen contribution), this results in a Υ of about 10–15 mrad.[13] An estimate of the contribution of the O_2 spectrum to the refractive index is about 4×10^{-6}. Thus the additional bending due to the O_2 spectrum around 55 GHz is negligible.

As can be seen in figures 7–10, there is a frequency dependent phase dispersion effect in the 50–70 GHz range. This would have an impact on very wideband (several GHz) digital transmissions over path lengths of several km, where relative phase must be preserved.

Rainfall has the very pronounced effect of rendering millimetre-wave transmission useless. Figure 30 (at the end of this section) shows the attenuation vs frequency at 100 mm/h rainfall.[14] At 60 GHz this attenuation is about 30 dB/km. Generally such a heavy rainfall occurs mostly at altitudes below 1 km but does not occur over long paths for extended periods of time. However, any millimetre-wave communication system should have a S/N ratio margin built into the design which allows for the short term extra loss. According to a BRL report,[15] the loss is due to both absorption and scattering. The relative importance of these effects vs frequency at various rain rates is listed in tables 3 and 4, taken from that report.

Millimetre-wave transmission loss through clouds at the present time is not well documented, but there are some data on loss incurred by propagation through fog. Table 5[14] lists measured values for various visibilities. In very heavy fog, a loss of 3 dB/km is not devastating over a communication range of 2 km. The effect due to clouds probably is

[13] M Skolnik, Weather Effects on Radar, Radar Handbook, chap 24, McGraw-Hill, 1970

[14] NOSC Technical Note NELC TN 1809, Precipitation Losses at Millimeter Wavelengths, by JW Carson, February 1971.

[15] US Army Ballistic Research Laboratories Memo Report 2710, A Review of Atmospheric Transmission Information in the Optical and Microwave Spectral Regions, by AR Downs, December 1976.

Table 3. Millimetre-wave rain absorption coefficients.

Rainfall rate, mm/hr	Rain absorption coefficient, (in inverse km)				
	9.375 GHz	35 GHz	94 GHz	140 GHz	240 GHz
1	2.0×10^{-3}	4.6×10^{-2}	1.2×10^{-1}	1.4×10^{-1}	1.4×10^{-1}
2	4.8×10^{-3}	8.7×10^{-2}	2.0×10^{-1}	2.3×10^{-1}	2.3×10^{-1}
4	1.2×10^{-2}	1.6×10^{-1}	3.3×10^{-1}	3.7×10^{-1}	3.7×10^{-1}
8	2.9×10^{-2}	3.0×10^{-1}	5.4×10^{-1}	6.2×10^{-1}	6.2×10^{-1}
16	6.5×10^{-2}	5.6×10^{-1}	8.7×10^{-1}	1.0×10^{0}	1.0×10^{0}
32	1.6×10^{-1}	1.0×10^{0}	1.5×10^{0}	1.7×10^{0}	1.7×10^{0}
64	3.8×10^{-1}	1.8×10^{0}	2.3×10^{0}	2.6×10^{0}	2.6×10^{0}

Table 4. Millimetre-wave rain scattering coefficients.

Rainfall rate mm/hr	Rain scattering coefficient, km^{-1} (in inverse km)				
	9.375 GHz	35 GHz	94 GHz	140 GHz	240 GHz
1	6.0×10^{-5}	1.7×10^{-2}	1.4×10^{-1}	1.6×10^{-1}	1.6×10^{-1}
2	1.7×10^{-4}	4.0×10^{-2}	2.3×10^{-1}	2.4×10^{-1}	2.4×10^{-1}
4	4.7×10^{-4}	8.5×10^{-2}	3.7×10^{-1}	3.8×10^{-1}	3.8×10^{-1}
8	1.4×10^{-3}	1.8×10^{-1}	6.4×10^{-1}	6.4×10^{-1}	6.4×10^{-1}
16	4.0×10^{-3}	4.0×10^{-1}	1.1×10^{0}	1.1×10^{0}	1.1×10^{0}
32	1.2×10^{-2}	8.2×10^{-1}	1.8×10^{0}	1.8×10^{0}	1.8×10^{0}
64	3.2×10^{-2}	1.7×10^{0}	2.9×10^{0}	2.9×10^{0}	2.9×10^{0}

Table 5. Attenuation by fog, experimental.

Visibility, m	Attenuation, dB/km	
	56–63 GHz	35 GHz
60	~2.5	
100	1	~.3
600	1/2	~.07
1000	~0	~.05

somewhat greater than that due to fog because of water droplet size difference, temperature difference, and dust density differences.

BRL has conducted a few preliminary tests of 94 GHz and 140 GHz transmissions through smoke.[15] First indications are that little attenuation was noted, but the parameters of the test that was conducted were not given. More controlled tests of this nature are needed before attenuation rates can be confidently stated.

For airborne system millimetre-wave transmission then, the principal atmospheric phenomena affecting the propagation characteristics are atmospheric oxygen, rain, clouds, and fog (and, in rare cases, ice particles). For the millimetre-wave communication system, the attenuation due to oxygen is utilized to achieve covertness.

INTERCEPT SYSTEM DESCRIPTION

It is assumed that the intercept receiver is a radiometer which is "tuned" to the transmit frequency and has its antenna pointed directly at the transmitter. Because it is a radiometer, no modulation can be recovered – only the knowledge of the presence of a signal (termed detection herein) and the location of the signal source are achieved.

It is assumed that the interceptor has a 40 dB gain dish with a corresponding 1.5° beamwidth. With such a beamwidth, a stabilized platform for the antenna is a must. If the antenna scans the horizon by swinging a full 360° about its axis, a reasonable period for one revolution is about 20 seconds. The antenna's main lobe covers an angular cell for about 80 milliseconds. If an intercept occurs, the integration time of the radiometer should be short

enough so that the scan will stop and the antenna will remain "trained" on the transmitter. A reasonable value for T, integration time, is 0.1 second. An intercept receiving system would normally have to scan in frequency as well as spatially. A large rf bandwidth window results in larger spectral coverage. If the radiometer front end has a scanning LO, a 4 GHz IF bandwidth is likely. To increase sensitivity, this bandwidth (in the 4–8 GHz range) could be split into 32 contiguous channels each 125 MHz wide. With integrated circuits this can be done readily. Hence, we assume a predetection bandwidth of 125 MHz. Finally, we assume an overall radiometer front-end noise figure of 10 dB, which is state-of-the-art and represents a high-quality front end. With such a receiver-antenna combination, the Δ_{intcp} characterizing the transmitter/interceptor characteristic is about 70 dB. The range curves then indicate the radius of a sphere or portion of a sphere in which intercept can occur.

If a potential interceptor lies beyond this radius, intercept is impossible with the parameters specified. The parameters of the interceptor listed are selected to favor interception and thus put an upper bound on intercept range.

INTERCEPTION OF A MILLIMETRE-WAVE COMMUNICATION SYSTEM

It follows that a millimetre-wave communication system operating at 60 GHz should be able to provide the necessary covertness required in a P-3 to P-3 hand-over. The ratio of maximum intercept range to communication range is about 2.5 to 1 even when the transmitter is at an altitude of 6.4 km and "looking" up with an elevation angle of 60°. Thus we see that intercept by either satellite or unfriendly aircraft is unlikely since it would have to be almost as close to the intended receiver as the transmitter. When the receiving aircraft is beneath the transmitting aircraft, intercept by surface platforms is possible only when the transmitter is at or below 1.6 km and uses a declination angle of 45° or more. When the transmitter is at 3.2 km, interception at the surface is possible only when θ_o is between −60° and −90°. At 6.4 km altitude, the transmitter's signal level at the surface is below the radiometer's threshold of detection.

At 57.6 GHz transmitting frequency, the distance ratio R_{intcp} (max)/R_{comm} increases from about 3 to 1 at the surface to about 4.5 to 1 at an altitude of 6.4 km. This ratio could be reduced somewhat, since the atmospheric loss is 8 dB lower at that altitude and the transmitted power level therefore could be reduced by that amount. Intercept by an airborne platform at an altitude greater than 1.6 km is virtually impossible. When the declination angle of the transmitting antenna is 30° or more at an altitude of 1.6 km, interception at the surface is possible. At an altitude of 3.2 km the declination angle must be 45° or more for detection. At 6.4 km, detection at the surface is not possible for any declination angle.

At a transmitting frequency of 55.2 GHz, the Δ for communications is about 15 dB instead of the 35 dB value required at 60 GHz. Thus either the transmitter power could be reduced or the antenna gain could be dropped from about 25 dB to roughly 15 dB. The corresponding beamwidth would increase from ~6° to ~30°. Δ_{intcp} would then be either 50 dB (for 20 dB transmit power drop) or 60 dB (for 10 dB decrease in transmit antenna gain). When the transmitter is at the surface and $\theta_o = 0°$, the intercept-range/comm-range is about 6 to 1. When $\theta_o = 60°$, that ratio is about 9 to 1. As the transmitter goes up in altitude, that ratio increases until at 6.4 km and $\theta_o = 60°$, the ratio is about 60 to 1. Interception by satellite still is not possible, but distant aircraft could intercept. Interception by surface platforms is possible for all declination angles at an altitude of 1.6 km, at all declination angles except from 0° to −12° at 6.4 km.

It can be seen from the range curves that use of the O_2 absorption peak centered at 60 GHz renders interception impossible beyond a range of 5-6 km. Communications should be conducted at an altitude of 3-6 km to eliminate reception by surface platform. At 60 GHz, millimetre-wave device and circuit technologies are developed sufficiently to enable implementing a small and relatively lightweight transceiver which can be hand held and pointed. The cost per unit probably would be $4k-5k.

Finally, it should be emphasized that this approach to evaluate such a system's covertness has sidestepped the issue of probability of intercept. In a realistic tactical situation, the likelihood of an interceptor's detecting a millimetre-wave transmission depends upon

having a receiver which "tunes" to the signal frequency.

having a sensitive receiver.

having his antenna's main beam trained on the transmitter.

having the transmitter antenna's main beam trained on the interceptor.

For interception to occur, all of the above factors must be coincident in time. Thus, to reduce this likelihood or probability of intercept, one should operate at a frequency where there are no intercept receivers and should operate with narrow antenna beamwidths, to spatially confine the emitted radiation. In more sophisticated (and costly) systems, techniques such as frequency hopping or spread spectrum could be used to reduce the probability of intercept.

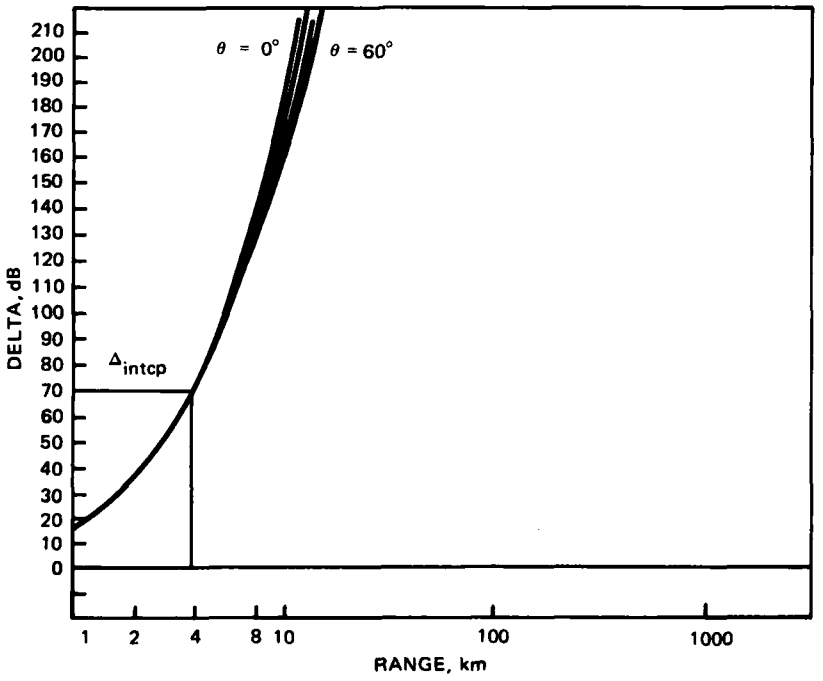

Figure 11. Range curve. Frequency, 60.306 GHz; height, 0.03 km.

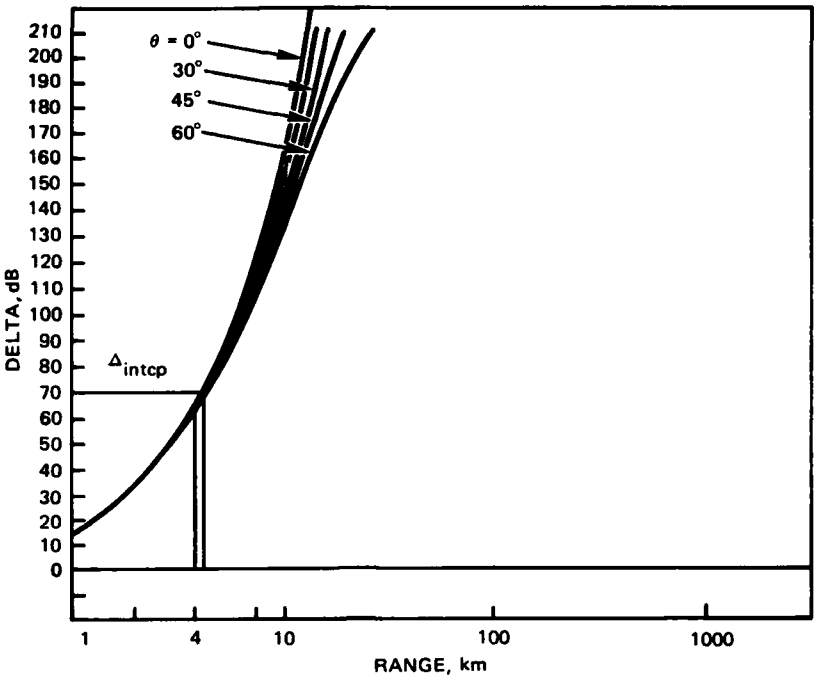

Figure 12. Range curve. Frequency, 60.306 GHz; height, 6.4 km.

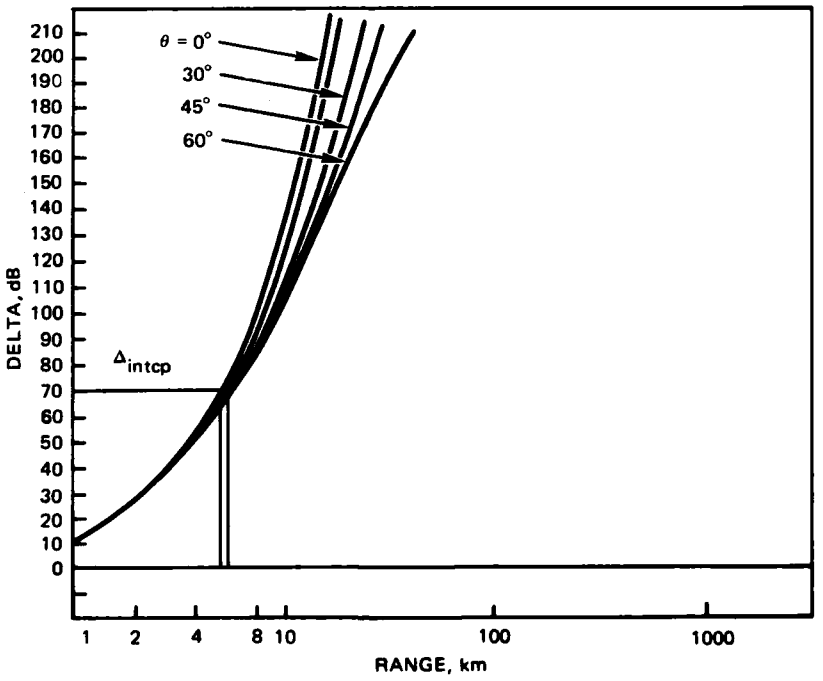

Figure 13. Range curve. Frequency, 57.6 GHz; height, .03 km.

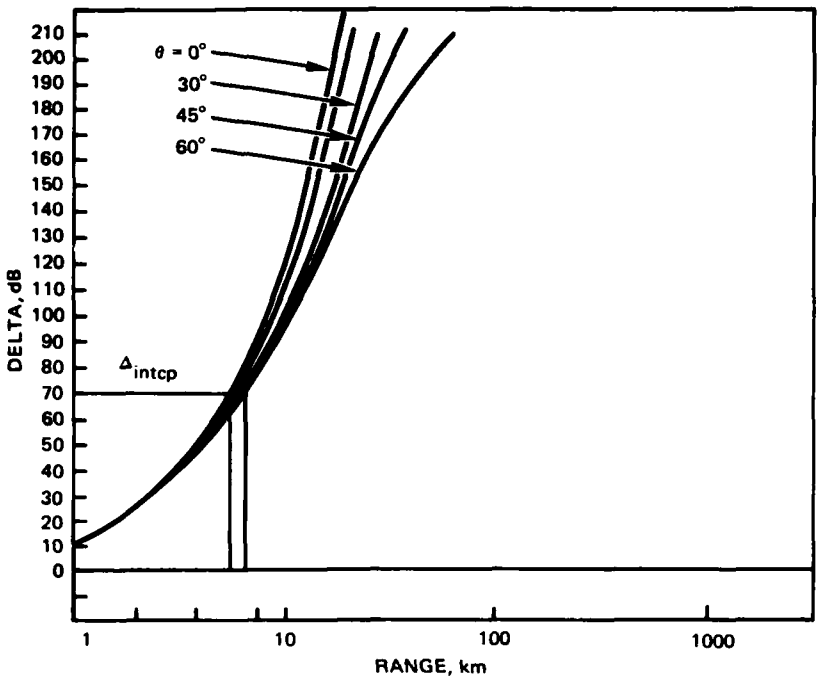

Figure 14. Range curve. Frequency, 57.6 GHz; height, 1.6 km.

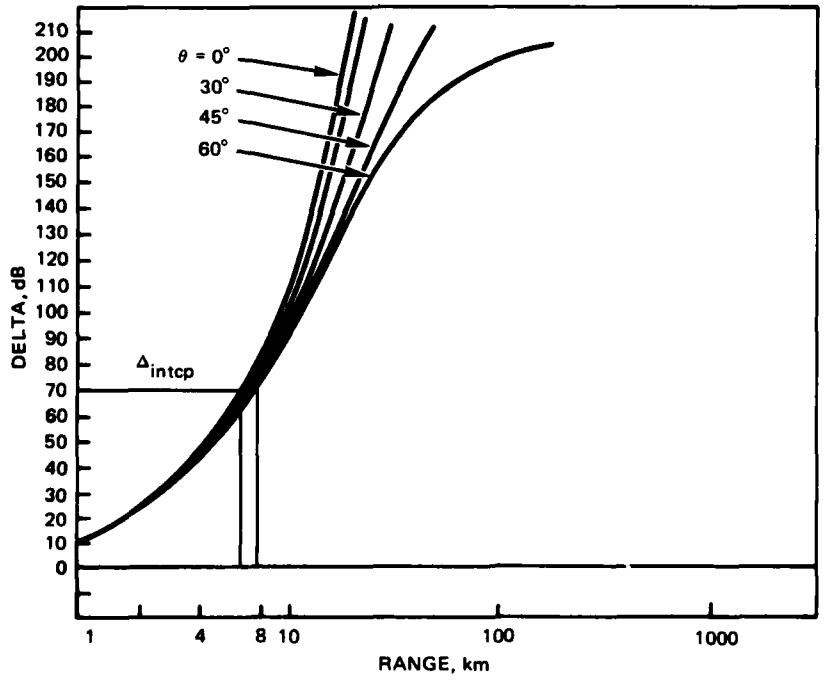

Figure 15. Range curve. Frequency, 57.6 GHz; height, 3.2 km.

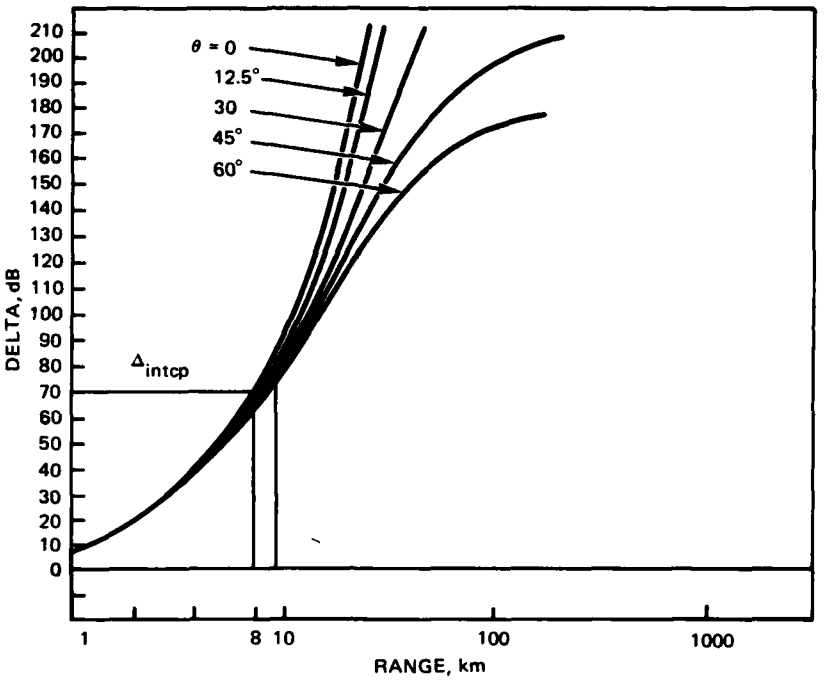

Figure 16. Range curve. Frequency, 57.6 GHz; height, 6.4 km.

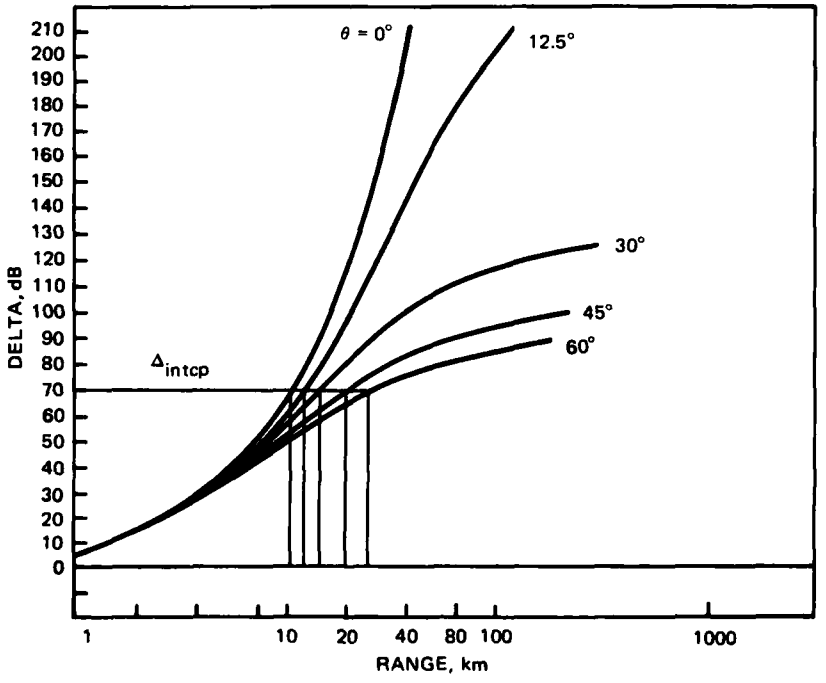

Figure 17. Range curve. Frequency, 55.2 GHz; height, 0.03 km.

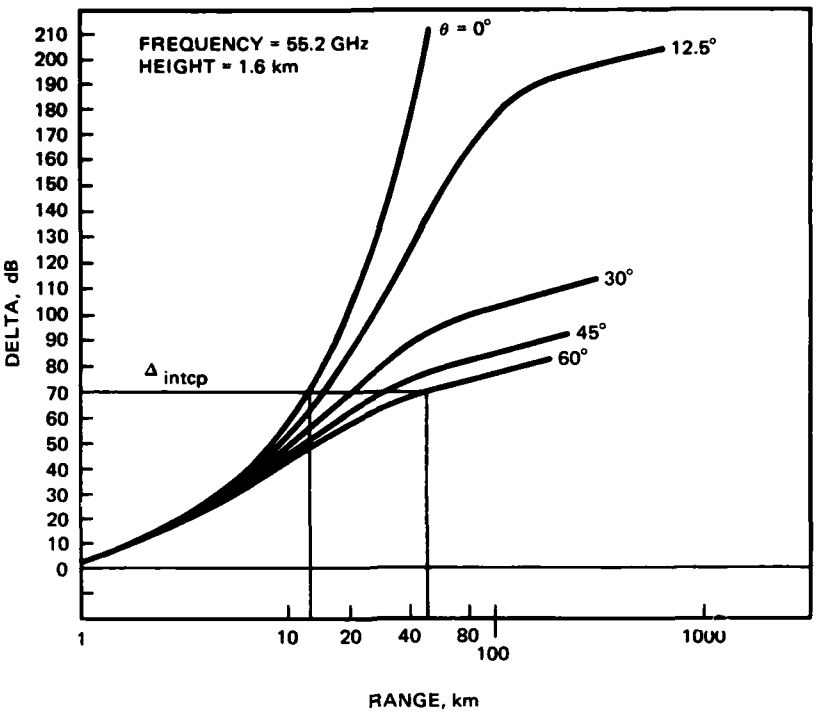

Figure 18. Range curve. Frequency, 55.2 GHz; height, 1.6 km.

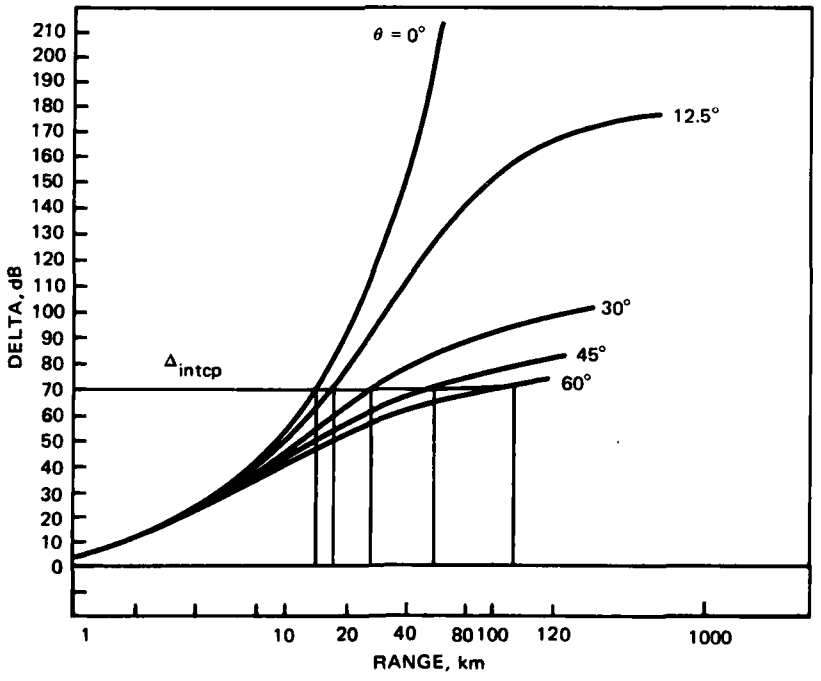

Figure 19. Range curve. Frequency, 55.2 GHz; height, 3.2 km.

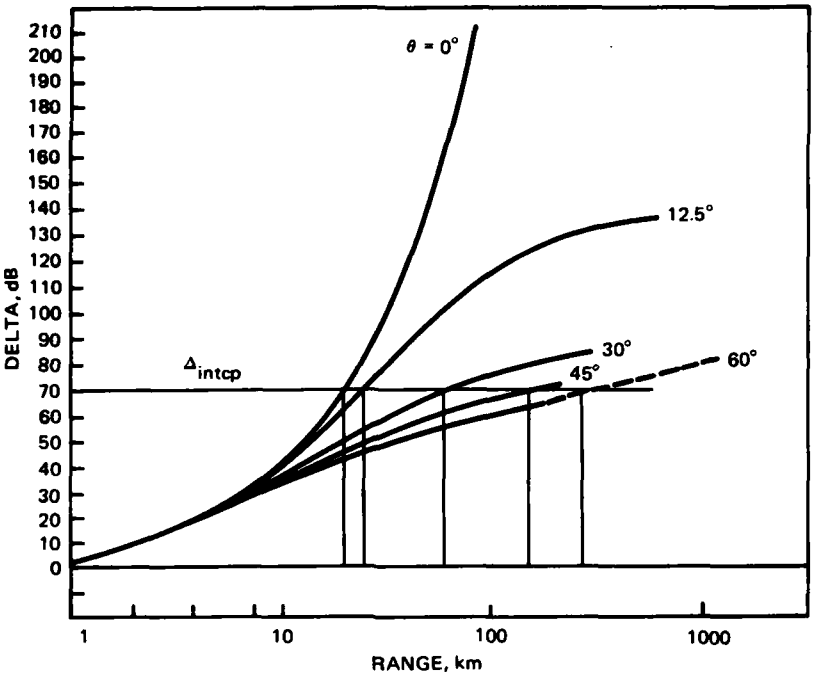

Figure 20. Range curve. Frequency, 55.2 GHz; height, 6.4 km.

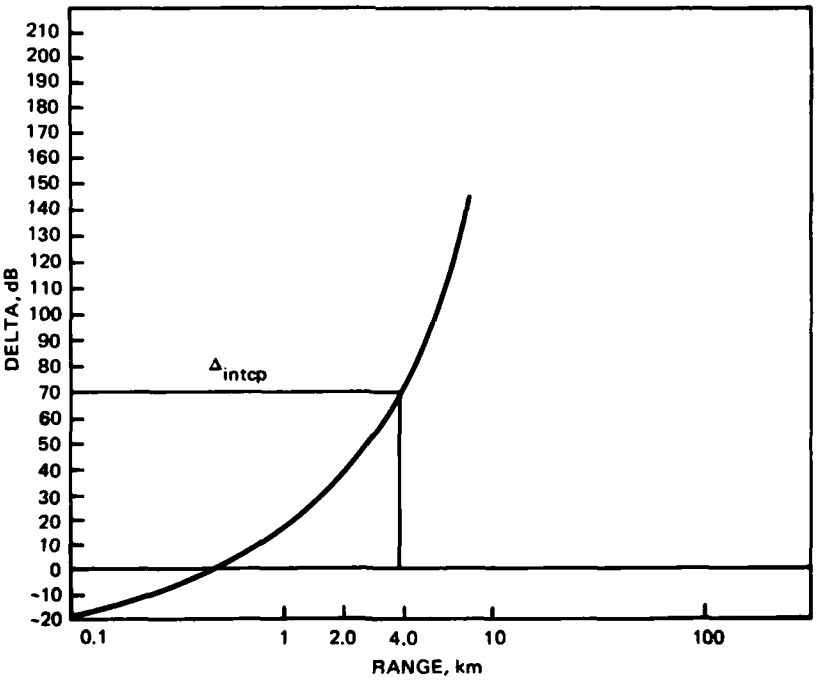

Figure 21. Range curve. Frequency, 60.306 GHz; height, 1.6 km.

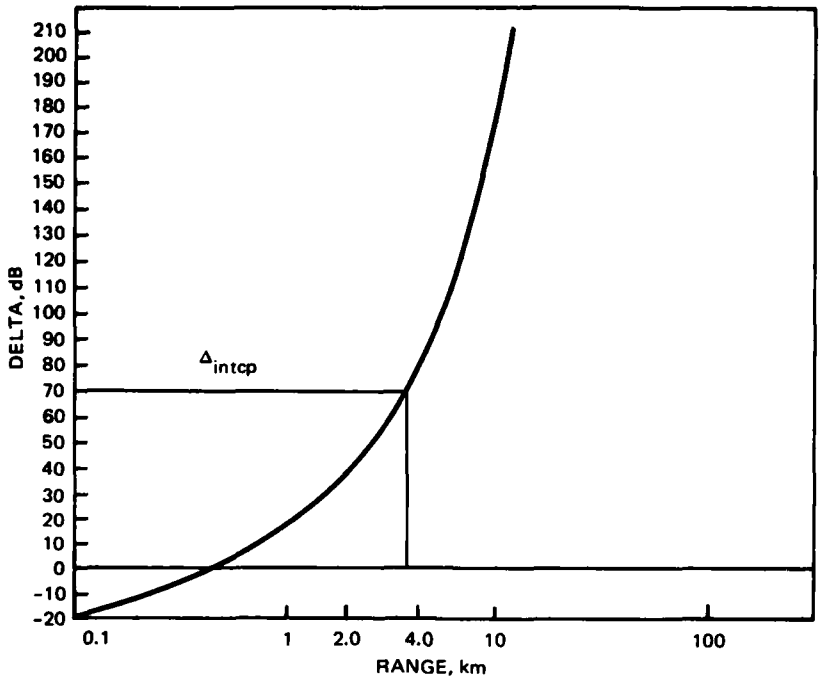

Figure 22. Range curve. Frequency, 60.306 GHz; height, 3.2 km.

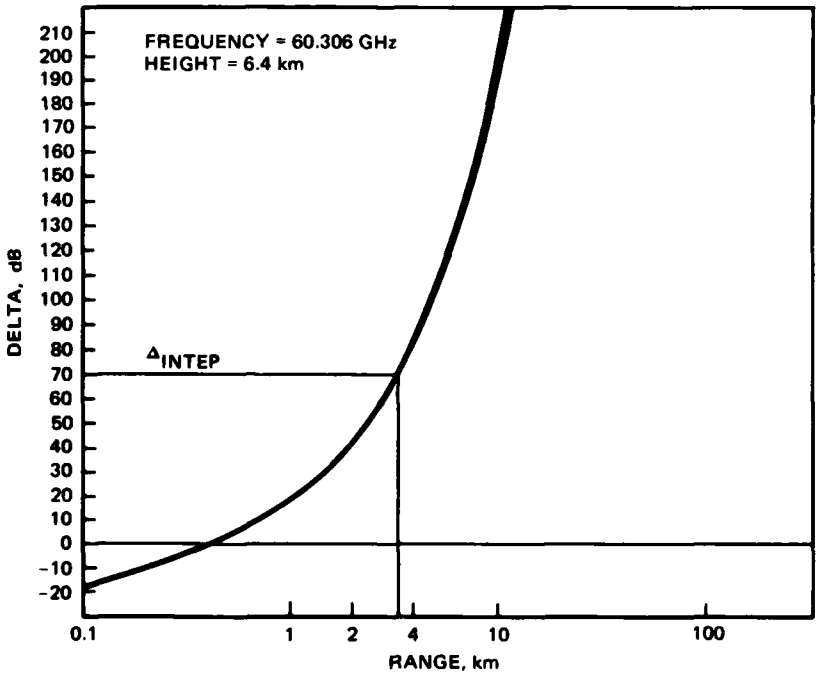

Figure 23. Range curve. Frequency, 60.306 GHz; height, 6.4 km.

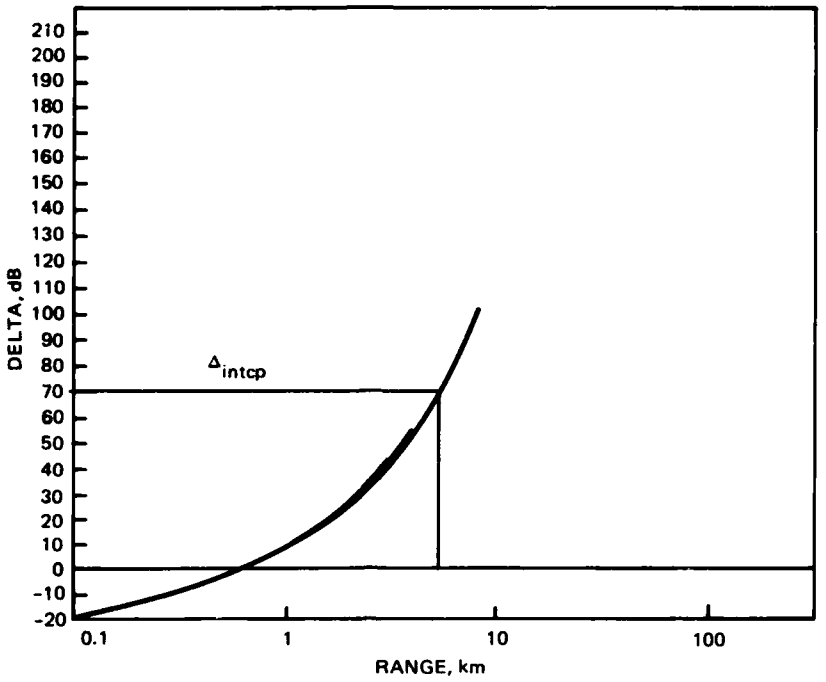

Figure 24. Range curve. Frequency, 57.6 GHz; height, 1.6 km.

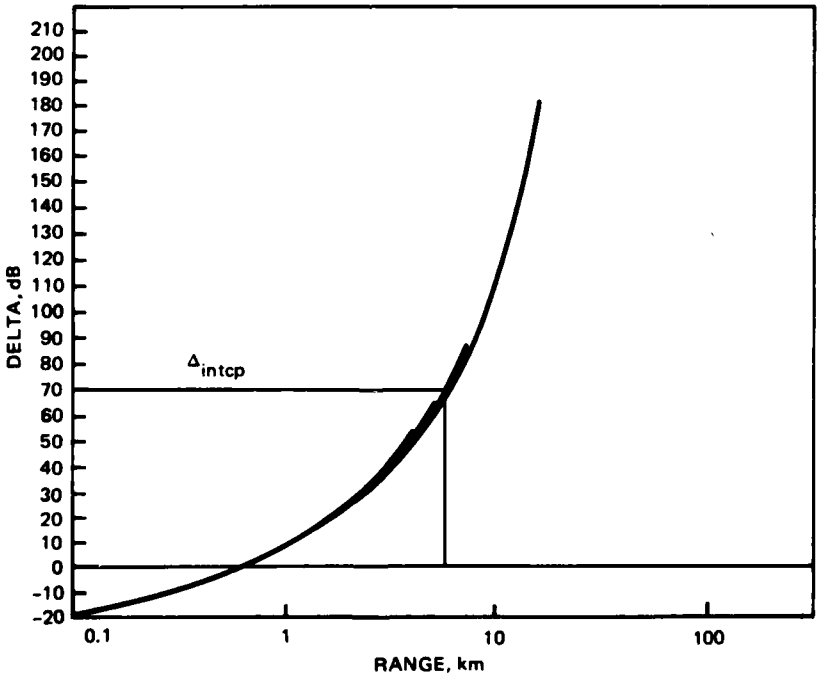

Figure 25. Range curve. Frequency, 57.6 GHz; height, 3.2 km.

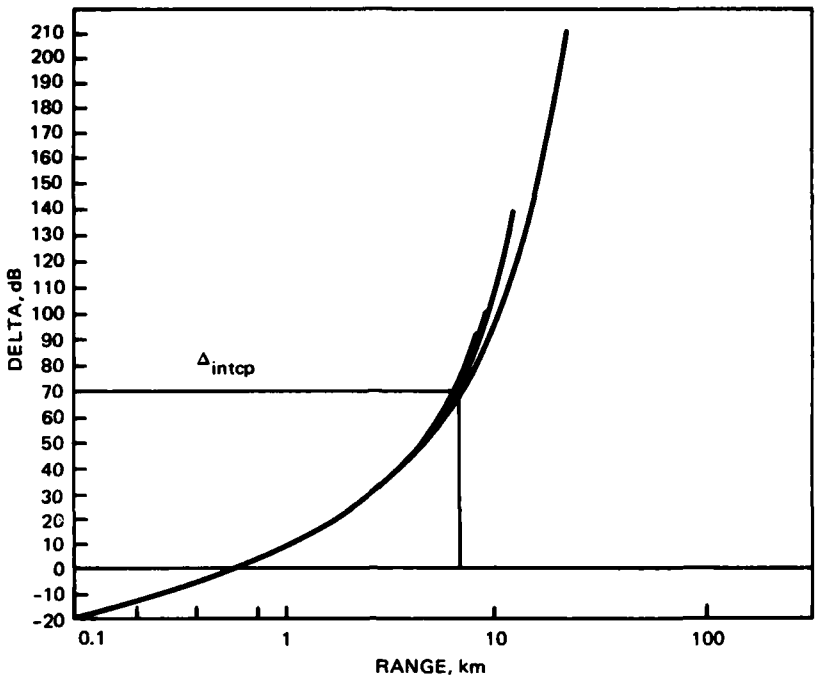

Figure 26. Range curve. Frequency, 57.6 GHz; height, 6.4 km.

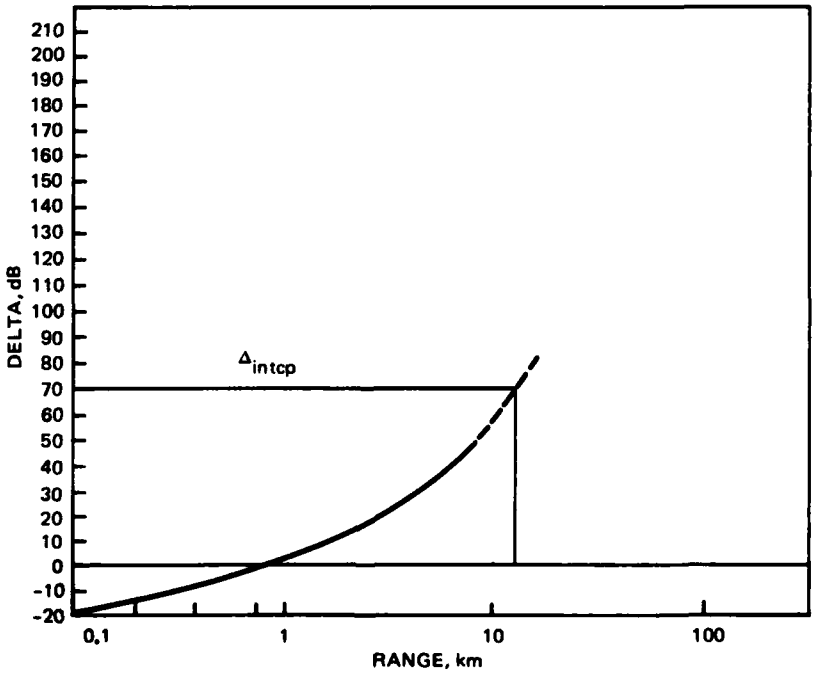

Figure 27. Range curve. Frequency, 55.2 GHz; height, 1.6 km.

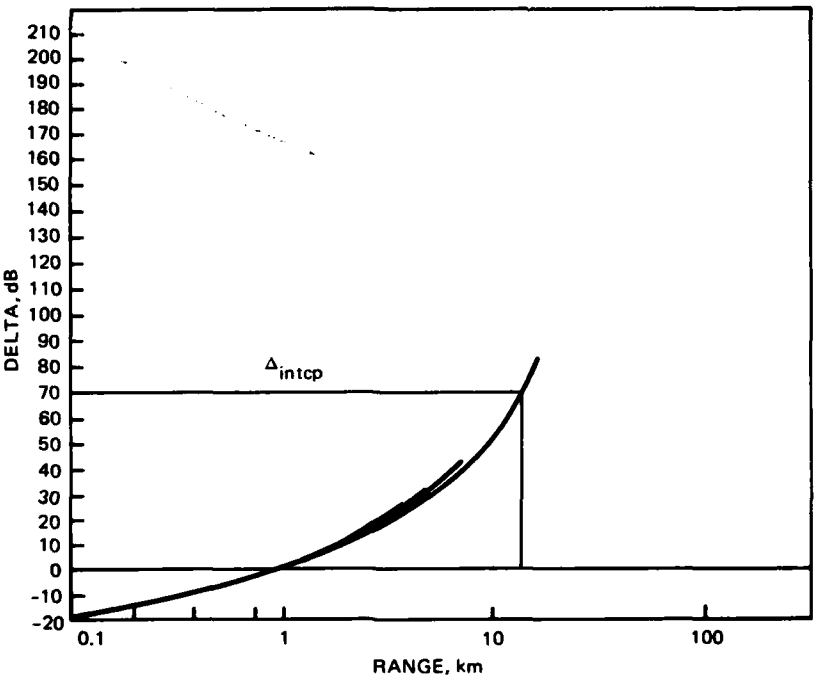

Figure 28. Range curve. Frequency, 55.2 GHz; height, 3.2 km.

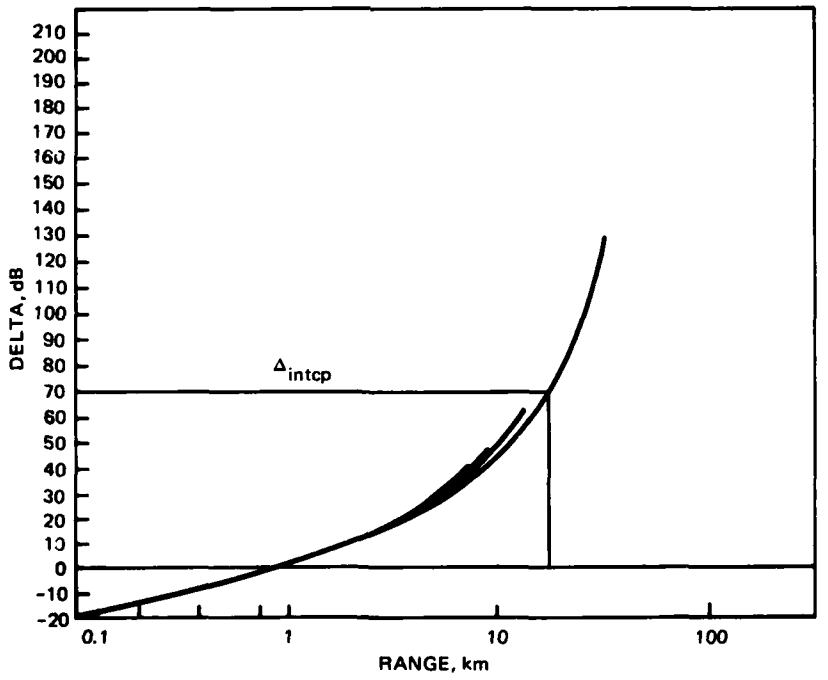

Figure 29. Range curve. Frequency, 55.2 GHz; height, 6.4 km.

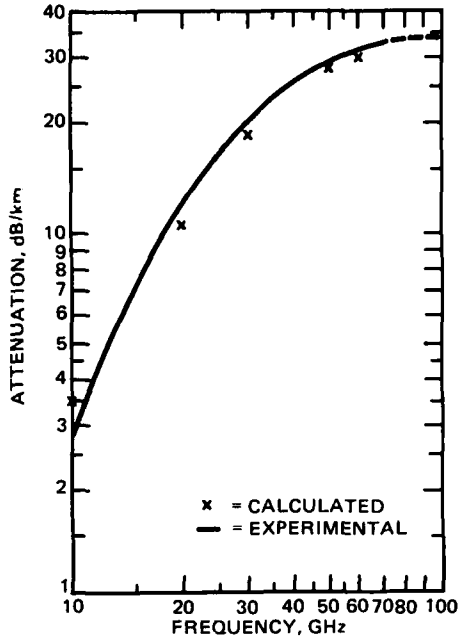

Figure 30. Attenuation vs frequency through 100 mm/h rainfall.

5 NEAR-INFRARED COMMUNICATION/INTERCEPTION

This section describes and evaluates the performance of a near-infrared optical communication system designed for P-3 to P-3 data exchange.

COMMUNICATION SYSTEM DESCRIPTION

Since the late 1930's, the venerable branch of physics known as optics has gradually developed ever-stronger ties with the communication and information processing fields. This trend is a rather understandable one, for both optical imaging systems and telecommunication systems are designed to collect or convey information. There are, however, two critical differences between microwave and optical systems. First, one cannot characterize optical noise as independent of the signal processing performed. Second, spatial problems really count in an optical system. The optical communications engineer must contend with antenna terminals which are not the receiver input and with fields across the aperture which are not totally coherent. Thus, one is left with a more complex design problem than was exemplified in the previous two sections.

OPTICAL TRANSMITTER

The source chosen for this study is a planar GaAs light emitting diode/reflector array designed for a total angular divergence of 23° and a peak wavelength of 0.94 μm. The average power emitted from each diode element is 0.5 watts and its current unit price is $280. However, it should be noted that this device should have a unit price in the vicinity of $20.00 within the next 2 years.* Referring to figures 31 and 32, we see that the 0.94 μm peak emission line of the diode coincides with an H_2O absorption band whose maximum attenuation rate is equal to −7.28 dB/km at sea level.

*From a conversation with RH Patterson

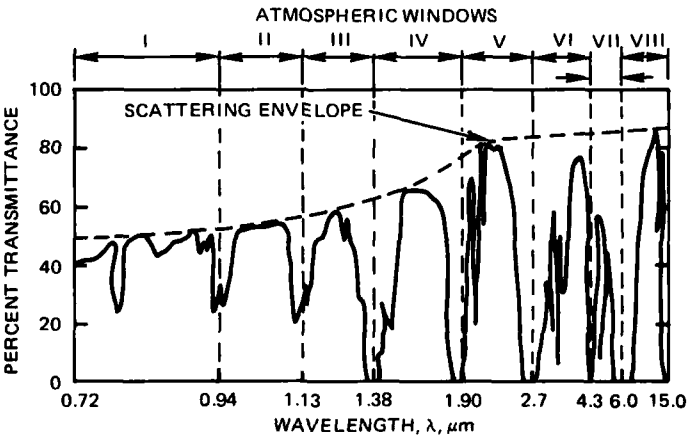

Figure 31. Transmissivity of the atmosphere.[16]

[16]Signal Corps Contract Report DA-36-039-SC-723351, Effects of Atmospheric Water Vapor on Near-Infrared Transmission at Sea Level, by RM Langer, JRM Bege Co, Arlington, Mass, May 1957.

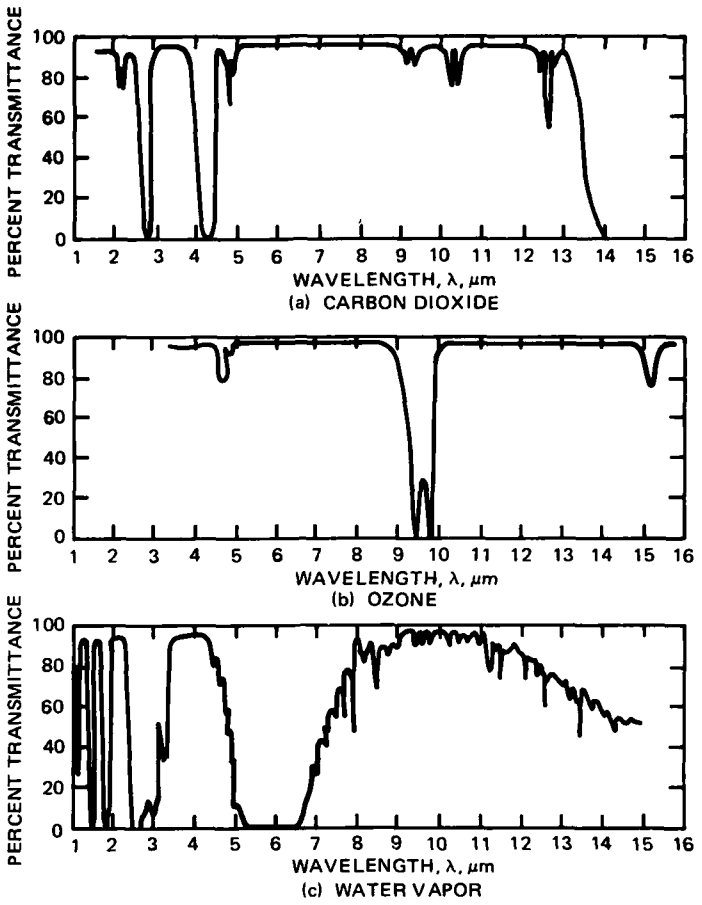

Figure 32. Transmissivities of atmospheric constituents.[17]

The information coding scheme chosen for the data transfer process is a minimum (frequency) shift keying (MSK) format.[18] Figure 33 illustrates a possible configuration for the transmitter. One important reason for choosing this scheme is that less postdetection bandwidth is required for a given data rate than with other schemes. In particular, we require only 20 kHz bandwidth for a 40 kbit per second data rate.

OPTICAL RECEIVER

The optical receiver chosen for this study is illustrated in figure 34. A simple reflective telescope is designed to incorporate a multilayer dielectric interference filter and a photodiode array in its focal plane and to be aplanatic. A typical photodiode array pattern is depicted in figure 35. Each element of the array subtends an angular field of view of θ_D degrees. The full field of view is denoted by θ_{FOV} and the convergence angle by ψ. Let $\Delta\lambda$ be the spectral bandwidth of the filter.

[17]PW Kruse, LD McGlauchlin, and RB McQuistan, Elements of Infrared Technology: Generation, Transmission, and Detection, John Wiley, New York, 1962.

[18]F Amoroso and JA Kivett, Simplified MSK Signaling Technique, IEEE Transactions on Communications, p 435-441, April 1977.

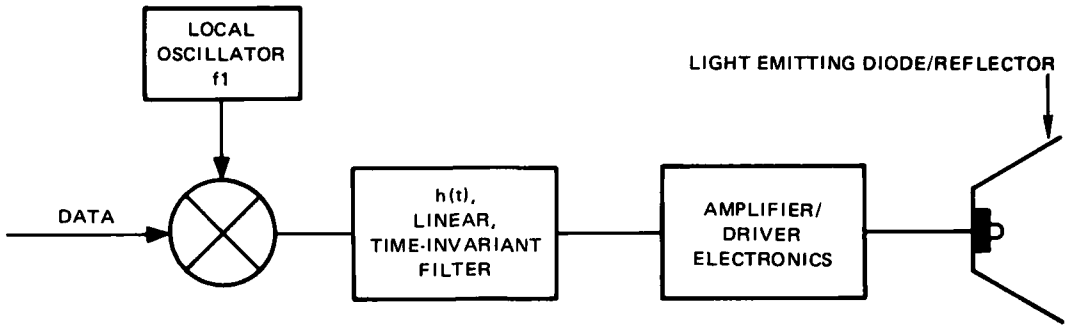

Figure 33. Block diagram of an MSK optical transmitter.

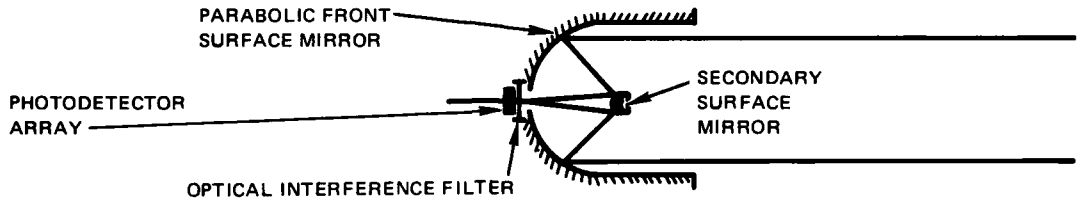

Figure 34. Cross-sectional view of the optical receiver.

From previous work,[19] it can be shown that the ratio of the detection surface diameter to the entrance aperture diameter

$$d_D/d_A = 2(f/\#)\tan(\theta_{FOV}/2) \ , \tag{17}$$

where

$d_D \equiv$ diameter of the detection array

$d_A \equiv$ diameter of entrance aperture

$f/\# \equiv$ f-number or speed of the optical system.

In general, most practical systems have an f-number of 1.2 or higher. For simplicity, let the f-number equal 1.20. Then, a field-of-view angle of 25° yields

$$d_D/d_A = 0.5321 \ .$$

If $\theta_D \lesssim 2°$,

then

$$d_{D_e}/d_A \lesssim 8.381 \times 10^{-2} \ ,$$

[19] RD Anderson and ME Hyde, Underwater Optical Communication Receivers, Paper presented at the SPIE meeting held in San Diego, Calif, 22-26 August 1977.

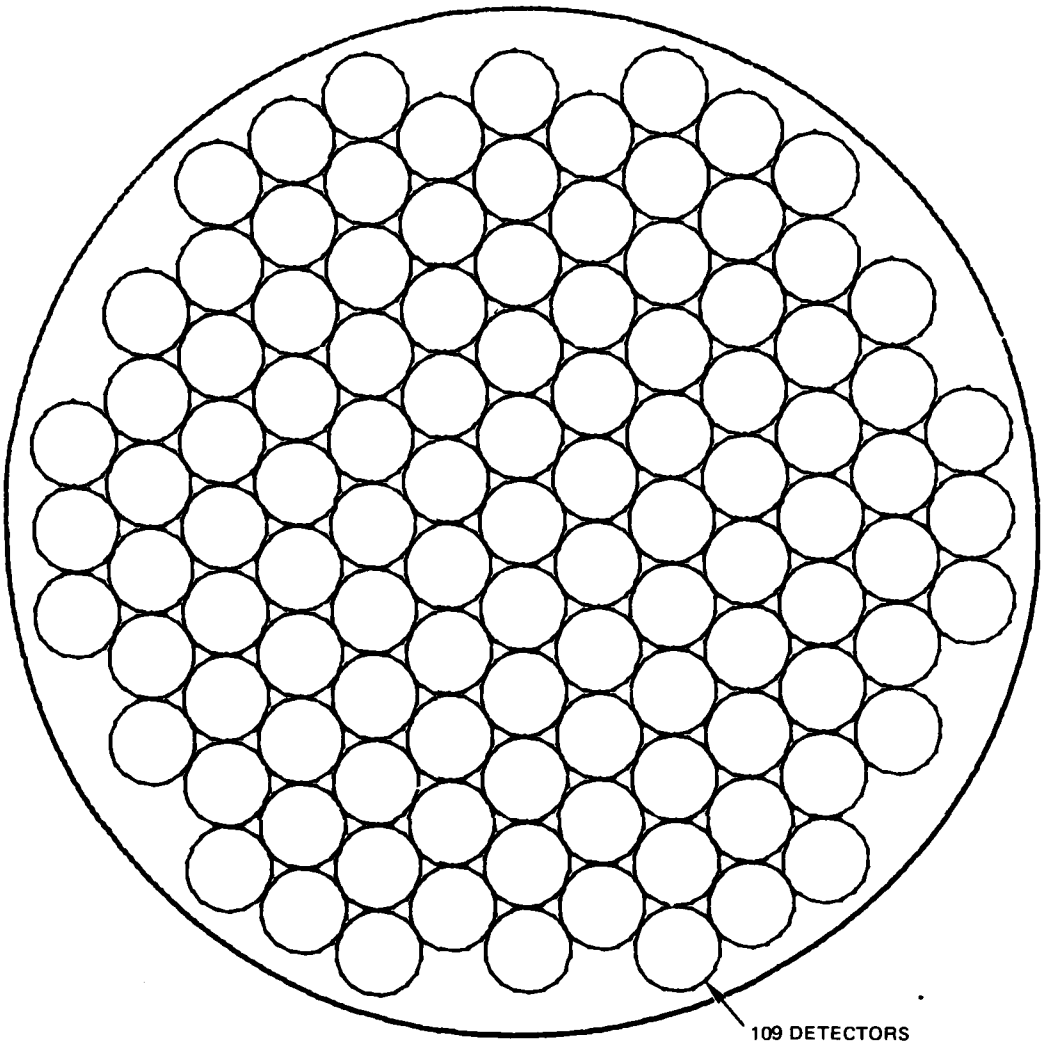

Figure 35. Photodiode array.

where d_{D_e} is the diameter of the individual diode elements. This type of array is shown in figure 35. There are two reasons for the choice of a diode array detector surface. One is the ease of large surface fabrication (greater than 1 inch) and the second is that the photodiode shuts off under intensive optical illumination. Thus, the optical system is never bothered by direct sunlight as long as the sun and transmitter angles are not collinear. For the discussion that follows, since the individual diodes subtend a much smaller angle than θ_{FOV}, we will assume the packing fraction of the array to be about unity.

In specifying the spectral bandwidth of the interference filter, one must take into account the operating characteristics of the source. The spectral bandwidth of a GaAs LED is approximately 300Å at room temperature. This spectrum, however, shifts 3Å/°C. Hence if we expect the system to operate within a 100°C temperature range about room temperature, $\Delta\lambda$ should be in the vicinity of 600Å.

Table 6 lists the pertinent characteristics of the assumed optical receiver.

Table 6. Operational characteristics of the receiver.

Characteristic	Value
Area of entrance aperture	7.3×10^{-2} m^2 (diameter 0.305 m)
Field-of-view solid angle	1.266×10^{-1} sr
Postdetection bandwidth	20 kHz
Spectral bandwidth	600Å
Telescope cost	$300 to $400
Interference filter cost	$200 to $300
Detection array cost	$200 to $300 (CCD) ~$1000 (silicon photodiode)

COMMUNICATION SYSTEM PERFORMANCE

In a given optical communication system, the current produced by the receiver is generally composed of four independent parts:

The current, I_S, resulting from a detected information-carrying signal P_S

The current, I_B, generated by undesired background power, P_B, incident on the detection surface

The current, I_T, derived from thermal noise

The dark current, I_D.

It can be shown[20,21] that both the signal current and the background current can be modeled as Poisson processes; they are directly proportional to the total detected optical power. That is, with P in watts, the average detected current in amperes

$$I = \frac{\eta q P}{h\nu}, \tag{18}$$

where

$\eta(\nu) \equiv$ detector quantum efficiency

$h \equiv$ Planck's constant

$q \equiv$ electronic charge

$\nu \equiv$ frequency of the optical radiation.

From appendix E, we know that the mean-square fluctuations of the noise about the rms value are equal to

$$2q I B ,$$

where B denotes the electrical bandwidth. In general, I_B is several orders of magnitude larger than any of the other components or all three combined. Thus we assume a

[20] WK Pratt, Laser Communication Systems, John Wiley, New York, 1969.

[21] M Ross, Laser Receivers: Devices, Techniques, Systems, John Wiley, New York, 1966.

background-limited situation for the purposes of this study. That is, we may write the mean-square fluctuations of the noise as

$$\overline{\Delta n^2} = 2q\,IB \sim \frac{\eta q^2 P_B}{h\nu} . \tag{19}$$

Therefore, the signal-to-noise power ratio for our communication system is given by

$$SNR \approx \frac{\eta}{2h\nu B} \cdot \frac{P_s^2}{P_B}, \tag{20}$$

where

$\eta/2h\nu = 1.890 \times 10^{18}\ J^{-1}$

$\nu = 3.191 \times 10^{14}$ Hz ($\lambda = 0.94\ \mu m$)

$B \equiv$ postdetection electrical bandwidth

$P_s =$ received information signal

$P_B \equiv$ received background signal

The received information signal can be shown[20,21] as

$$P_s \approx T_\lambda \left(\frac{d_A}{\theta_{DIV} R}\right)^2 \tau_a P_T , \tag{21}$$

where

$T_\lambda \equiv$ transmissivity of the optical system

$\tau_a \equiv$ atmospheric transmissivity of source/receiver path

$R =$ source/receiver separation

$d_A \equiv$ diameter of receiver's entrance aperture

$\theta_{DIV} \equiv$ angular divergence of the source

$P_T \equiv$ total source input power

Unfortunately, the transmissivity, τ_a, for a gradient atmosphere in the presence of a curved earth at $\lambda = 0.94\ \mu m$ has yet to be reported in the literature. Thus, a model had to be developed. We do not discuss its development here, but rather refer the reader to appendix F for its mathematical derivation.

The background radiation for a gradient atmosphere and curved earth at $\lambda = 0.94$ also has not been reported in the literature. Hence, a model for this process had to be developed. This is the subject of appendix E. Referring to figure 36, the background power produced by a gradient atmosphere in the presence of a curved earth is given by

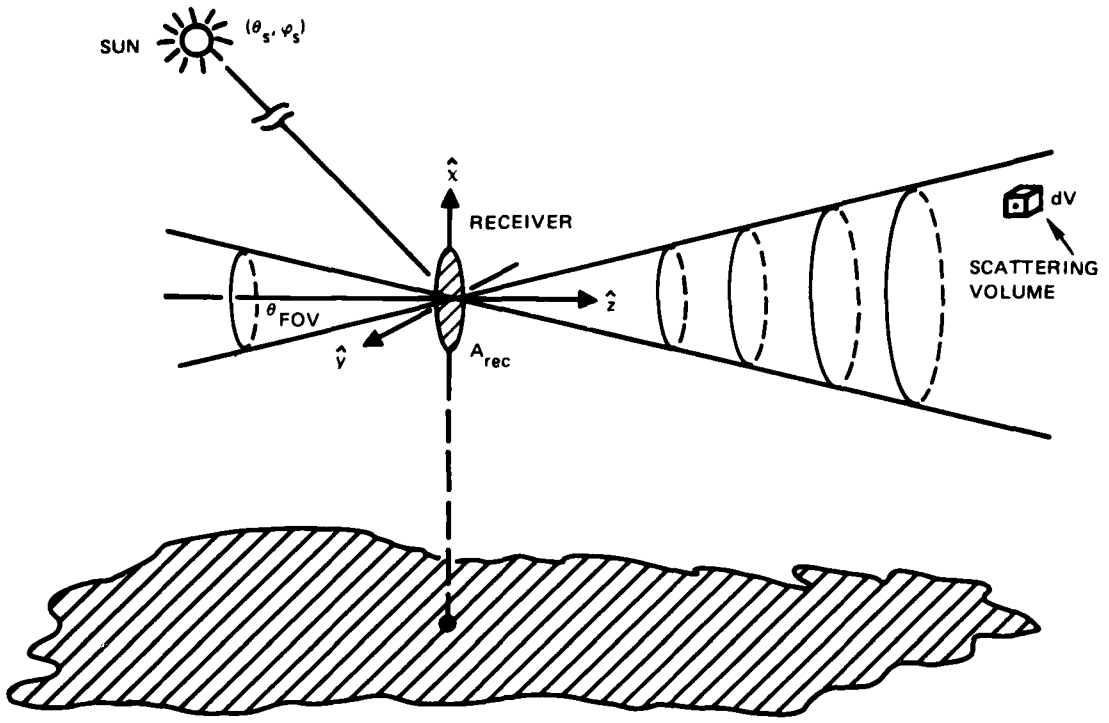

Figure 36. Typical communications scenario for $(\theta_R, \varphi_R) = (0°, 0°)$.

$$P_B \sim A_{rec} \int_0^{r_{max}} \int_{\substack{\text{Spectral} \\ \text{range}}} H_{\lambda s} \iint_{4\pi} T(\gamma,\lambda)\, \tau_0(\underset{\sim}{r}_0)\, \tau_a(\underset{\sim}{r}_0)\, \beta(\gamma, \underset{\sim}{r}_0) \cdot$$

$$\cos\theta \, d\Omega \, d\lambda \, dr \, , \qquad (22)$$

where

$H_{\lambda s} \equiv$ unattenuated spectral solar irradiance

$$= \frac{2hc\,\Omega_{sun}}{\lambda^5} (\exp[hc/\lambda kT] - 1)^{-1} \Big|_{T = 5900\ K}$$

$\Omega_{sun} \equiv$ solid angle subtended by the sun

$\approx 6.79 \times 10^{-5}$ sr

$\lambda \equiv$ wavelength of optical radiation

$k \equiv$ Boltzmann's constant

$T \equiv$ Source temperature in kelvins

$A_{rec} \equiv$ area of the receiver's entrance aperture

$T(\gamma,\lambda) \equiv$ angular/spectral transmissivity of the receiver

$\tau_0(\underset{\sim}{r}_0)$ ≡ transmissivity from sun to scattering volume (See appendix E)

$\tau_0(\underset{\sim}{r}_0)$ ≡ transmissivity from scattering volume to receiver (See appendix E)

$\beta(\gamma, \underset{\sim}{r}_0)$ ≡ volume scattering function at the point $\underset{\sim}{r}_0$.

c ≡ speed of light

The scenario atmosphere is assumed to be exponentially graded[10,22] and to possess a Barnhardt and Street[23] particle distribution. In particular, we have assumed the volume scattering function

$$\beta(\gamma, \underset{\sim}{r}_0) = k_{sca} \frac{P(\gamma)}{4\pi} e^{-h/0.8\ km} ,$$

where

k_{sca} = 0.46/km

h ≡ height of the scattering volume from the earth's surface

$$P(\gamma)/4\pi = \frac{1}{8\pi}(P_{TE} + P_{TM})$$

P_{TE}, P_{TM} ≡ unnormalized scalar phase function for transverse electric (TE), transverse magnetic (TM) waves.

Table 7 is a list of the values for P_{TE} and P_{TM} assumed for this study under the Barnhardt and Street assumption. In addition, the molecular absorption coefficient, α, referenced in appendices E and F, has been assumed to have the form[23]

$$\alpha = (1.676/km)\, e^{-h/0.8\ km} .$$

It should be noted that the only loss incurred by the transmitted beam is that due to absorption. That is, we are assuming that the scattered photons contribute to the total received signal based on our assumption of a large field of view and a clear-weather atmosphere.

Figures 37 to 47 (at the end of this section) are graphs of the signal-to-noise power ratio, SNR, as a function of range, for various altitudes and transmitter/receiver orientations (see fig 1). In all these graphs, receiver area = 0.07297 m^2, solid angle = 0.1266 sr, and bandwidth = 20 kHz. The sun is located at $(\theta_S, \varphi_S) = (45°, 0°)$, and the source is assumed to be variable power. We are assuming that the system possesses an electronic capability for adjusting the transmitter power to the correct value necessary for communication at 1.5 km. This can be done by monitoring received background radiation, aircraft altitude, and received signal level from the other aircraft. From these graphs, we see that the largest optical transmit power occurs when the sun/receiver and transmitter/receiver projections are essentially collinear, ie $\gamma_S \sim 0$. This implies that the projected LED array cost is $1960. It is fairly apparent that both the transmitter and receiver are pointable, but with $\theta_D \sim 23°$, one need not track closely. For nonclear weather conditions, one would expect the attenuation to remain essentially constant but the background to increase. Experimental measurements

---

[22] WC Wells, G Gal, and MW Munn, Aerosol Distributions in Maritime Air and Predicted Scattering Coefficients in the Infrared, Applied Optics, vol 16 no 3, p 654-659, 1977

[23] EA Barnhardt and JL Street, A Method for Predicting Atmospheric Aerosol Scattering Coefficients in the Infrared, Applied Optics, vol 9 no 6, p 1337-1344, June 1970

Table 7. Values for the TE and TM components of the scalar phase function, $P(\gamma)/4\pi$.

γ	$P_{TE}(\gamma)/4\pi$	$P_{TM}(\gamma)/4\pi$
.0	2.0404822 + 001	2.0404822 + 001
.2	2.0719146 + 001	2.0311434 + 001
.4	2.0440732 + 001	2.0036026 + 001
.6	1.9988940 + 001	1.9591562 + 001
.8	1.9384193 + 001	1.8998091 + 001
1.0	1.8652196 + 001	1.8280759 + 001
1.2	1.7821357 + 001	1.7467310 + 001
1.4	1.6920532 + 001	1.6585879 + 001
1.6	1.5977076 + 001	1.5663100 + 001
1.8	1.5015479 + 001	1.4722801 + 001
2.0	1.4056478 + 001	1.3785138 + 001
2.2	1.3116811 + 001	1.2866371 + 001
2.4	1.2209206 + 001	1.1978865 + 001
2.6	1.1342756 + 001	1.1131453 + 001
2.8	1.0523431 + 001	1.0329935 + 001
3.0	9.7546383 + 000	9.5776324 + 000
4.0	6.7201667 + 000	6.5555431 + 000
5.0	4.6812851 + 000	4.5678580 + 000
6.0	3.3672898 + 000	3.2817434 + 000
7.0	2.5095086 + 000	2.4418277 + 000
8.0	1.9349040 + 000	1.8817958 + 000
9.0	1.5385351 + 000	1.4974470 + 000
10.0	1.2565848 + 000	1.2250573 + 000
12.0	9.0011483 - 001	8.7509175 - 001
14.0	6.8627307 - 001	6.6578110 - 001
16.0	5.4668064 - 001	5.3097439 - 001
18.0	4.4948722 - 001	4.3757183 - 001
20.0	3.7710569 - 001	3.6997997 - 001
22.0	3.2072399 - 001	3.2467150 - 001
24.0	2.8010732 - 001	2.8925323 - 001
26.0	2.4920856 - 001	2.5423969 - 001
28.0	2.2297012 - 001	2.2117782 - 001
30.0	2.0036466 - 001	1.9210913 - 001
35.0	1.4048294 - 001	1.4557978 - 001
40.0	1.0098947 - 001	1.1190301 - 001
45.0	7.6164116 - 002	8.6203167 - 002

Table 7. Values for the TE and TM components of the scalar phase function, $P(\gamma)/4\pi$ (Continued).

γ	$P_{TE}(\gamma)/4\pi$	$P_{TM}(\gamma)/4\pi$
50.0	5.8081307 - 002	6.5924760 - 002
55.0	4.2929378 - 002	5.1789219 - 002
60.0	3.3287967 - 002	4.0805321 - 002
65.0	2.5223013 - 002	3.1051815 - 002
70.0	1.9592502 - 002	2.6183686 - 002
75.0	1.5757830 - 002	1.8836767 - 002
80.0	1.5800945 - 002	1.6609443 - 002
85.0	1.0325098 - 002	1.3199536 - 002
90.0	8.2182273 - 003	1.1398269 - 002
95.0	8.0639212 - 003	9.5464706 - 003
100.0	7.1316148 - 003	8.2197606 - 003
105.0	6.3165194 - 003	6.2028421 - 003
110.0	5.6295425 - 003	6.8883400 - 003
115.0	5.7623922 - 003	5.3610677 - 003
120.0	5.0940931 - 003	5.6653513 - 003
125.0	4.9397149 - 003	5.8440132 - 003
130.0	5.1104149 - 003	6.0436248 - 003
135.0	5.8306391 - 003	6.9005404 - 003
140.0	8.7602681 - 003	8.9722958 - 003
145.0	1.4622755 - 002	1.0859597 - 002
150.0	2.3789838 - 002	1.3337544 - 002
155.0	3.0286344 - 002	1.3677890 - 002
160.0	3.0007686 - 002	1.9964599 - 002
162.0	2.7733605 - 002	2.3210705 - 002
164.0	2.4719489 - 002	2.5293168 - 002
166.0	2.3178350 - 002	2.6852630 - 002
168.0	2.3510361 - 002	2.9400418 - 002
170.0	2.4601564 - 002	3.1521049 - 002
172.0	2.5224564 - 002	3.2494484 - 002
174.0	2.7153237 - 002	3.1975146 - 002
176.0	2.8937702 - 002	2.8618934 - 002
178.0	3.1262037 - 002	2.5968881 - 002
180.0	3.6509125 - 002	3.5895456 - 002

at lower wavelengths indicate that P_B can vary from a 2-3 dB increase on a cloudy day to approximately a 10 dB increase on a cloudy day in those directions noncollinear with the sun.[24] The background power collinear with sun direction will decrease due to the Rayleigh-type scattering associated with severe haze and cloudy conditions. Thus, we expect the transmit power to increase up to a factor of 3 for those directions not collinear with the sun and to remain constant or to decrease in those collinear situations.

INTERCEPT SYSTEM DESCRIPTION

As in the millimetre-wave intercept system description, we have assumed the intercept receiver to be a radiometer tuned to the transmit carrier/subcarrier frequencies and directed collinear with the maximum lobe position. Table 8 describes the operational characteristics of the intercept receiver.

The communications transmitter input powers are assumed to be the same values as used in figures 37 to 47. The sun again is assumed to be at (45°,0°). We are again assuming background-limited operation with the scattered photons contributing to the received signal. Figures 48 to 58 (at the end of this section) depict the signal-to-noise power ratio of the received signal as a function of range, for various altitudes and transmitter/interceptor orientations. In all these graphs, receiver area ≈ 0.2919 m^2, solid angle = 5.383 X 10^{-4} sr, and bandwidth = 5 Hz. The minimum detectable SNR for the interceptor is 1 dB. From figures 48 through 52, our communicator is fairly susceptible to any surface or air-based platform within a distance h sec (θ_I) of it for the ($90° \leqslant \theta_I \leqslant 165°, \varphi_I = \pi$) sector, where ($\theta_I, \varphi_I$) are the angular coordinates of the interceptor. Figures 53 through 58 tell us that the communication transmitter can generally be picked up within a 125 to 150 km radius of the source.

[24]HS Stewart and RF Hopfield, Atmospheric Effects, Applied Optics and Optical Engineering, R Kingslake, Ed, vol 1, p 131-140, Academic Press, New York, 1965.

Table 8. Intercept receiver characteristics.

Characteristic	Value
Area of entrance aperture	2.919 X 10^{-1} m^2
Field-of-view solid angle	5.383 X 10^{-4} sr
Electrical bandwidth	5 Hz

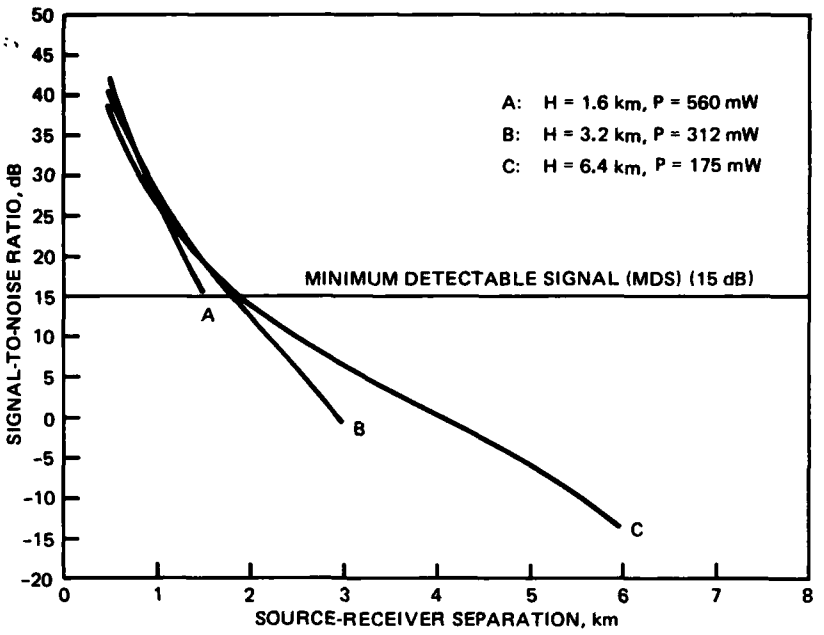

Figure 37. SNR vs range for a P-3 to P-3 communication link. Receiver angular orientation (90°, 180°).

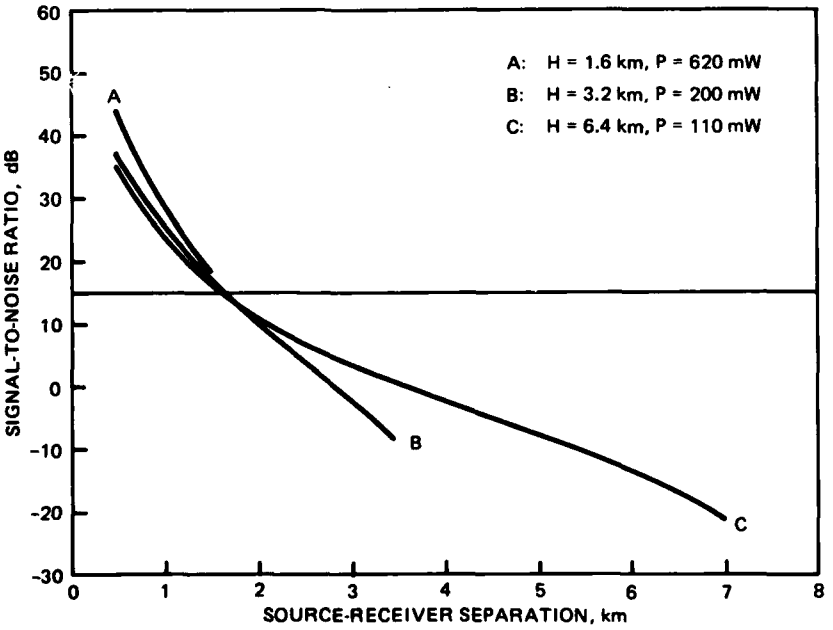

Figure 38. SNR vs range for a P-3 to P-3 communication link. Receiver angular orientation (120°, 180°).

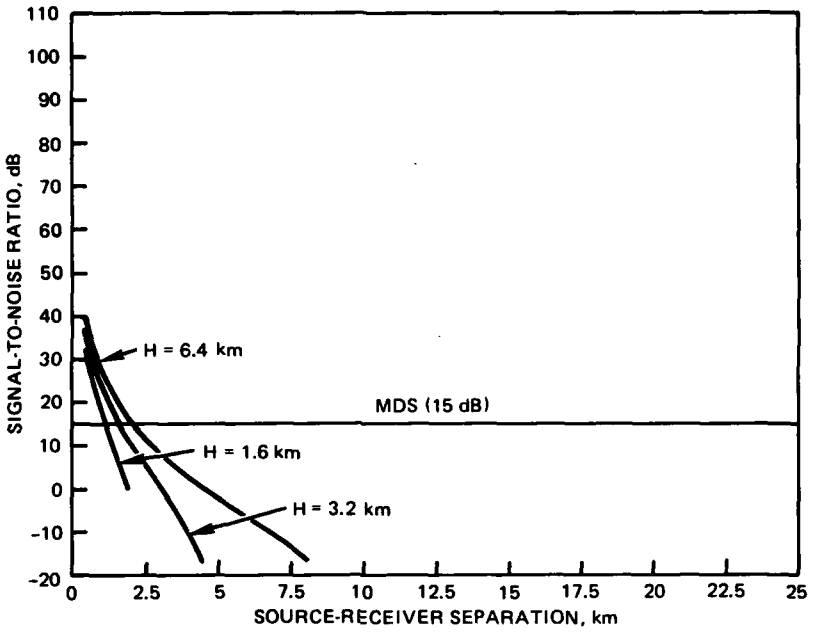

Figure 39. SNR vs range for a P-3 to P-3 communication link. Receiver angular orientation (135°, 180°).

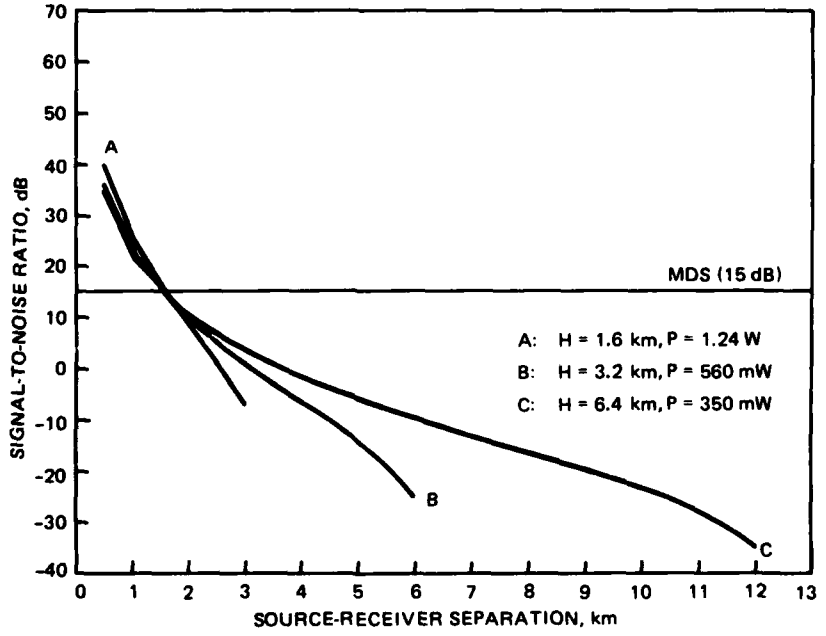

Figure 40. SNR vs range for a P-3 to P-3 communication link. Receiver angular orientation (150°, 180°).

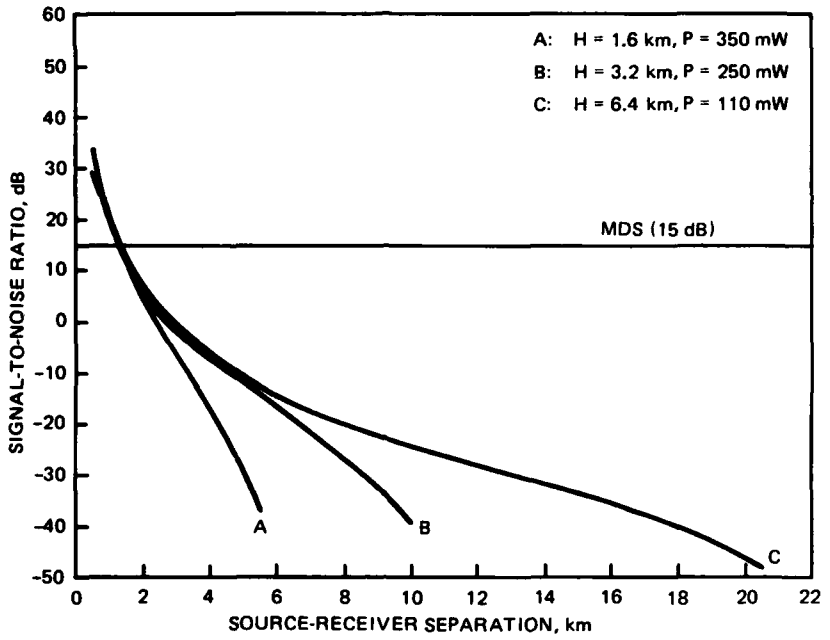

Figure 41. SNR vs range for a P-3 to P-3 communication link. Receiver angular orientation (165°, 180°).

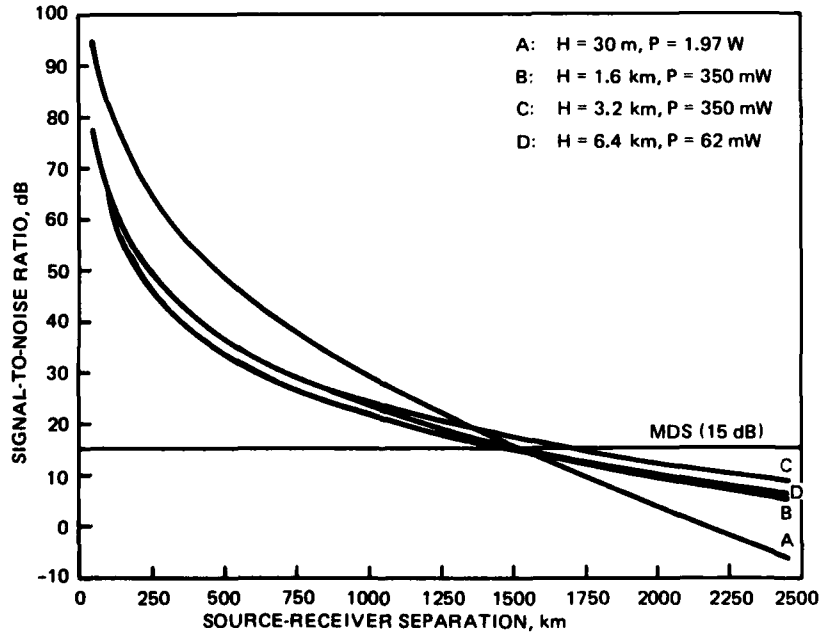

Figure 42. SNR vs range for a P-3 to P-3 communication link. Receiver angular orientation (180°, 0°).

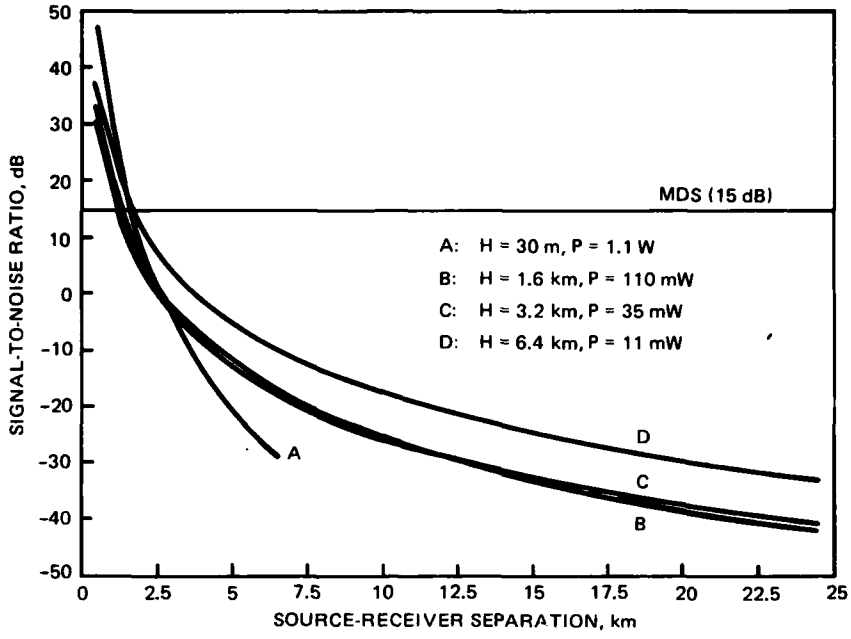

Figure 43. SNR vs range for a P-3 to P-3 communication link. Receiver angular orientation (165°, 0°).

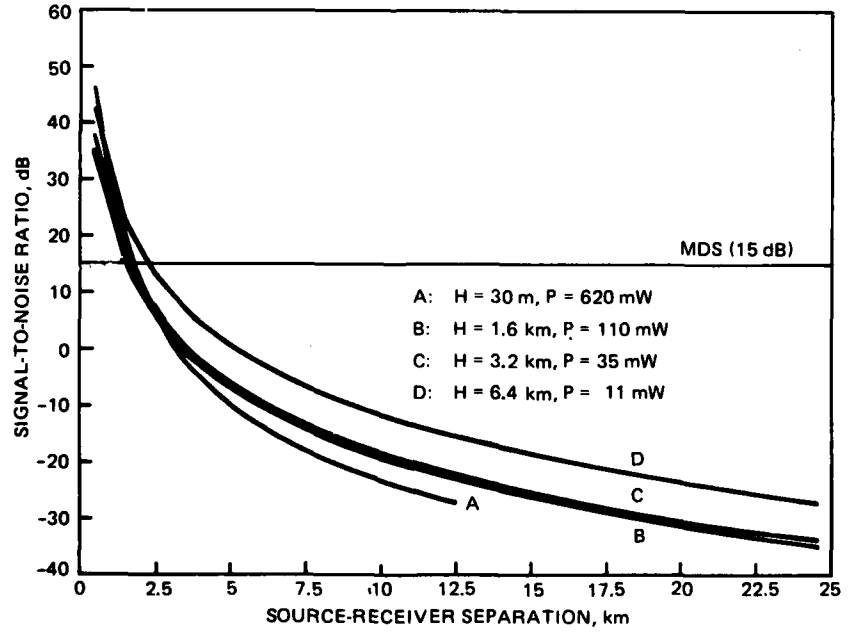

Figure 44. SNR vs range for a P-3 to P-3 communication link. Receiver angular orientation (150°, 0°).

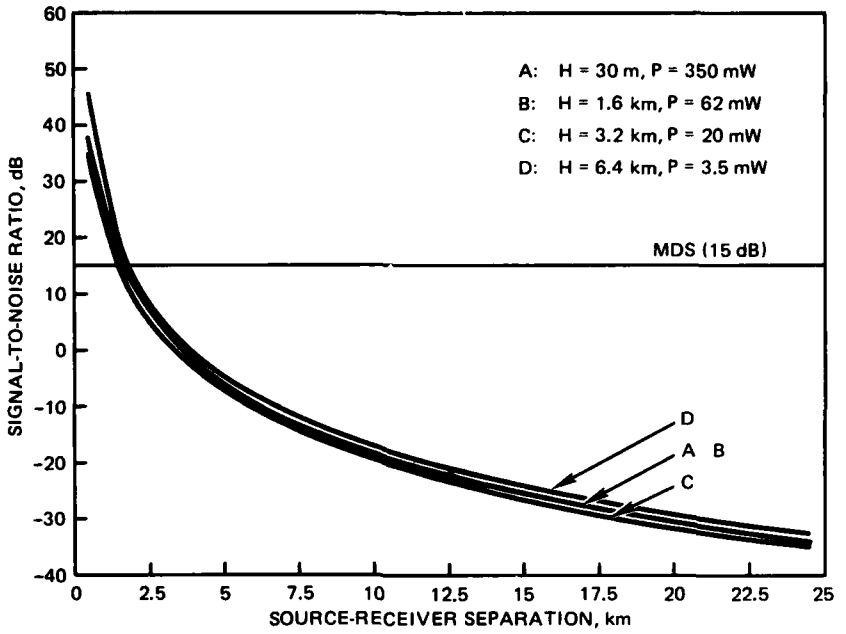

Figure 45. SNR vs range for a P-3 to P-3 communication link. Receiver angular orientation (135°, 0°).

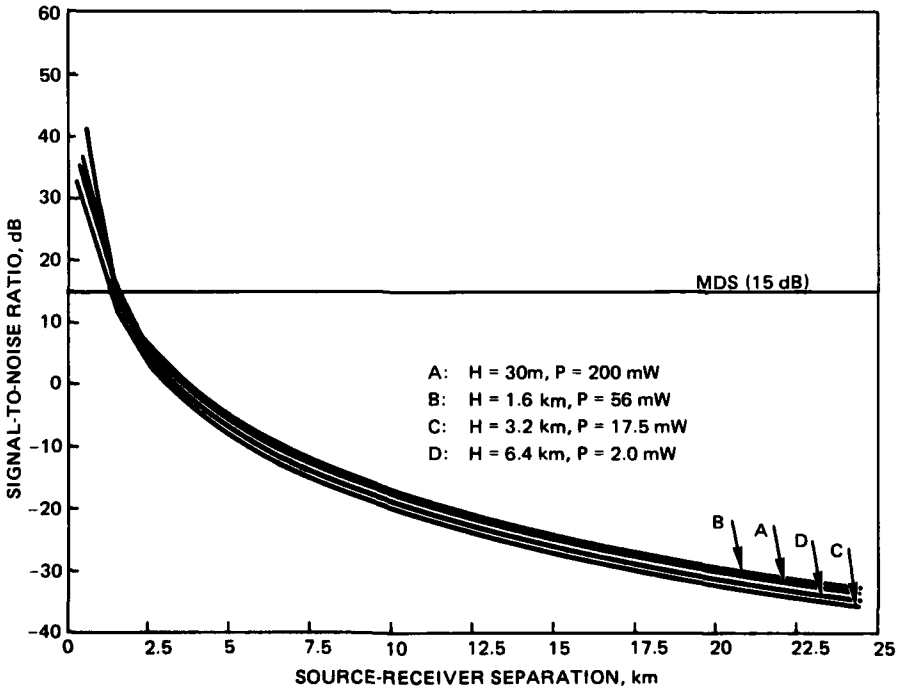

Figure 46. SNR vs range for a P-3 to P-3 communication link. Receiver angular orientation (120°, 0°).

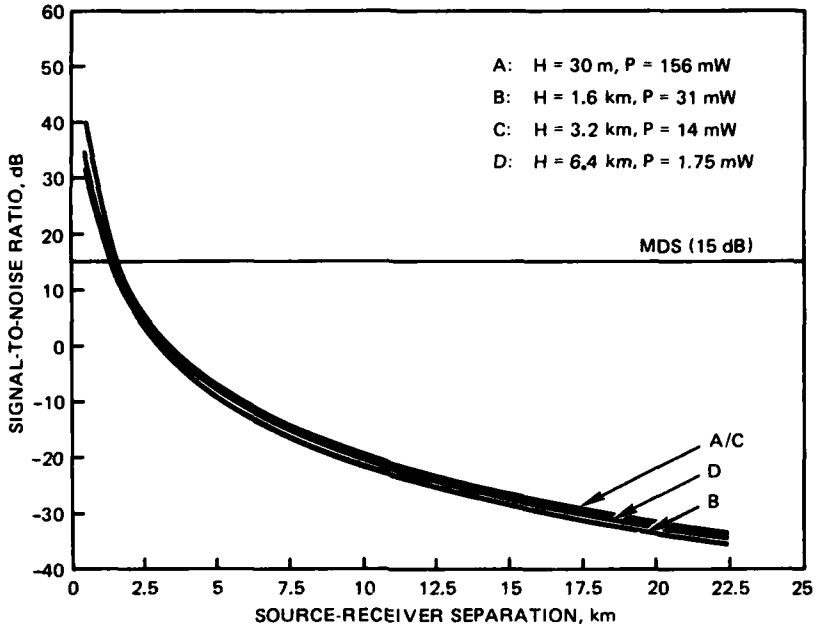

Figure 47. SNR vs range for a P-3 to P-3 communication link. Receiver angular orientation (90°, 0°).

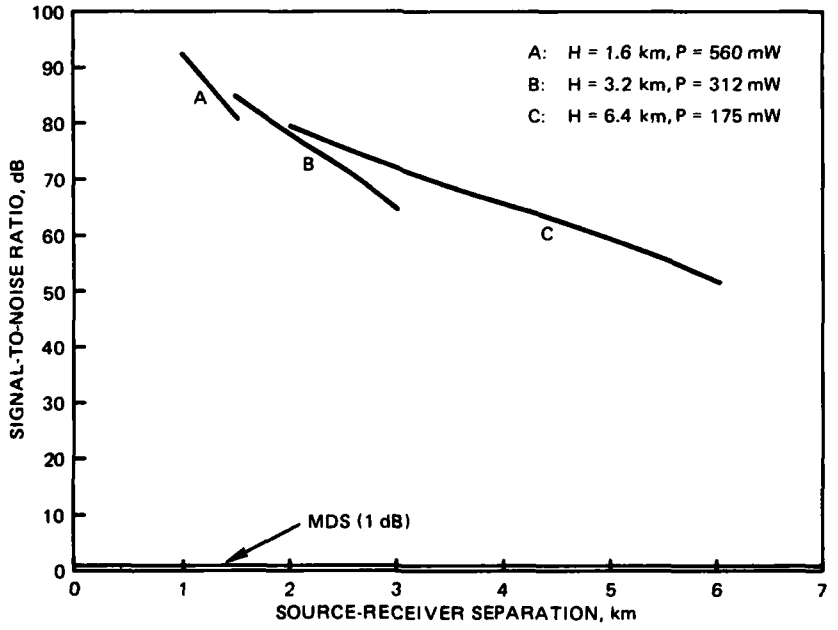

Figure 48. SNR vs range for a P-3 to enemy interception link. Receiver angular orientation (90°, 180°).

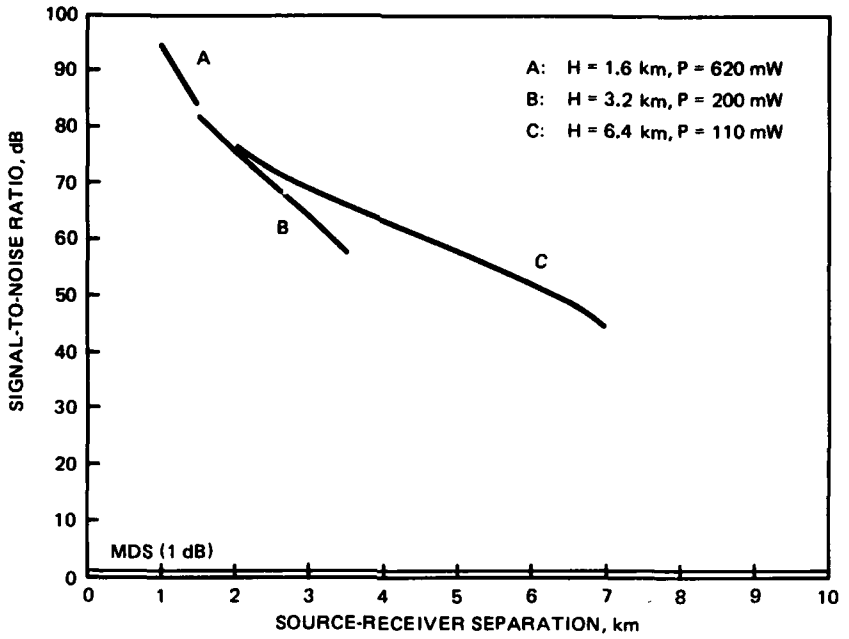

Figure 49. SNR vs range for a P-3 to enemy interception link. Receiver angular orientation (120°, 180°).

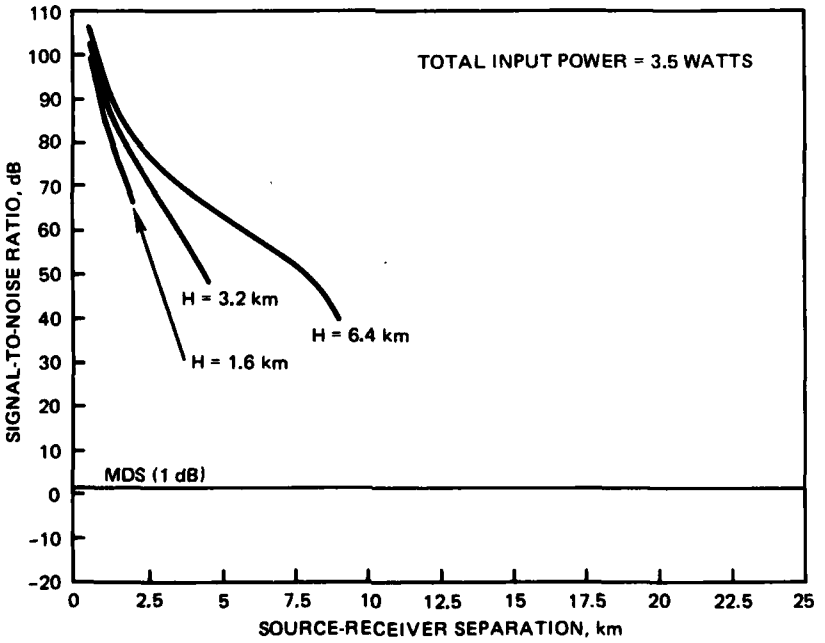

Figure 50. SNR vs range for a P-3 to enemy interception link. Receiver angular orientation (135°, 180°).

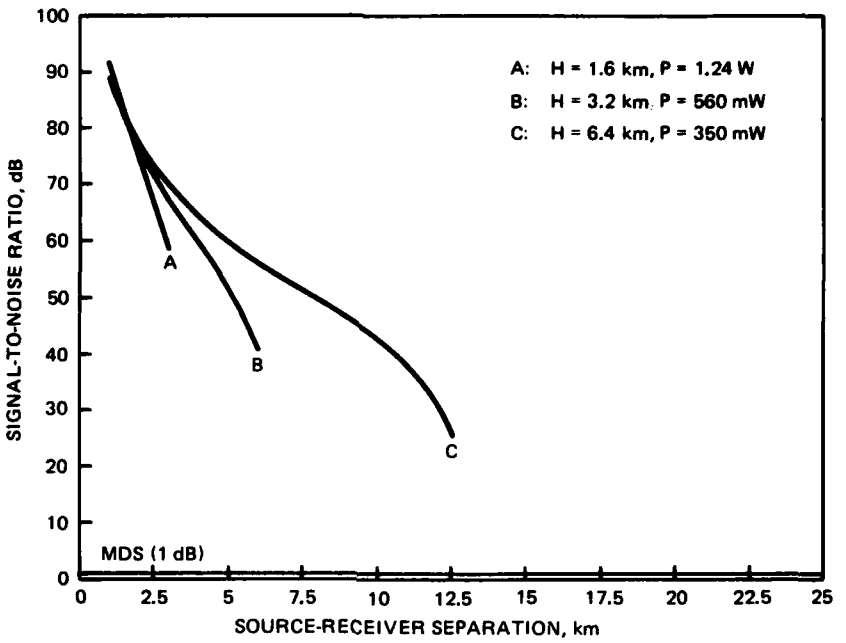

Figure 51. SNR vs range for a P-3 to enemy interception link. Receiver angular orientation (150°, 180°).

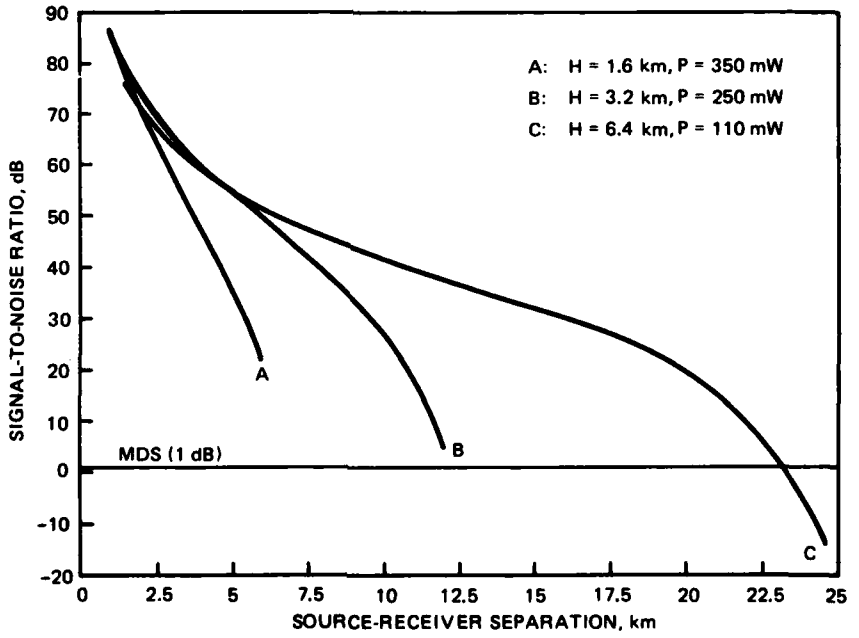

Figure 52. SNR vs range for a P-3 to enemy interception link. Receiver angular orientation (165°, 180°).

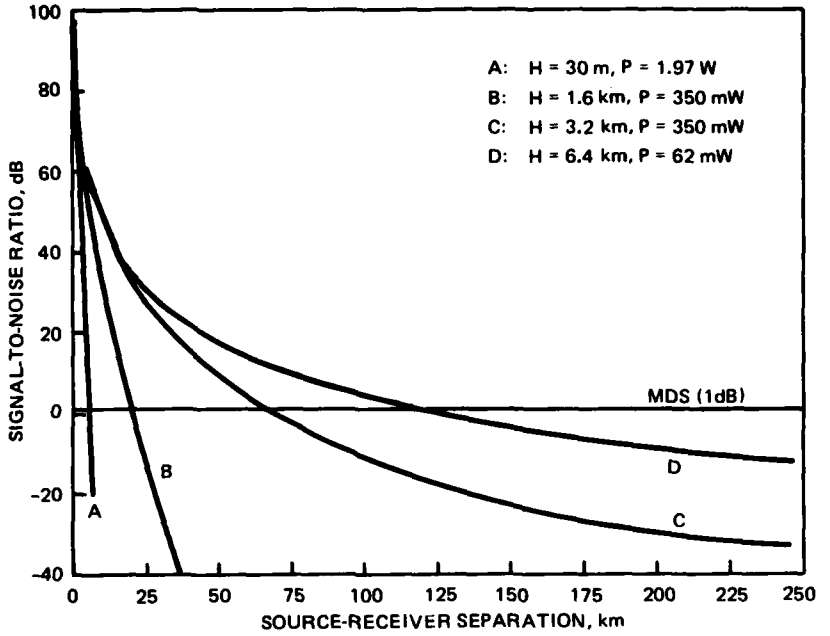

Figure 53. SNR vs range for a P-3 to enemy interception link. Receiver angular orientation (180°, 0°).

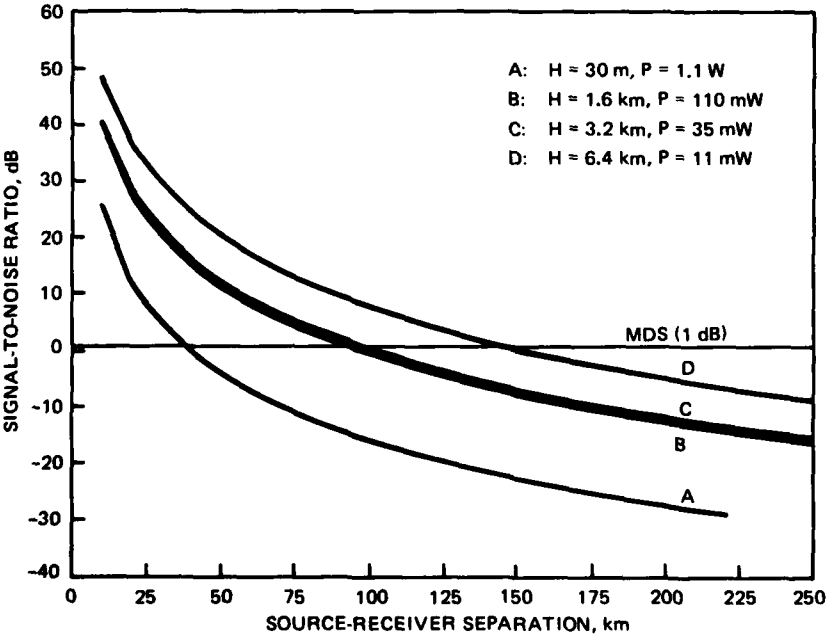

Figure 54. SNR vs range for a P-3 to enemy interception link. Receiver angular orientation (165°, 0°).

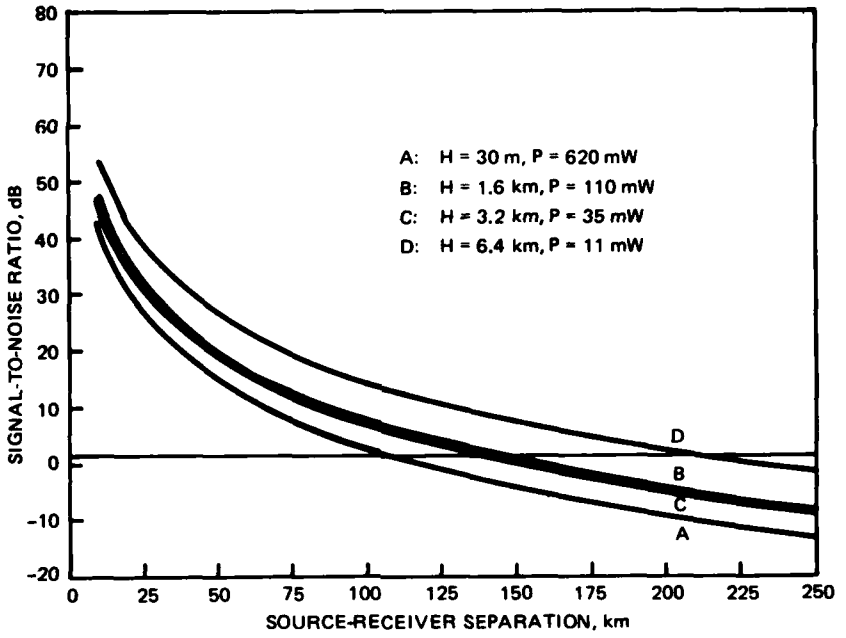

Figure 55. SNR vs range for a P-3 to enemy interception link. Receiver angular orientation (150°, 0°).

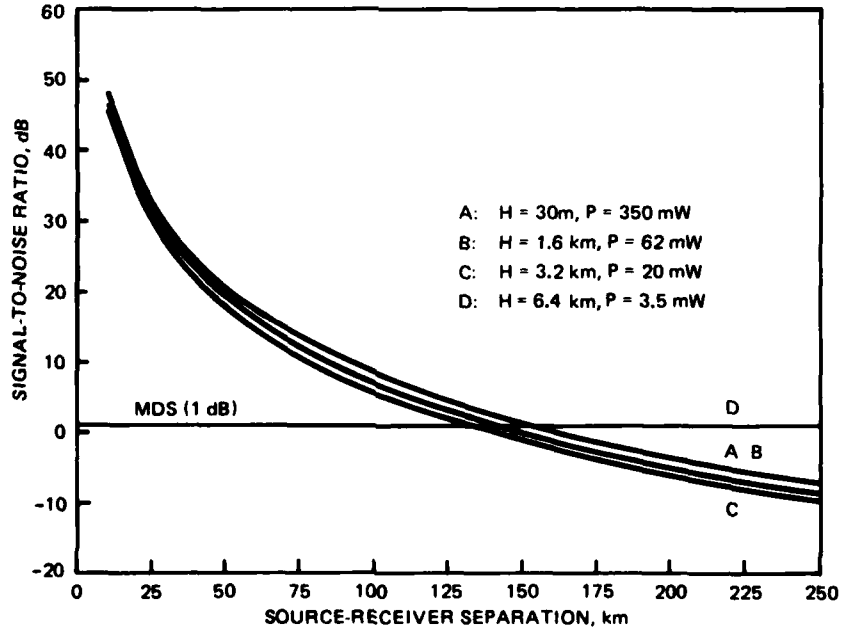

Figure 56. SNR vs range for a P-3 to enemy interception link. Receiver angular orientation (135°, 0°).

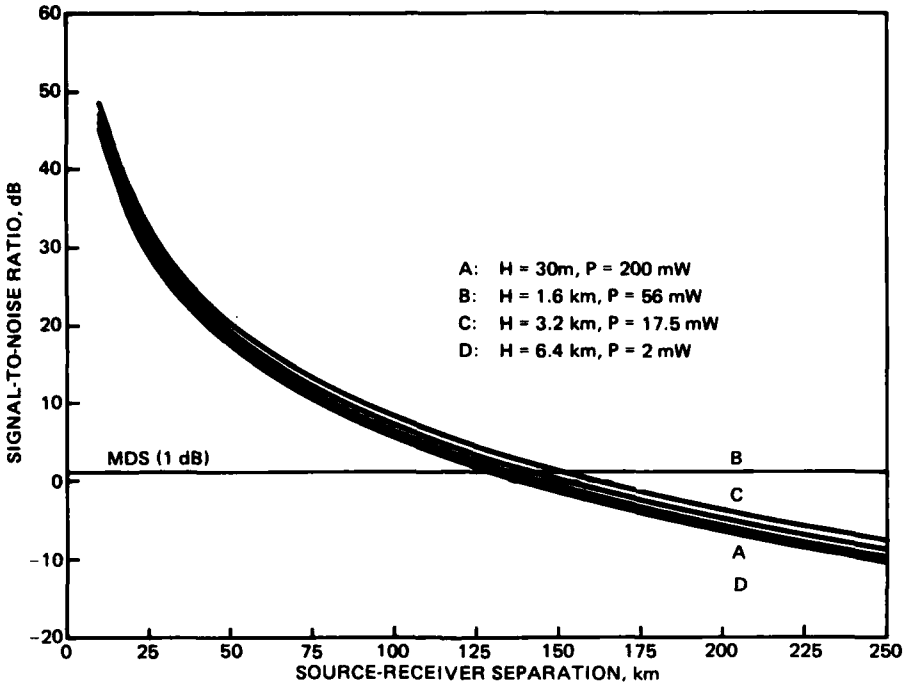

Figure 57. SNR vs range for a P-3 to enemy interception link. Receiver angular orientation (120°, 0°).

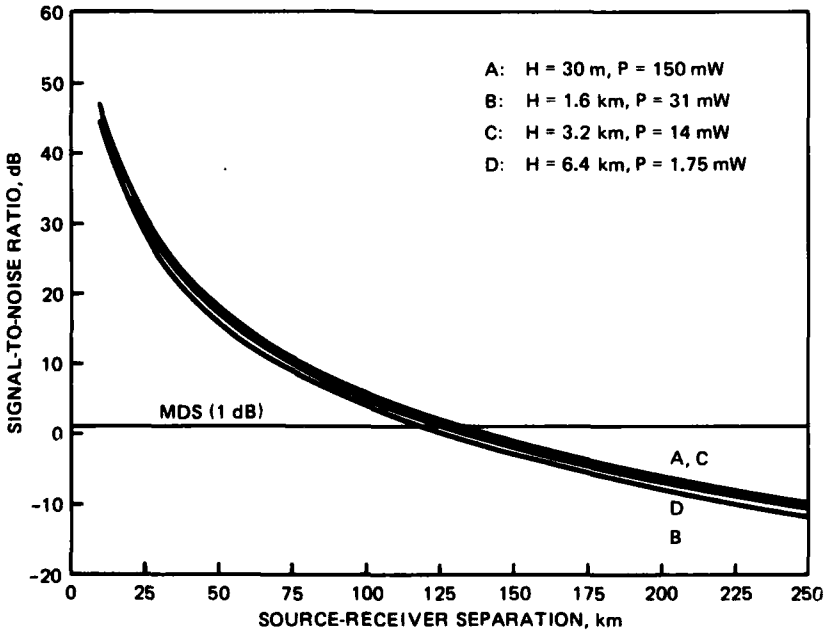

Figure 58. SNR vs range for a P-3 to enemy interception link. Receiver angular orientation (90°, 0°).

6 COMPARISON, SUMMARY, AND RECOMMENDATIONS

COMPARISON OF INTERCEPTABILITY

As stated in section 1, the objective of this study was to address the trade-off between millimetre-wave and electro-optical communication systems designed for covert hand-over between two P-3 surveillance aircraft. The hand-over is assumed to occur in a maritime environment and within a corridor running 0.03 to 6.4 km in altitude. The major comparison criterion is the system covertness, and this was defined in section 2 to be the energy detectability of a 1.5 km communication link by an interceptor under his most ideal conditions. The benchmark of the study is the present Navy communication capability, Link 4.

Table 1 of section 3 indicates that the maximum detectable range of a Link 4 type of system is about 0.8×10^4 to 5.1×10^4 km, assuming a highly directive intercept antenna. Referring to figures 10 through 28 and 36 through 46, we find that both proposed systems possess significantly lower maximum detectable ranges than these, again assuming highly directive intercept antennas. Moreover, it is apparent from these graphs that the 60 GHz millimetre-wave system has a significantly lower maximum detectable range than the electro-optical. In particular, the electro-optical communication system possesses a maximum detectable range* on the order of 30 times that of the proposed 60 GHz system, regardless of link orientation with few exceptions. The exceptions occur in situations in which the earth intersects the link path projector. However, the magnitude of this difference can be attributed more to the chosen system design than to the superiority of one technology over the other. Let us discuss this point in a little more detail.

Table 9 is a comparison of some of the characteristic differences between the millimetre-wave and the near-infrared systems described in sections 4 and 5, respectively. The first difference that we note is the type of operation mode used during communication: thermal-noise-limited operation for the millimetre-wave system and background-limited operation for the optical system. In general, the use of a wide-field-of view receiver will keep the system noise level high and link-orientation dependent, relative to the thermal-noise-limited system. Unfortunately for the near-infrared approach, there is really not

*It should be noted that for the interceptor, the narrow field of view will cause many of the scattered photons to be lost to the received signal. The attenuation rate under this condition would be 9.23 dB/km at sea level instead of the assumed 7.3 dB/km rate at sea level. However, since we assumed the most ideal conditions for the interceptor, we assumed no additional loss due to decreased FOV.

Table 9. Characteristic differences between the proposed millimetre-wave and near-infrared communication systems.

Characteristic	Value	
	mm	IR
System operation mode	Thermal-noise-limited	Background-noise-limited
Source divergence	5°	23°

that much that one can do about this if one wants to use a GaAs emitting diode/reflector similar to the one described in section 5.

The second characteristic difference, on the other hand, is quite a different story. It would be legitimate to decrease the optical source divergence angle to 5° and not expect any operational degradation. Therefore, with just this difference, assuming the same receiver FOV and transmitter power as before, the maximum detectable range will decrease from 30 times that of the 60 GHz system to just 6.5 times. If one were also to lower the transmitter power and receiver field of view (and thus the background noise power), the maximum detectable range of both proposed systems would be comparable. That is, they would have comparable maximum detectable ranges for source divergence angles and receiver fields of view equal to 5°. This should come as no great surprise; it was very pointedly stated in section 4 that directive antennas are more desirable for covertness. But the use of directive antennas increases system complexity and requires a closer tolerance on link alignment. One might then ask whether the added complexity actually constitutes a "sacrifice" in practice. On the basis of limited discussions with COMPATWINGPAC personnel (see section 1), we think not. Depending on specific fleet and operational requirements, hand-over might be carried out with a lower maximum detectable range and less "omnidirectionality" by means of a very simple system that eliminates any tracking requirement: fixed-wing systems would be used and rendezvousing aircraft would be restricted to parallel flight paths within an established cone of angular orientations about their wing axes. In particular, a fixed-wing system whose transmit/receive cone angle lies between 5° and 23° and whose separation range for hand-over is between 1 and 1.5 km appears, at least on the surface, to be not too restrictive a configuration for the P-3 to P-3 SWAP procedure. This configuration would also restrict intercept platforms to only other surveillance aircraft, based on the results of sections 4 and 5.

As noted in section 4, the interceptor must scan both spatially and in frequency for the transmitter under nonideal conditions. Since the near-infrared's subcarrier can lie anywhere between dc and 300 kHz, the problem of frequency scan is totally analogous for both systems. However, optical interceptors with this capability are still in their development infancy, and they would, furthermore, be forced to work in a high ambient background environment. Thus, an enemy would be forced to divert a significant amount of money towards a sophisticated optical interceptor development. On the other hand, both millimetre-wave and microwave interceptors with this capability are probably available for field installation, if not already installed, due to the maturity of both technologies. Thus, an electro-optical approach may hold a slight edge. A more detailed discussion concerning the general intercept problem for all three technologies can be found in appendix G.

Before this discussion is left, something should be said about system construction and installation costs. Since both systems are new to the aircraft, their installation costs should be fairly equivalent. Construction cost for the near-infrared system should be in the vicinity of $10k–11k, whereas a millimetre-wave system runs only about $4k–5k. It should be noted that the optical system has the potential to drop in price to the $7k–8k region within the next few years. In any event, millimetre-wave technology holds the edge in this respect.

SUMMARY

We have shown that under the most ideal interception conditions, both millimetre-wave and electro-optical communication systems have the potential to provide a significantly better covertness capability in P-3 to P-3 hand-over than the present uhf capability

utilized in the fleet. Furthermore, both systems have comparable performance levels under identical source divergence and receiver field-of-view conditions.

RECOMMENDATIONS

1. Incorporate the analytical models developed in this study with the graphical comparison techniques described in appendix G; extend the total intercept/communication analysis to more detailed fleet operational scenarios.

2. Extend the above analysis to the total probability-of-intercept problem.

3. Investigate the feasibility of hybrid millimetre-wave/electro-optical communications for increased performance and atmospheric channel availability.

7 REFERENCES

1. NRL Memorandum Report 2873, Fundamentals of Covert Communications, by PJ Crepeau, July 1974.
2. NOSC Technical Note NELC TN 2722, Detection of Covert Signals, by RA Dillard, 27 June 1974. (TNs are informal documents intended chiefly for internal use.)
3. Naval Electronic Systems Command paper, Covert Communications Notes (on work performed by NOSC Tactical Command Control Division).
4. BR Hatcher, Probability of Intercept and Intercept Time, Watson-Johnson Company Tech-note, vol 3 no 3, May/June 1976.
5. CA Robinson, Jr, Computer Enhances P-3C Effectiveness, Aviation Week and Space Technology, p 34–35, 15 November 1976.
6. CA Robinson, Jr, S-3A Strengthens Carriers' ASW Role, Aviation Week and Space Technology, p 30–41, 22 November 1976.
7. HR Reed and CM Russel, UHF Propagation, Boston Technical Publishers, Lexington, Mass, 1964.
8. ITT Handbook for Radio Engineers, chap 29, 1975.
9. M Skolnik, Radar Handbook, McGraw-Hill, New York, chap 24, 1970.
10. NPS 620 L 76103, Shipboard RFI in UHF SATCOM, October 1976.
11. EE Reber, RL Mitchell, CJ Carter, Oxygen Absorption in the Earth's Atmosphere, The Microwave Journal, November 1969.
12. US Dept of Commerce Office of Telecommunications Report OT 73-10, Molecular Attenuation and Phase Dispersion Between 40 and 140 GHz for Path Models from Different Altitudes, by HJ Liebe and WM Welch, May 1973.
13. M Skolnik, Weather Effects on Radar, Radar Handbook, chap 24, McGraw-Hill, 1970.
14. NOSC Technical Note NELC TN 1809, Precipitation Losses at Millimeter Wavelengths, by JW Carson, February 1971.
15. US Army Ballistic Research Laboratories Memo Report 2710, A Review of Atmospheric Transmission Information in the Optical and Microwave Spectral Regions, by AR Downs, December 1976.
16. Signal Corps Contract Report DA-36-039-SC-723351, Effects of Atmospheric Water Vapor on Near-Infrared Transmission at Sea Level, by RM Langer, JRM Bege Co, Arlington, Mass, May 1957.
17. PW Kruse, LD McGlauchlin, and RB McQuistan, Elements of Infrared Technology: Generation, Transmission, and Detection, John Wiley, New York, 1962.
18. F Amoroso and JA Kivett, Simplified MSK Signaling Technique, IEEE Transactions on Communications, p 435–441, April 1977.
19. RD Anderson and ME Hyde, Underwater Optical Communication Receivers, Paper presented at the SPIE meeting held in San Diego, Calif, 22–26 August 1977.

20. WK Pratt, Laser Communication Systems, John Wiley, New York, 1969.

21. M Ross, Laser Receivers: Devices, Techniques, Systems, John Wiley, New York, 1966.

22. WC Wells, G Gal, and MW Munn, Aerosol Distributions in Maritime Air and Predicted Scattering Coefficients in the Infrared, Applied Optics, vol 16 no 3, p 654–659, 1977.

23. EA Barnhardt and JL Street, A Method for Predicting Atmospheric Aerosol Scattering Coefficients in the Infrared, Applied Optics, vol 9 no 6, p 1337–1344, June 1970.

24. HS Stewart and RF Hopfield, Atmospheric Effects, Applied Optics and Optical Engineering, R Kingslake, Ed, vol 1, p 131–140, Academic Press, New York, 1965.

APPENDIX A
ELECTROMAGNETIC SYSTEM ANALYSIS

The purpose of this appendix is to provide a concise introductory treatment of some of the more important quantities and equations common to both radio and optical systems analysis. The topics include antenna fundamentals, brightness, radiance, flux density, thermal and blackbody radiation, and effects of the antenna pattern on observation.

ANTENNA FUNDAMENTALS

An antenna may be defined as the region of transition between a free-space wave and a guided wave, or vice versa, depending on whether one has a receiving or transmitting system in mind. The precise description of this transition is usually specified in terms of one of the following parameters: antenna gain, power gain, directive gain, or directivity. These quantities can then in turn be used to generate other important antenna characteristics such as effective aperture and main-beam solid angle. It is the intent of this part to review these important parameters and to establish the relationship with other key antenna characteristics.

The power radiated per unit area in a given direction relative to the source is described by its associated Poynting vector $\underset{\sim}{S}$. If we assume both the electric and magnetic fields to be orthogonal in a plane normal to the radius vector and related by the equation $|\underset{\sim}{E}| = Z\,|\underset{\sim}{H}|$ in the far field, then the power flow per unit area is given by

$$S = |\underset{\sim}{E} \times \underset{\sim}{H}^*| = E^2/Z \ (\text{in W/m}^2) \ ,$$

where

$E = E(\theta,\varphi) \equiv$ electric field pattern in the far field

$Z \equiv$ intrinsic impedance of the transmission medium.

Referring to figure A1, noting that there are R^2 square metres of surface area per unit solid angle (or steradian), we define the radiation intensity, $P(\theta,\varphi)$, to be the power per unit solid angle in the (θ,φ)-direction and thus equal to

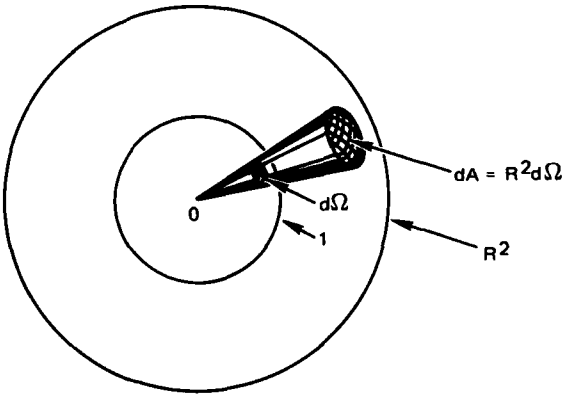

Figure A1. Radiation pattern.

$$P(\theta,\varphi) = R^2 S$$

$$= \frac{R^2 E^2(\theta,\varphi)}{Z} \text{ (in W/sr)} .$$

It should be noted that $P(\theta,\varphi)$ is independent of R. The total power radiated is then

$$P_{TR} = \iint_{4\pi} P(\theta,\varphi)\, d\Omega ,$$

with 4π being the total enclosed solid angle and $d\Omega$ equal to $\sin\theta\, d\theta\, d\varphi$. Therefore, the average power radiated per unit solid angle is defined to be

$$P_{AVG} = P_{TR}/4\pi .$$

This quantity represents the radiation intensity which would be produced by an isotropic radiator generating the same total power P_{TR}.

The directive gain in a given direction, denoted by $D(\theta,\varphi)$ is defined as the ratio of the radiation intensity in that direction to the average radiated power. That is,

$$D(\theta,\varphi) = P(\theta,\varphi) \Big/ P_{AVG}$$

$$= 4\pi\, P(\theta,\varphi) \Big/ \iint_{4\pi} P(\theta,\varphi)\, d\Omega .$$

The directivity, D^*, of an antenna is just its maximum directive gain, or

$$D^* = 4\pi\, P(\theta,\varphi)_{max} \Big/ \iint_{4\pi} P(\theta,\varphi)\, d\Omega .$$

If the total input power P_T is used in the above expressions instead of P_{TR}, the result is a power gain rather than directive gain. The power gain g_p is thus defined as

$$g_p = \frac{4\pi\, P(\theta,\varphi)}{P_T}$$

where

$$P_T = P_{TR} + P_{TL} ,$$

P_{TL} being the ohmic losses in the device incurred within the frequency band of interest. It is fairly evident that

$$g_p/D = \frac{P_{TR}}{P_{TR} + P_{TL}}$$

is a measure of the efficiency of the antenna. When g_p is approximately equal to D, one can refer to either one of these quantities as just the antenna gain of the system.

Although the above definitions were developed under the assumption of a transmitting antenna, the same analysis can be performed for a receiving system. This fact is a direct

consequence of the reciprocity theorem. However, one should remember that the gain of any receiving antenna assumes proper impedance matching and appropriate polarization of the incoming fields.

A term which has special significance for a receiving system is its effective aperture, or alternatively, effective area. It is generally defined to be given by

$$A_e = \frac{\lambda^2}{4\pi} g_p$$

where λ denotes the incident radiation's wavelength. For a lossless system, the expression reduces to

$$A_e = \frac{\lambda^2}{4\pi} D \ .$$

In some situations, it is often advantageous to describe the antenna system in terms of its effective subtended solid angle. Let us define a new parameter $\Phi(\theta,\varphi)$ given by

$$\Phi(\theta,\varphi) = P(\theta,\varphi)\, Z/R^2$$

$$= E^2(\theta,\varphi) \ .$$

$\Phi(\theta,\varphi)$ is generally referred to as the antenna power pattern. If we now perform a quasi-normalization by dividing by its maximum, then we can write

$$\Phi_n(\theta,\varphi) = \frac{\Phi(\theta,\varphi)}{\Phi(\theta,\varphi)_{max}}$$

$$= \frac{P(\theta,\varphi)}{P(\theta,\varphi)_{max}}$$

as the normalized antenna power pattern. Therefore we define the beam solid angle to be

$$\Omega_A = \iint_{4\pi} \Phi_n(\theta,\varphi)\, d\Omega \ \ (\text{in rad}^2) \ .$$

Ω_A is the angle through which all the power from the antenna would flow if the radiation intensity were constant over this angle and equal to its maximum value. In general, the antenna power pattern is composed of a number of lobes; a typical pattern is suggested in figure A2. Figure A2 is an example of a symmetric pattern. This is not necessarily true in practice and one is forced to rely on several pattern drawings for a complete picture of the power pattern. The lobe with the largest maximum is called the main lobe, while the smaller lobes comprise the minor, or side and back, lobes. Thus, if one restricts the angular integration to just the main lobe, then the above integral yields the main-beam solid angle. That is, we have

$$\Omega_M = \iint_{\text{main-lobe}} \Phi_n(\theta,\varphi)\, d\Omega \ \ (\text{in rad}^2) \ ,$$

with $\Omega_M \equiv$ main-beam solid angle. The minor lobe solid angle is hence

$$\Omega_m = \Omega_A - \Omega_M \ .$$

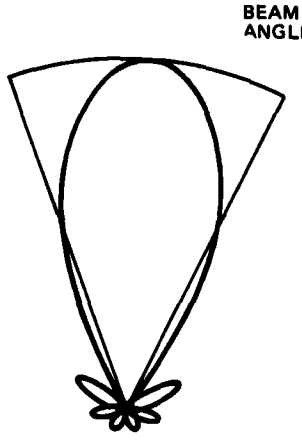

Figure A2. Typical symmetric antenna pattern.

Therefore it is readily apparent that

$$\Omega_A = \frac{4\pi}{D^*}$$

and

$$\Phi_n(\theta,\varphi) = \frac{D(\theta,\varphi)}{D^*} .$$

POWER AND BRIGHTNESS

Suppose that an arbitrary but known electromagnetic source is located a certain fixed distance away from a flat receiving surface of area A. Then the infinitesimal power dP from a solid angle $d\Omega$ of the source incident on an incremental area dA of that surface is given by

$$dP = B \cos\theta \, d\Omega \, dA \, d\nu \ \text{(in W)} ,$$

where

$B \equiv$ brightness of the source at the position of $d\Omega$ (in $W/m^2 \cdot sr \cdot Hz$)

$d\Omega = \sin\theta \, d\theta \, d\varphi$

$dA \equiv$ infinitesimal area of surface (in m^2)

$d\nu \equiv$ infinitesimal element of bandwidth (in Hz) .

The basic geometry for this situation is shown in figure A3. The quantity B is called the surface brightness, or simply brightness of the source. It is a fundamental parameter to both optical and radio communications and is a measure of the power radiated per unit area per unit solid angle per unit bandwidth. The element of bandwidth $d\nu$ is assumed to lie between a parameter frequency ν and $\nu + \Delta\nu$. It will be shown shortly that the brightness is directly proportional to the source's specific intensity or spectral radiance.

The total power contained in bandwidth $\Delta\nu$ about $\nu + \Delta\nu/2$ is given by

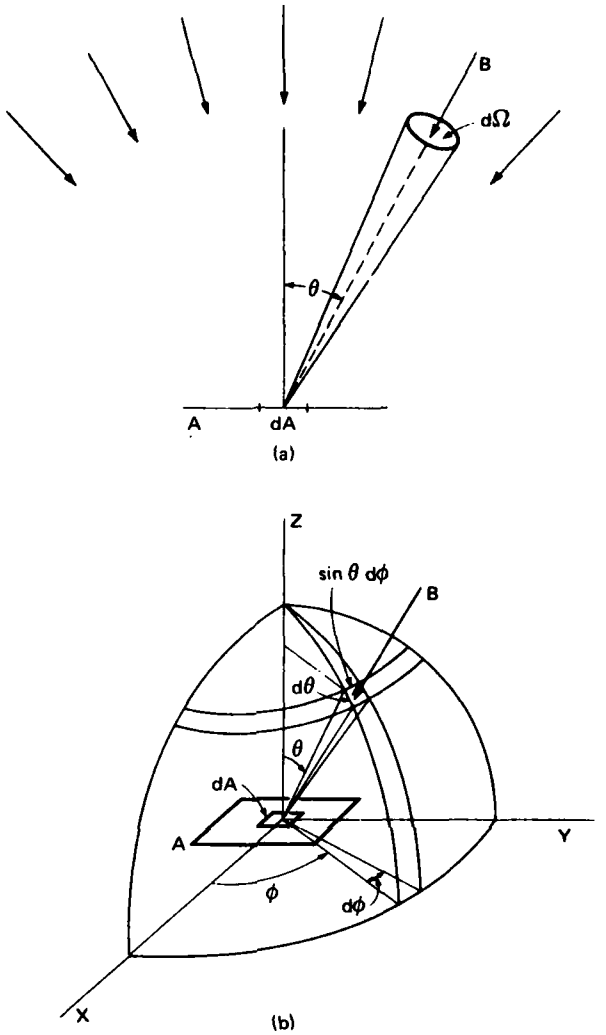

Figure A3. Basic geometry for radiation of brightness B incident on a flat area shown in elevation at (a) and in perspective view at (b).

$$P = \int dP = \int_A \int_\Omega \int_\nu^{\nu+\Delta\nu} B \cos\theta \, dA \, d\Omega \, d\nu \ ,$$

where Ω denotes the total solid angle subtended by the source relative to the receiving surface.

In general the brightness is a function of both the direction of incidence and of frequency. The variance of brightness with frequency is called the brightness spectrum. The integration of B over a bandwidth $\Delta\nu$ extending from a frequency ν to a frequency $\nu + \Delta\nu$ gives the total brightness B', ie

$$B' = \int_{\nu}^{\nu+\Delta\nu} B \, d\nu \ (\text{in W/m}^2 \cdot \text{sr}) \ ,$$

with

$B' \equiv$ total brightness

$B \equiv$ brightness of the source .

If the integration is extended over the radio spectrum, the total radio brightness spectrum is obtained. Likewise, if the integration is over the optical spectrum, the total optical brightness is obtained.

Introducing the total brightness, we can rewrite the total power as

$$P = \int_A \int_\Omega B' \cos\theta \, d\Omega \, dA \ .$$

In many situations, the power per unit bandwidth is more pertinent than the power contained in an arbitrary bandwidth $\Delta\nu$. This power per unit bandwidth is often called the spectral power, since its variation with frequency constitutes the power spectrum. Its units are watts per hertz. Thus, introducing the concept of spectral power allows us to write

$$dP_\nu \equiv \frac{dP}{d\nu} = B \cos\theta \, d\Omega \, dA$$

where dP_ν represents the spectral power, or infinitesimal power, per unit bandwidth. This implies that

$$P_\nu = \int_A \int_\Omega B \cos\theta \, d\Omega \, dA$$

is the total spectral power.

Another term commonly used in system analysis is the flux density, F. It is defined as

$$F = \int_{\Omega_S} B(\theta,\varphi) \, d\Omega \ ,$$

where Ω_S is the solid angle subtended by the source. In optics, this quantity is known as the source irradiance.

RADIANCE AND BRIGHTNESS

Consider an elemental area dA which radiates power into an elemental solid angle $d\Omega$ as shown in figure A4. The spectral radiance, or specific intensity, N_ν, of this source is defined to be the power per unit bandwidth radiated into $d\Omega$ from a projected area of source $dA \cdot \cos\theta$. The spectral radiant emittance (or spectral irradiance), W_ν, is the power per unit bandwidth radiated into the total solid angle subtended by the source from an

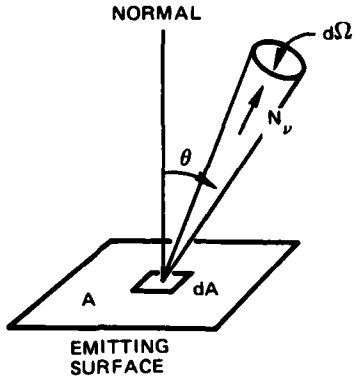

Figure A4. Emitting surface of radiance N_ν.

actual area dA. In the above situation, the total solid angle subtended is a hemisphere. In general, the source need not be a flat emitter for the analysis to be valid; the geometry was chosen for simplicity. Thus, the above two quantities are related by

$$W_\nu = \iint_{\text{hemisphere}} N_\nu(\theta,\varphi) \cos\theta \, d\Omega \ .$$

The spectral power from a source element dA flowing out through a solid angle $d\Omega$ is hence

$$dP_\nu = N_\nu \cos\theta \, d\Omega \, dA$$

It is readily apparent that the above is just the transmitting version of the analysis given under the previous discussion, Power and Brightness. Therefore, under the above conditions, it follows that

$$B \cos\theta \, d\Omega \, dA = -N_\nu \cos\theta \, d\Omega \, dA$$

or

$$B = -N_\nu \ .$$

THERMAL AND BLACKBODY RADIATION

All objects at temperatures above absolute zero radiate energy in the form of electromagnetic waves. This process is commonly known as thermal radiation. It was shown by Kirchoff that a good absorber of electromagnetic energy is also a good radiator. A perfect absorber, hence a perfect radiator, is called a blackbody. In particular, a blackbody absorbs all radiation falling upon it, regardless of the frequency, and concurrently produces an emission spectrum determined solely by its surface temperature. Such a body is an idealization, since no known materials possess those properties. However, one finds in practice that many real sources behave like blackbody radiators fixed at a certain temperature for limited portions of the electromagnetic spectrum. For example, the spectral irradiance of the sun is very similar to that of a 5900 K blackbody in the 0.1 to 10 μm wavelength region. Hence,

knowledge of blackbody radiation can oftentimes make communication system design and analysis quite straightforward.

The brightness of a blackbody is given by Planck's radiation law. This law, formulated by Max Planck in 1901, states that the brightness of a blackbody radiator at a temperature T and frequency ν is given by the equation

$$B_b = \frac{2h\nu^3}{c^2} \frac{1}{\exp\left(\frac{h\nu}{kT}\right) - 1} ,$$

where

$B_b \equiv$ blackbody brightness (in $W/m^2 \cdot sr \cdot Hz$)

$h \equiv$ Planck's constant

$= 6.63 \times 10^{-34}$ J · s

$\nu \equiv$ frequency (Hz)

$c \equiv$ speed of light

$\cong 3 \times 10^8$ m/s

$k \equiv$ Boltzmann's constant

$= 1.38 \times 10^{-23}$ J/K

$T \equiv$ temperature, K.

It is interesting to note that the peak brightness shifts to higher frequency as the temperature increases.

It is often convenient to express the above radiation law in terms of unit wavelength instead of unit bandwidth. Recall that

$$\nu\lambda \equiv c .$$

This implies that

$$d\nu = \frac{-c}{\lambda^2} d\lambda .$$

Therefore if we define $B_\lambda = /B\, d\nu/$ to be the power per unit area per unit solid angle per unit wavelength, then we have

$$B_\lambda = \frac{2h\,c^2}{\lambda^5} \frac{1}{\exp\left(\frac{hc}{kT\lambda}\right) - 1} ,$$

where $\lambda \equiv$ wavelength in meters.

The Wien displacement law describes the maximum or peak wavelength for blackbody radiation. It can be shown that

$$\lambda_m T = 0.0051 \text{ m/K} ,$$

for brightness in terms of unit frequency, and

$$\lambda_m T = 0.0029 \text{ m/K} ,$$

for brightness in terms of unit wavelength, with λ_m being the peak wavelength.

Recall from previous work that the total brightness is defined as the total integrated brightness over the frequency band of interest. If we assume $\Delta\nu$ to extend over all frequencies, then

$$B'_\Omega = \frac{2h}{c^2} \int_0^\infty \frac{\nu^3 \, d\nu}{\exp\left(\frac{h\nu}{kT}\right) - 1}$$

$$= \sigma T^4 ,$$

where

$$B'_\Omega = \iint_{\Omega_s} B'(\theta,\varphi) \, d\Omega$$

$\equiv$ total spectral emittance

$\sigma = 5.67 \times 10^{-8}$ (in $W/m^2 \cdot K^4$)

This is known as the Stefan-Boltzmann equation.

Before ending this discussion of thermal and blackbody radiation, we should note two important approximate expressions for the brightness of a blackbody for $kT \gg h\nu$ and $kT \ll h\nu$. The first expression, developed before Planck's general law, is called the Rayleigh-Jeans law and is valid for $h\nu \ll kT$. It has the form

$$B \approx \frac{2kT}{\lambda^2} .$$

The second expression, valid for $h\nu \gg kT$, is known as the Wien radiation law and is given by

$$B \approx \frac{2h\nu^3}{c^2} e^{-h\nu/kT} .$$

THE EFFECT OF THE ANTENNA PATTERN ON OBSERVATION

In the discussion of power and brightness, we assumed the receiving surface to be a flat, horizontal square of area and subject to a $\cos\theta$ angular response. Unfortunately, most receiving antennas are not that way and usually possess a more complicated angular response. In particular, they are generally described in terms of an effective area A_e and an antenna power pattern $\Phi_n(\theta,\varphi)$. (See the discussion on antenna fundamentals.) We will now examine the effects of the antenna on electromagnetic source observations.

Consider the receiving situation suggested in figure A5. The area A in figure A3(b) is replaced by a flat horizontal surface of a receiving antenna with the power pattern of the antenna directed towards the zenith ($\theta = 0°$). The pertinent area is now the effective area A_e of the antenna. For an antenna of large aperture, A_e is always less than its physical aperture. Therefore, if we assume that Φ_n is uniform across the aperture, the spectral power, P_ν, from a solid angle, Ω, of the source is given by

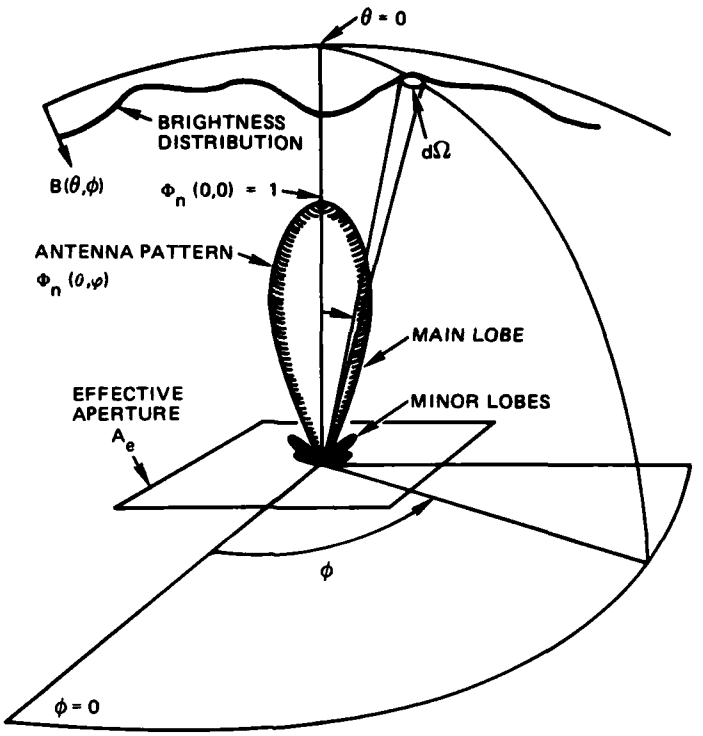

Figure A5. Relation of antenna pattern to incoming brightness distribution.

$$P_\nu = \frac{1}{2} A_e \iint_\Omega B(\theta,\varphi)\, \Phi_n(\theta,\varphi)\, d\Omega \ ,$$

with

$P_\nu \equiv$ received spectral power

$A_e \equiv$ effective aperture

$B \equiv$ brightness distribution of the source

$\Phi_n \equiv$ normalized power pattern.

The 1/2 factor comes from the fact that the source is assumed to be incoherent and unpolarized, and antennas respond to only one polarization.* In general, the polarization properties of the source will alter this value to some new one lying between 0 and 1.

If the brightness $B(\theta,\varphi)$ is constant and the minor lobe response is negligible, the above reduces to

$$P_\nu \approx \frac{1}{2} A_e B_c \Omega_M \ ,$$

*This is not true for direct detection optical receivers. In that particular case, the 1/2 factor would be omitted.

where

$$B_c = B(\theta,\varphi)$$

$$\equiv \text{a constant}$$

$$\Omega_A \equiv \text{beam solid angle (see section on antenna fundamentals)}$$

$$= \iint_{\text{main lobe}} \Phi_n(\theta,\varphi)\, d\Omega \ .$$

In the general case, where the brightness varies with both position and frequency, the total power contained in bandwidth $\Delta\nu$ centered about $\nu + \Delta\nu/2$ is given by

$$P = \frac{1}{2} A_e \int_{\nu}^{\nu+\Delta\nu} \iint_{\Omega} B(\theta,\varphi)\, \Phi_n(\theta,\varphi)\, d\Omega\, d\nu \ .$$

Previously we defined the flux density of a source as the integral of its brightness over the total solid angle it subtends. That is,

$$F = \iint_{\Omega_s} B(\theta,\varphi)\, d\Omega$$

is the total flux density of the source. When that source is observed with an antenna of power pattern $\Phi_n(\theta,\varphi)$, the observed flux density

$$F_0 = \iint_{\Omega_s} B(\theta,\varphi)\, \Phi_n(\theta,\varphi)\, d\Omega \ .$$

It is apparent that the antenna will generally, but not in all cases, lower the observed flux density from its true value and hence will decrease the total sensitivity of the system.

APPENDIX B
PROBABILITY OF INTERCEPT AND COVERTNESS

As seen from the text of this report, transmitted signals are never completely undetectable. Does this mean that there is no such thing as covert communications? If one bases his definition upon absolute undetectability, then the answer is yes, there is not. If, however, one's definition is grounded on reducing the likelihood (probability) of interception, then it can be said that a system is more covert than another. Actually, interception must occur first then successful detection must be achieved before an interceptor is "aware" of the transmitter. Interception relies on the coincidence of many events, whereas detection is a function merely of signal level, noise level, and threshold of detection. Thus, even though the interceptor's receiver may be sensitive enough, without the necessary coincidence of events, the signal does not reach the receiver and the interceptor is unaware of the transmitter.

By way of example, assume that the interceptor's antenna rotates at a rate of S degrees per second. The period of revolution is T_1, where $T_1 = 360°/S_1$. Let ϕ = the 3 dB beamwidth of the antenna. The time that the antenna's main beam points in a given direction is $\tau_1 = \phi_1/S_1$. Further assume that the intercept receiver sweeps in frequency over a band, D, in time, T_2, and has a receiver passband, B. The time that a particular frequency remains in the passband is $\tau_2 = BT_2/D$. We can plot these "window functions" as shown in figure B1. In order for intercept to occur, these window functions must overlap. If $t_1 = t_2$, in the relationship shown in the figure, an intercept will occur immediately, otherwise there

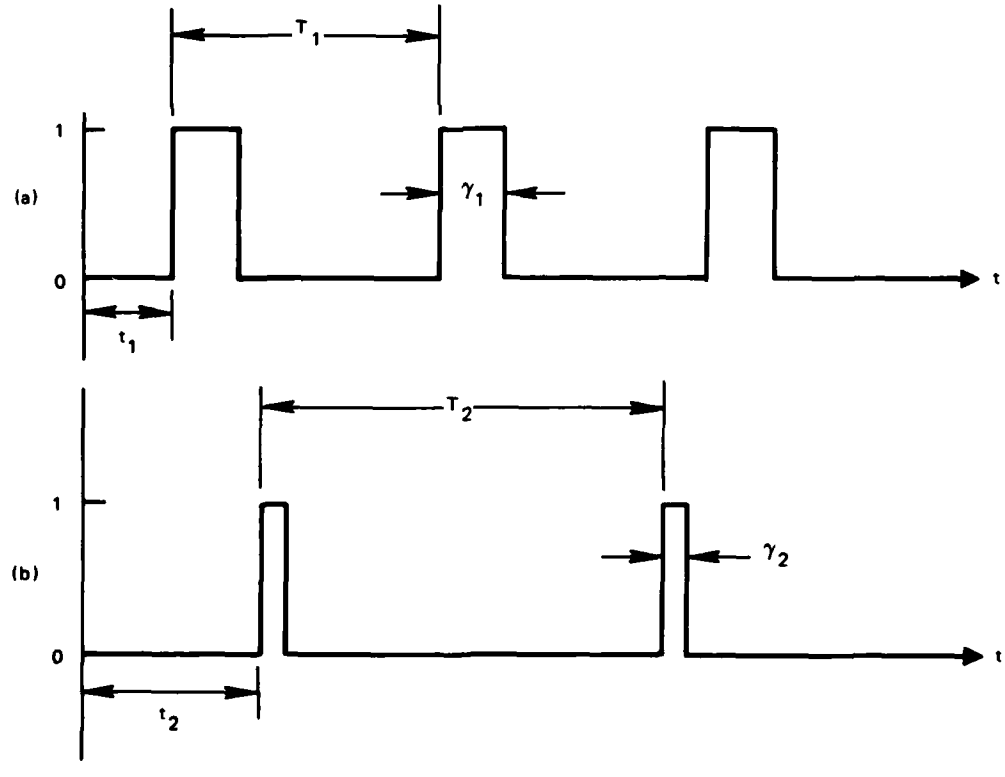

Figure B1. Reception as a function of beamwidth of intercept receiver rotating antenna (a) and passband of frequency-scanning intercept receiver (b).

will be partial overlap within the first period of the more rapidly occurring function (t_1), provided $-\tau_1 \leq t_1 - t_2 \leq \tau_2$. Since the starting times of t_1 and t_2 actually are independent of each other, the probability of coincidence during the first period of the window function with the shorter period, can be found. Table B-1 gives this probability.* The probability that at least one intercept will occur in time, T, is as follows:

$$P_{12} = 1 - (1 - P_{12}(T_1))^{T/T_1} \qquad (\text{if } T_1 \leq T_2)$$

$$P_{12} = 1 - (1 - P_{12}(T_2))^{T/T_2} \qquad (\text{if } T_2 \leq T_1)$$

Note that the probability approaches unity when $T \gg T_1$ or T_2, implying a relatively long observation time. This probability can be made smaller by reducing the length of communication transmission time.

If the transmissions are made in short bursts irregularly spaced in time, the intercept requires the overlap of three window functions. The overall probability of intercept then would be expressed as

$$P(T) = P_{12}(T) \times P_{13}(T) \times P_{23}(T) \ .$$

The more complex the situation (ie, the more events that are required to be coincident), the larger the number of conditional probabilities needed to compute the overall intercept probability.

*BR Hatcher, Probability of Intercept and Intercept Time, Watson-Johnson Company Tech-note, vol 3, no 3, May/June 1976

Table B1. Probability of reception coincidence by a rotating directional antenna feeding a frequency-scanning receiver.

$T_1 \leq T_2$			$T_2 \leq T_1$		
$P_{12}(T_1)$			$P_{12}(T_2)$		
For	$\tau_2 \leq T_1$	$T_1 \leq \tau_2$	$\tau_1 \leq T_2$	$T_2 \leq \tau_1$	For
$\tau_1 \leq T_2 - T_1$	$\frac{1}{T_2}\left[\tau_1 + \tau_2\left(1 - \frac{\tau_2}{2T_1}\right)\right]$	$\frac{1}{T_2}\left(\tau_1 + \frac{T_1}{2}\right)$	$\frac{1}{T_1}\left[\tau_2 + \tau_1\left(1 - \frac{\tau_1}{2T_2}\right)\right.$	$\frac{1}{T_1}\left(\tau_2 + \frac{T_2}{2}\right)$	$\tau_2 \leq T_1 - T_2$
$T_2 - T_1 \leq \tau_1$	$1 \equiv \frac{(T_1-\tau_2)^2 + (T_2-\tau_1)^2}{2T_1T_2}$	$1 \equiv \frac{(T_2-\tau_1)^2}{2T_1T_2}$	$1 \equiv \frac{(T_2-\tau_1)^2 + (T_1-\tau_2)^2}{2T_1T_2}$	$1 \equiv \frac{(T_1-\tau_2)^2}{2T_1T_2}$	$T_1 - T_2 \leq \tau_2$
Probability of intercept for a time T $P_{12}(T) = 1 - [1 - P_{12}(T_1)]^{T/T_1}$			Probability of intercept for a time T $P_{12}(T) = 1 - [1 - P_{12}(T_2)]^{T/T_2}$		
Observation time for a desired probability of intercept (P_{oi}) $T_o = T_1 \cdot \frac{\ln(1 - P_{oi})}{\ln[1 - P_{12}(T_1)]}$			Observation time for a desired probability of intercept (P_{oi}) $T_o = T_2 \cdot \frac{\ln(1 - P_{oi})}{\ln[1 - P_{12}(T_2)]}$		

The question then becomes "What parameters of the system design and operation are available that can be suitably altered to reduce the probability of intercept?" PJ Crepeau* has expressed the interceptor's postdetection S/N ratio as

$$(S/N)_i = \left(\frac{G_{ti}}{G_t}\right)\left(\frac{G_{ri}}{G_r}\right)\left(\frac{L_i}{L}\right)\left(\frac{T}{T_i}\right) q\, M\, r_d \frac{E_b}{n_o}\sqrt{\frac{t}{w}}$$

for the transmitter, intended-receiver/intercept-receiver scenario, where

t = integration time

w = rcvr noise bandwidth

$q = \frac{w}{B_s}$ for $w < B_s$

$= 1$ for $w \geq B_s$

For the interceptor, $(S/N)_i$ must exceed some a priori threshold value. Nevertheless, some of the parameters to be exploited become apparent in that equation. G_{ti}/G_t is the ratio of transmitter antenna gain in the direction of the interceptor to that in the direction of the intended receiver. This implies that a high-gain, narrow beamwidth transmitting antenna should be used. Likewise the intended receiving antenna should be as narrow beamed as is practical. L_i/L is the interceptor/intended-receiver atmospheric loss ratio which can be successfully employed around 60 GHz as indicated by the range curves. Assuming intended and interceptor receiver noise temperatures are equal, $T/T_i = 1$. M is the required communication system margin for assuring successful communication. The quantity $M\, r_d\, E_b/n_o$ is the carrier/noise ratio and should be kept as low as possible. Spread spectrum techniques achieve this. Finally $q\sqrt{t/w} = \sqrt{tw}/B_s$ if signal bandwidth, B_s, is greater than the intercept receiver's predetection bandwidth and $q\sqrt{t/w} = \sqrt{t/w}$ if $w > B_s$. If the message can be transmitted in a very short burst, advantage can be taken of the fact that the signal bandwidth $B_s > w$ and that the time of transmission is less than t, the interceptor's integration time. Finally, the carrier frequency could be "hopped" in time so that the intercepting receiver will lose the signal for significant portions of time.

In summary, a communication system is covert if its operating parameters have been adjusted so that it has low probability of intercept and has signal time-bandwidth characteristics which are incompatible with those of the intercept receiver.

*NRL Memorandum Report 2873, Fundamentals of Covert Communications, by PJ Crepeau, July 1974

APPENDIX C
ANTENNA TEMPERATURE AND THE MINIMUM DETECTABLE SIGNAL

Communication systems which use only a limited amount of power to send messages great distances must contend at the receiving terminal with the problem of detecting (demodulating) a weak signal in the midst of random noise. The receiver must distinguish the information-bearing electromagnetic signals from random noise and from each other as effectively as possible. Thus the basic problem in any system design is a receiver problem: to differentiate signal from noise and to process the composite so as to convey the intended information to the output with the lowest possible probability of error. In appendix A we discussed signal propagation and the reception of electromagnetic energy by a receiver from an arbitrary electromagnetic source. In this appendix, we discuss how to determine whether the signal power at the receiver is of sufficient magnitude to allow signal detection and demodulation.

It was shown in 1928 by Nyquist[C1] that the noise power associated with a particular antenna is given by

$$N_A = k T_A B \tag{C1}$$

where

$N_A \equiv$ Noise power at the antenna, in watts

$k \equiv$ Boltzmann's Constant

$= 1.38 \times 10^{-23}$ J/K

$T_A \equiv$ Antenna temperature, in K

$B \equiv$ electrical bandwidth of antenna, in Hz

The receiver also contributes noise to the detection process due to the thermal noise in the receiver components, shot noise in the tubes or transistors, etc. In addition, losses in the transmission line between the antenna and receiver will add noise. Thus, the total system noise power referenced to the antenna terminals is equal to

$$\begin{aligned} N_{sys} &= N_A + N_R \\ &= k (T_A + T_R) B \\ &= k T_{sys} B \end{aligned} \tag{C2}$$

where

$N_R \equiv$ receiver noise power referenced to the antenna terminals, watts

$T_{sys} = T_A + T_R$

$\equiv$ total system temperature referenced to the antenna terminals, in K

$T_R =$ receiver noise temperature (including the transmission line), in K

[C1] H Nyquist, Thermal Agitation of Electrical Charge in Conductors, Phys Rev 32, p 110, 1928

Let us now relate the above quantities to a system's minimum detectable signal.

The minimum antenna temperature which a receiver can detect (demodulate) is limited by fluctuations in the receiver's output produced by the statistical nature of the input noise waveform. Equation (C2) tells us that the noise is proportional to the system temperature. In theory,[C2] the system noise power can be reduced to any desired extent by increasing the postdetection integration time, increasing the predetection bandwidth, and/or taking the average of one or more observations. In practice, however, one cannot perform the above improvement without suffering certain consequences; eg, by increasing the integration, one reduces the system's data rate. Therefore, one must take into account system requirements and operational scenarios in a preliminary system design before trying to make trade-offs.

It can be shown, using classical detection theory,[C2] that the minimum detectable temperature (signal) is equal to the rms noise temperature of the system. In particular, we can write

$$\Delta T_{min} \approx \frac{R_s T_{sys}}{\sqrt{B\tau n}} \qquad \text{(C3)}$$

where

$R_s \equiv$ sensitivity constant of the receiver

$\tau \equiv$ postdetection integration time, in s

$B \equiv$ predetection bandwidth, Hz

$n \equiv$ number of observations averaged.

The constant R_s depends on the type of receiver used, its mode of operation, and the format of the data conveyed. The accompanying table gives a representative sample of R_s for several types of receivers.

Receiver type	R_s
Total power	1
Correlation interferometer	0.71
Correlation receiver	1.41
Dicke receiver	2.–2.83*

*Depends on type of input signal modulation/demodulation

It is sometimes desirable to describe the effective noise of a system in terms of a noise figure. The noise figure of a receiver, denoted by NF, is defined as the ratio of actual noise power output when the receiver is connected at its input to a source at standard temperature $T_0 = 290$ K to the noise power output that would exist for the same input if the system were noiseless. Hence, we have

$$NF = 1 + T_R/T_0 \ , \qquad \text{(C4)}$$

[C2] CW Helstrom, Statistical Theory of Signal Detection, Pergamon Press, New York, 1968.

where T_R is the effective noise temperature of the receiving network. Conversely, if NF is known, T_R can be found.

The antenna temperature, T_A, is the sum of all the temperature contributions from external sources, either man-made or naturally occurring. Figure C1 depicts typical sky noise temperatures which might occur at the receiving aperture as a function of frequency and antenna direction.[C3–C7] In general, T_A is totally dependent on the operational scenario of the system.

[C3] CCIR, Documents of the Xth Plenary Assembly, Geneva, 1963, Rept 322, ITU, Geneva, 1964.

[C4] DL Croom, Naturally Occurring Thermal Radiation in the Range 1–10 Gc/s, Proc Inst Elec Engrs, London, vol 111, p 967–980, May 1964.

[C5] RH Dicke, PJE Peebles, PG Roll, and DT Wilkinson, Cosmic Black-body Radiation, Astrophys J, vol 142, p 414–419, 1965.

[C6] JD Kraus and HC Ko, Celestial Radio Radiation, Ohio State Univ Radio Obs Rept 7, May 1957.

[C7] AA Penzias and RW Wilson, A Measurement of Excess Antenna Temperature at 4080 Mc/s, Astrophys J, vol 142, p 419–421, 1965.

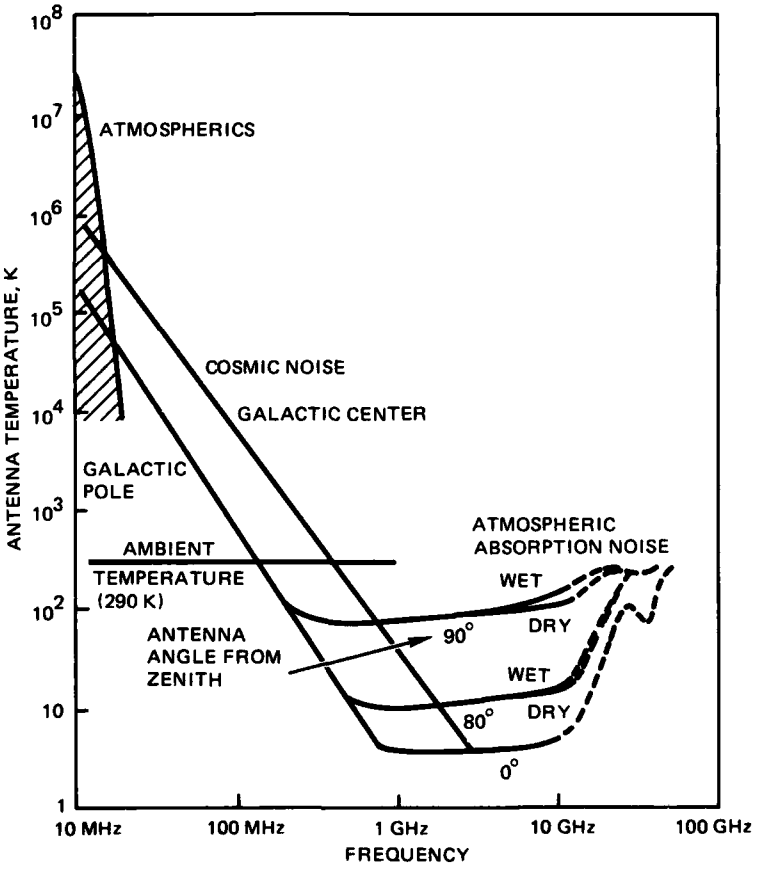

Figure C1. Antenna sky noise temperature as a function of frequency and antenna angle. A beam angle (HPBW) of less than a few degrees and 100 percent beam efficiency are assumed.

REFERENCES

C1. H Nyquist, Thermal Agitation of Electrical Charge in Conductors, Phys Rev 32, p 110, 1928.

C2. CW Helstrom, Statistical Theory of Signal Detection, Pergamon Press, New York, 1968.

C3. CCIR, Documents of the Xth Plenary Assembly, Geneva, 1963, Rept 322, ITU, Geneva, 1964.

C4. DL Croom, Naturally Occurring Thermal Radiation in the Range 1–10 Gc/s, Proc Inst Elec Engrs, London, vol 111, p 967–980, May 1964.

C5. RH Dicke, PJE Peebles, PG Roll, and DT Wilkinson, Cosmic Black-body Radiation, Astrophys J, vol 142, p 414–419, 1965.

C6. JD Kraus and HC Ko, Celestial Radio Radiation, Ohio State Univ Radio Obs Rept 7. May 1957.

C7. AA Penzias and RW Wilson, A Measurement of Excess Antenna Temperature at 4080 Mc/s, Astrophys J, vol 142, p 419–421, 1965.

APPENDIX D
MILLIMETRE-WAVE RANGE CURVE CALCULATIONS

The geometry describing the slant range from the transmitting aircraft to either the intended receiving aircraft or an intercept receiving platform is depicted in figure D1. Using R as the independent quantity, it can be shown that

$$h = \left[R^2 + (r_o + h_o)^2 - 2R(r_o + h_o)\cos(\theta_o + 90°)\right]^{1/2} - r_o$$

By starting at $h = h_o$ and incrementing R in suitable steps, ϵR, h_i can be determined for each step. Using the appropriate function for $\alpha(h_i)$, the values for α from $h = h_o$ to h_{max} can be calculated. Using a mean value of α over the step, ϵR, and summing α over all steps yields an approximation to the total O_2 attenuation over the slant path, R. The total attenuation, L_t, is thus

$$L_t = \sum_{h=h_o}^{h_{max}} \alpha(h_i)\,\epsilon R \ \text{(in dB)} \ .$$

The computer program used to generate the curves when the transmitter "looks up" stops calculating when the total attenuation exceeds 200 dB or when h_{max} reaches 160 km (satellite altitude). For the "down look," the program stops when the signal reaches sea level.

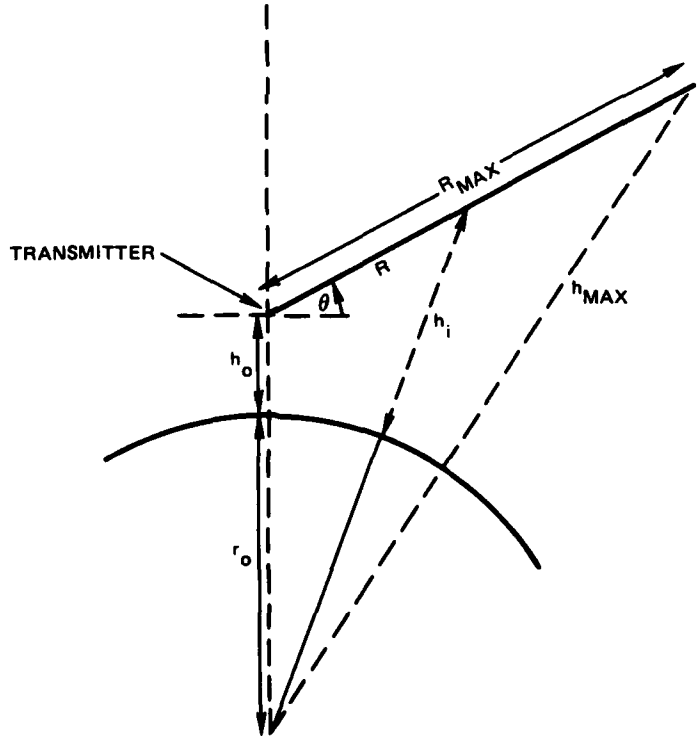

Figure D1. Geometry describing slant range from transmitting aircraft to either the intended receiving aircraft or an intercept receiving platform.

APPENDIX E
BACKGROUND NOISE FROM AN ABSORPTIVE, SCATTERING ATMOSPHERE IN THE PRESENCE OF A TOTALLY ABSORBING SURFACE

In designing any optical communication system, one must contend with two distinct types of naturally-occurring noise: thermal (or Johnson) noise and quantum (or shot) noise.[E1] Thermal noise originates within amplifiers and load resistors and internal to the detection process; quantum noise has components both internal and external in origin.[E2] Internally generated quantum noise is caused by electronic dark current. The quantum noise produced by external sources is proportional to the received power and thus can be traced back to the information signal and the background radiation environment in which the system operates. In the near-IR to UV situation, one does not usually refer to noise temperatures but refers rather to noise photons in a description of noise. It is the purpose of this appendix to develop an analytical model for describing the background noise generated by direct and indirect solar irradiance.

In a given optical receiver, the output current produced can generally be considered as four independent parts: the thermal noise current I_{Th}, the dark current I_D, the current I_S produced by the detected information-carrying signal P_S, and the current I_B derived from the undesired background power, P_B, that reaches the detection surface. It can be shown[E3,E4] that the photoelectron output can be modelled as a Poisson statistical process possessing a rate parameter proportional to the detected optical power. In particular, the average detected current is given by

$$I = \frac{\eta q}{h\gamma} P \ ,$$

where

$I \equiv$ average detected current (in A)

$P \equiv$ average detected optical power (in W)

$\eta = \eta(\nu) \equiv$ detection quantum efficiency

$q \equiv$ electronic charge $= 1.6 \times 10^{-19}$ C

$h \equiv$ Planck's constant $= 6.63 \times 10^{-34}$ J·s

$\gamma \equiv$ frequency of the incident radiation (in Hz).

Thus, the total average detected current

$$I_T = \frac{\eta q}{h\nu} [P_S + P_B] + I_D + I_{Th} \ .$$

The mean-square fluctuation about this average current

$$\Delta I_T^2 = 2q I_T B \ ,$$

[E1] BM Oliver, Thermal and Quantum Noise, Proc IEEE, 53, p 436–454, May 1965

[E2] WK Pratt, Laser Communication Systems, Wiley, New York, 1969

[E3] M Ross, Laser Receivers, Wiley, New York, 1966

[E4] JI Gordon, Optical Properties of Objects and Background, Applied Optics, vol 3 no 5, p 556–562, May 1964

where B denotes the electrical bandwidth of the receiver. Numerical values for I_D and I_{Th} can be obtained from the open literature. Equations for the received signal power P_S can be derived by using the results derived in appendix A. Hence, the remaining portions of this appendix are concerned only with the quantification of the received background power, P_B.

BACKGROUND POWER FROM DIRECT SOLAR ILLUMINATION

Consider a spherical source, eg the sun, of diameter, d_S, which possesses a uniform radiation pattern and a subtended solid angle, Ω_S, less than the receiver's field-of-view solid angle. Let $B(\gamma,\theta,\varphi) = B(\nu)$ denote the source's spectral brightness. Then from appendix A, we know that the total received power within the receiver

$$P_{BS} = \int_{\substack{\text{spectral}\\ \text{range}}} d\nu\, \tau_a(\nu)\, T_\nu \iint_{\substack{\text{entrance}\\ \text{aperture}}} dA \iint_{4\pi} B(\gamma,\theta,\varphi)\, P(\theta,\varphi)\, d\Omega \ ,$$

where

$\tau_a(\nu) \equiv$ atmospheric transmissivity between source and receiver at optical frequency ν.

$T_\nu \equiv$ receiver transmittance.

$dA \equiv$ incremental aperture area

$P(\theta,\varphi) \equiv$ receiver's antenna pattern

$d\Omega \equiv$ incremental solid angle.

If we now assume a simple lens receiver, then we have

$$P_{BS} \approx \int_{\substack{\text{spectral}\\ \text{range}}} d\nu\, \tau_a(\nu)\, T_\nu \iint_{A_{rec}} dA \iint_{\Omega_S} B(\gamma,\theta,\varphi)\, d\Omega \ ,$$

for $\Omega_{FOV} > \Omega_S$. Let R denote the source receiver separation in metres, and assume that $R \gg d_S$. Therefore, under the above conditions, the total background power from direct solar illumination can be written as

$$P_{BS} \simeq \frac{\pi\, d_S^{\,2}}{4R^2}\, A_{rec} \int_{\text{spectral}} d\nu\, \tau_a(\nu)\, T_\nu\, B(\nu)$$

with A_{rec} being the area of the receiver's entrance aperture. In terms of the source's spectral radiant emittance, the total received power can be written

$$P_{BS} \simeq \frac{d_S^{\,2}\, A_{rec}}{4R^2} \int_{\substack{\text{spectral}\\ \text{range}}} d\nu\, \tau_a(\nu)\, T_\nu\, W(\nu) \ ,$$

where $W(\nu)$ represents the spectral radiant emittance of the source. Recall that the subtended solid angle of the source, Ω_S, can be shown to be approximately equal to $\pi d_S^2/4R^2$. Hence,

$$P_{BS} \simeq A_{rec} \int_{\substack{\text{spectral} \\ \text{range}}} d\nu\, \tau_a(\nu)\, T_\nu\, H(\nu) \ ,$$

where $H(\nu)$ is the source's spectral irradiance.

BACKGROUND POWER FROM SCATTERED SOLAR IRRADIANCE

A communication receiver need not be directly pointed at an optical noise source to be susceptible to its presence. The reflection and scattering of optical radiation by background objects and atmospheric constituents within the receiver's field of view (FOV) can adversely affect the system performance. Since we are assumably operating in a totally maritime environment, we limit our discussion to just the background radiation produced by an absorptive, scattering atmosphere.

Consider an elemental volume, dV, located at a point $\underset{\sim}{r}_o$ within the receiver's field of view but not at, or below, the sea surface. Then, by placing the coordinate axes at the receiver (see fig E1), we have

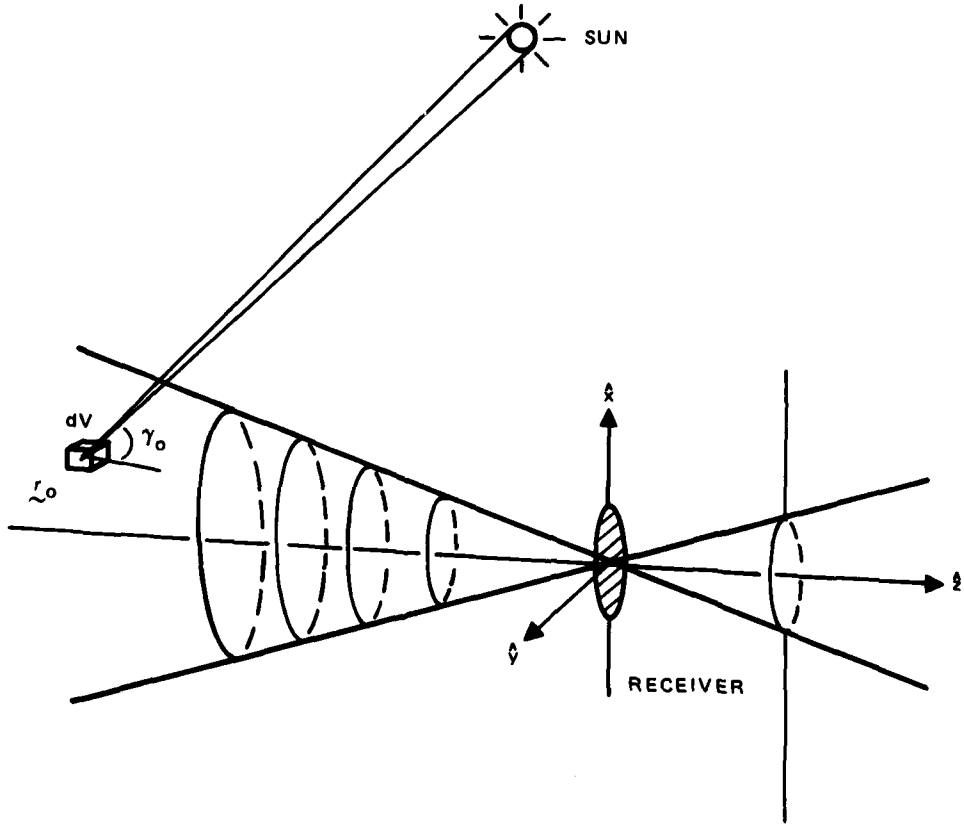

Figure E1. Scattering geometry for background contribution.

$$dV = r_o^2 \sin\theta \, d\theta \, d\varphi \, dr_o$$

The power emitted by this volume can be traced back to two distinct sources: direct solar irradiance scattering and surface-reflected solar irradiance scattering. For a calm-water, infinite depth situation, the directional reflectance is on the order of 20–50%.[E4] Thus, for simplicity, we will assume that near the ocean surface, the total scattered power

$$P_{BSS} = 1.35 \, P_{BSD}$$

where

$P_{BSS} \equiv$ total scattered background power

$P_{BSD} \equiv$ total scattered background power from direct solar radiance in the presence of a totally absorbing surface

Recall that the sun is an isotropic radiator. This implies that the spectral solar irradiance at $\underset{\sim}{r}_o$ is

$$\tau_o(\underset{\sim}{r}_o) H_{\lambda s}$$

where $\tau_o(\underset{\sim}{r}_o)$ is the atmospheric transmissivity to point $\underset{\sim}{r}_o$ and $H_{\lambda s}$ is the unattenuated solar irradiance at wavelength λ. Let γ_o denote the angle between $\underset{\sim}{r}_o$ and the $\underset{\sim}{r}_o$–sun projection vector. Then the power per steradian per unit wavelength interval is equal to

$$\tau_o(\underset{\sim}{r}_o) H_{\lambda s} \beta(\gamma_o, \underset{\sim}{r}_o) \, dV \ .$$

$\beta(\gamma_o, \underset{\sim}{r}_o)$ is the volume scattering function at $\underset{\sim}{r}_o$ and has units of inverse sr·m. The solid angle subtended by the receiver is given by

$$\frac{\pi a^2 \cos\theta}{a^2 + r_o^2} \simeq \frac{A_{rec} \cos\theta}{r_o^2} \ ,$$

where a is the radius of the entrance aperture and A_{rec} its area. Therefore, the power received by dV is equal to

$$T_\lambda(\gamma_o) \tau_o(\underset{\sim}{r}_o) \tau_a(\underset{\sim}{r}_o) H_{\lambda s} A_{rec} \beta(\gamma_o, \underset{\sim}{r}_o) \cos\theta \, d\Omega \, dr_o \ ,$$

where

$\tau_a \equiv$ atmospheric transmissivity between $\underset{\sim}{r}_o$ and the origin

$T_\lambda(\gamma_o) \equiv$ spectral transmittance of the receiver at angle γ_o.

It can easily be shown, by using the law of sines and the fact that $R_s \gg r_o$ for all r_o values of interest (R_s being equal to the distance from the earth to the sun) that

$$\gamma_o \approx \cos^{-1}[\cos\theta_s \cos\theta_o + \sin\theta_s \sin\theta_o \cos(\varphi_o - \varphi_s)]$$

where

$(\theta_s, \varphi_s) \equiv$ angular coordinates of sun

$(\theta_o, \varphi_o) \equiv$ angular coordinates of receiver's look direction within the FOV.

The contributing surface is defined by the intersection of the sea surface and the receiver's FOV cone. Thus the total received power from the $/\underset{\sim}{r}_o/ = r_o$ surface is equal to

$$H_{\lambda s} A_{rec} \, dr_o \int_0^{2\pi} \int_0^{\theta_{FOV}/2} \tau_0(\underset{\sim}{r}_o) \, \tau_a(\underset{\sim}{r}_o) \, T_\lambda(\gamma_o) \, \beta(\gamma_o, \underset{\sim}{r}_o) \, \zeta(\underset{\sim}{r}_o) \cos\theta \, d\Omega \ ,$$

where $\zeta(\underset{\sim}{r}_o)$ is the contributing surface's structure function. $\zeta(\underset{\sim}{r}_o)$ is equal to 1 for no intersection, less than 1 otherwise. The total contribution within the FOV cone is then equal to

$$P_{BSD} \cong A_{rec} H_{\lambda s} \int_0^{r_{max}} \int_0^{2\pi} \int_0^{\theta_{FOV}/2} dr_o \, d\Omega \, \tau_0(\underset{\sim}{r}_o) \, \tau_a(\underset{\sim}{r}_o) \, T_\lambda(r_o) \, \beta(\gamma_o, \underset{\sim}{r}_o) \, \zeta(\underset{\sim}{r}_o)$$

$$\cos\theta \ ,$$

where r_{max} is the maximum distance of integration ($\leqslant \infty$).

REFERENCES

E1. BM Oliver, Thermal and Quantum Noise, Proc IEEE, 53, p 436–454, May 1965.

E2. WK Pratt, Laser Communication Systems, Wiley, New York, 1969.

E3. M Ross, Laser Receivers, Wiley, New York, 1966.

E4. JI Gordon, Optical Properties of Objects and Background, Applied Optics, vol 3 no 5, p 556–562, May 1964.

APPENDIX F
ATMOSPHERIC OPTICAL LOSS MODEL

Figure F1 depicts the assumed source/receiver geometry. Let

$R \equiv$ radius of the "4/3" earth

$= 8393$ km

$R+h_o \equiv$ distance from the center of the earth to the source at $\underset{\sim}{r}_o$

$R+h_R \equiv$ distance from the center of the earth to the receiver

$R+h \equiv$ distance from the center of the earth to the point $\underset{\sim}{p}$.

Referring to the figure, let the coordinate origin be located at the transmitter such that the $\hat{z}$ axis points to the right, $\hat{x}$ points upwards, and $\hat{y}$ points out of the page. Thus, the position of the center of the earth would be given by

$$\underset{\sim}{r}_e = (R + h_R, \pi/2, \pi) \ .$$

Hence, the angle, α, between $\underset{\sim}{r}_o$ and r_e is equal to

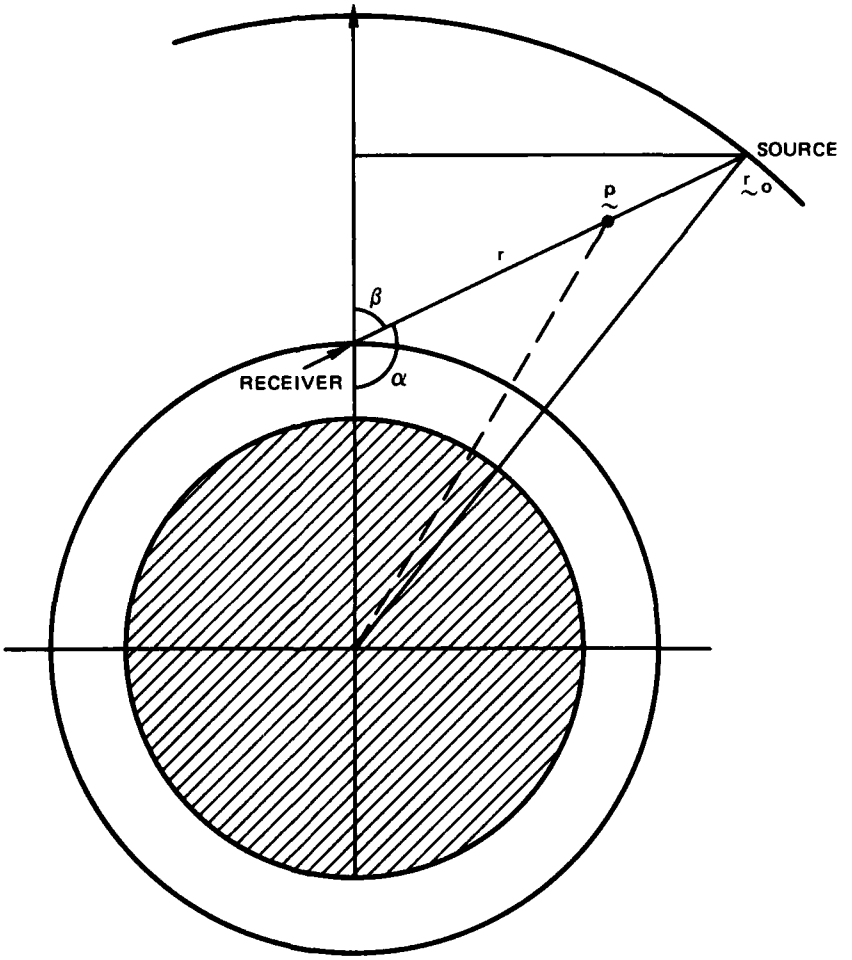

Figure F1. Source/receiver geometry.

$$\cos^{-1}(-\sin\theta_o \cos\varphi_o)$$

where $\underset{\sim}{r}_o = (r_o, \theta_o, \varphi_o)$. This implies that the distance from the surface of the earth to the point $\underset{\sim}{p}$ along the (R+h)-projection is given by

$$h = \sqrt{R' + r^2 + 2R' r \sin\theta_o \cos\varphi_o} - R$$

where $|\underset{\sim}{p}| = r$ and $R' = R + h_R$.

Using classical radiative transfer theory, ie the Lambert-Bouger law, it can be shown that the atmospheric attenuation term, or transmissivity, has the form

$$\tau(\underset{\sim}{r}_o) = \exp\left\{ - \int_0^{r_o} \alpha\,[h(r)]\, dr \right\},$$

where α is the total atmospheric attenuation coefficient. In general, one finds that this coefficient falls off exponentially.[F1] That is,

$$\alpha = A_o \exp\left[- A_1 \left(\sqrt{R'^2 + r^2 + 2R' r \sin\theta_o \cos\varphi_o} - R \right) \right],$$

where A_o, A_1 denote coefficients proportional to inverse meters. Unfortunately, the integration of α over the range does not yield a closed form solution. However, the fact that $R' \gg r_o$ within our range of interest does allow us to approximate α in such a way as to give closed form representations for τ.

CASE I: $R'^2 \gg r_o^2 \gg |2 r_o R' \sin\theta_o \cos\varphi_o|$.

Under this condition, we find that

$$\sqrt{R'^2 + r^2 + 2r R \sin\theta_o \cos\varphi_o} - R \cong h_R + \frac{r^2}{2R'} \left[1 - \sin^2\theta_o \cos^2\varphi_o \right] + r \sin\theta_o \cos\varphi_o .$$

This implies that

$$\int_0^{r_o} \alpha(r)\, dr \approx A_o \sqrt{\frac{\pi R'}{A_1 \left(1 - \sin^2\theta_o \cos^2\varphi_o\right)}} \cdot \exp\left[- \frac{2A_1 R' \cos^2\varphi_o \sin^2\theta_o}{1 - \sin^2\theta_o \cos^2\varphi_o} - A_1 h_R \right] \cdot \left[\operatorname{erf}\left(\sqrt{\frac{A_1 \left(1 - \sin^2\theta_0 \cos^2\varphi_o\right)}{2R'}}\; r_o + \frac{\sqrt{2R' A_1}\, \sin\theta_o \cos\varphi_o}{\sqrt{1 - \sin^2\theta_o \cos^2\varphi_o}} \right) \right.$$

[F1] WC Wells, G Gal, and MW Munn, Aerosol Distributions in Maritime Air and Predicted Scattering Coefficients in the Infrared, Applied Optics, vol 16 no 3, p 654-659, 1977

$$- \text{erf} \left(\frac{\sqrt{2R' A_1 \sin\theta_o \cos\varphi_o}}{\sqrt{1 - \sin^2\theta_o \cos^2\varphi_o}} \right) \quad ,$$

where erf(x) is the error function.

CASE II: $R'^2 \gg /2r_o R' \sin\theta_o \cos\varphi_o / \gg r_o^2$.

Under this condition,

$$\sqrt{R'^2 + r^2 + 2r R' \sin\theta_o \cos\varphi_o} - R \cong h_R + r \cos\varphi_o \sin\theta_o \ .$$

Hence,

$$\int_0^{r_o} \alpha(r)\, dr \cong \frac{A_o \sec\varphi_o \csc\theta_o}{A_1} e^{-A_1 h_R} \left(1 - e^{-A_1 r_o \sin\theta_o \cos\varphi_o}\right) \ .$$

APPENDIX G
A GENERAL DISCUSSION OF THE DETECTABILITY OF MILLIMETRE-WAVE AND ELECTRO-OPTICAL COMMUNICATION SYSTEMS IN THE P-3 SCENARIO

This appendix is written as a subreport with its own internal logic. The goal is a well-defined quantitative score for detectability. The use of some previously developed computer programs is demonstrated, and exhibits of graphical output from them are shown to give a spatial understanding of the detectability problem.

The table of contents which follows shows the internal organization of this appendix. A quick-reading summary is followed by a discussion of military operational considerations, then by a section on the communications properties of several systems—including both those that are under consideration and some that are evaluated to form a context for the systems under consideration—and finally by calculated interception properties.

Atmospheric propagation calculations intentionally follow methods that are described elsewhere in this report. There are many points of comparison between results presented here in appendix G and those presented elsewhere. They should agree. But little detail is included that would be repetitious. The optical computations were not available early enough to allow them to be fully adapted to the present computer programs. In consequence they are poorly represented.

Certain items of nomenclature might be noted. The kilometre is generally used as a unit of length. In the P-3 series of aircraft, the P-3C has a standard communications suite that seems to contain representative present-day equipment. Near-optical refers to radiation frequencies within, say, a factor of ten of frequencies to which the eye is sensitive. Near-infrared refers to infrared frequencies near frequencies to which the eye is sensitive.

CONTENTS

SUMMARY

PROBLEM

The problem is that by intercepting communication signals between P-3 aircraft, an enemy can gain important information on the timing and location of our antisubmarine activities. To solve the problem by forbidding communications altogether would sacrifice the effectiveness of patrol activities. The solution explored here is low-intercept communications between P-3 aircraft in rendezvous. A way is required to evaluate or score a communication system for susceptibility to interception. One goal is to compare two generic types of communication systems—millimetre-wave and near-optical.

RESULTS

It was found that communication systems in general could not be evaluated but that specific communication/interceptor system combinations could be. Several combinations were selected for evaluation from systems presently on board the P-3C, systems of that type modified for reduced transmitter power, and some candidate millimetre-wave and near-optical systems.

The evaluation is in terms of a detectability score, which is proportional to the rate of detection by an interceptor that is assumed to be uniformly distributed, geographically, on a constant-altitude surface. The geometrical concept is defined by figure G1. The detectability score is expressed as a geographical area (in km^2) on the Earth's surface.*

The probability of detection by the interceptor during a communications interlude is the product of (1) the ratio of the detectability score (area) to the total area under search by the interceptor and (2) the ratio of the transmitter-on time to the total search time of the interceptor. The interceptor is assumed to have no information before detection occurs that would allow him to localize his search area or limit his search time. Detection control of P-3 communications might be executed by assigning a detection budget (the product of detectability and transmitter-on time in $km^2 \cdot s$) for each mission.

The detectability scores for combinations of systems, P-3 transmitter heights, and interceptor altitudes are summarized graphically in figure G2.

In discussing these scores it is noted that other means of detecting the aircraft would have a detectability score on the order of 1000 km^2. The scores obtained varied from about 10000 times larger for systems presently on board the P-3C to 10000 times smaller for one of the candidate systems. Detectabilities very much less than the detectability by other means are, in fact, negligible in their contribution to the enemy. All of the candidate systems evaluated had a detectability below 1000 km^2. Candidate systems were chosen that utilize atmospheric absorption to minimize detection, but it is probable that the detectability may be made less than 1000 km^2 without utilizing atmospheric absorption. In fact, this value of detectability would almost be achieved merely by reducing the transmitter power of the systems presently on board the P-3C. The very high detectabilities for the on-board systems (with their present transmitters) justifies restricting their use when interception is of concern.

*Naval Electronic Systems Command Covert Communications Notes, section 3.7.1 of Detection of Covert Signals, by RA Dillard, 1974.

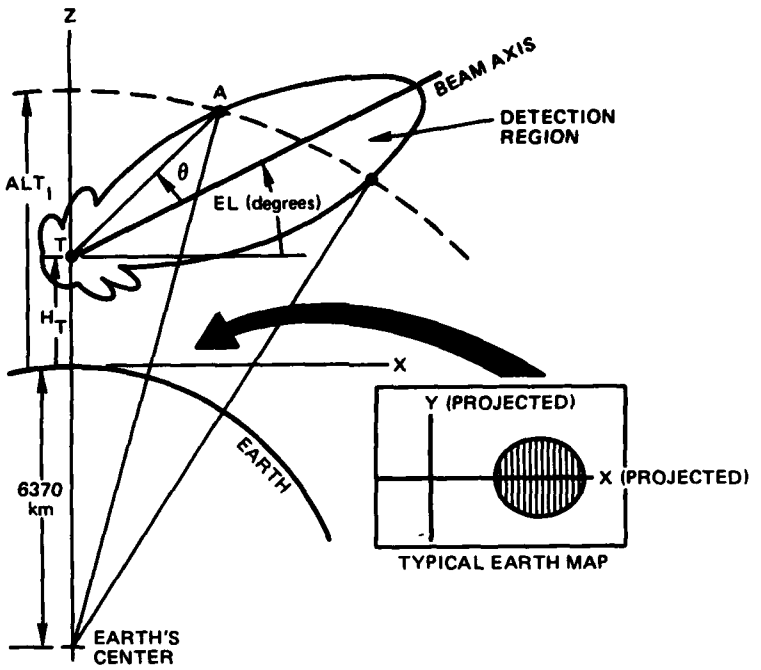

Figure G1. The concept defining the detectability score. A vertical plane containing the communication beam axis and the Earth's center also cuts the surface which bounds the region of detection by the assumed interceptor. The transmitter, T, is at height, H_T (km), above the Earth's surface and the elevation angle of the beam is EL (degrees). An interceptor is located somewhere on a spherical surface of constant altitude, ALT_I (km), above the Earth's surface. This surface also cuts the detection region, and the projection of this cut onto the Earth's surface is a "footprint" (shown shaded in the insert) whose area (in km^2) is taken as the detectability score of the communication system.

Systems presently on board the P-3C are intended primarily for communication over long ranges (say 1000 km), in all orientations and all weather. (Everyone can receive their signals, including the enemy.) The low-detectability systems, on the other hand, sacrifice operational convenience. These low-detectability systems are short-range (say 10 km or less) communication systems which require special rendezvous maneuvers for the aircraft involved. Under certain weather or flight conditions it is apparent that these maneuvers may not be permissible. The near-optical systems are predicted to be poor communicators in cloud or fog, and both the millimetre-wave and near-optical systems would be poor in rain. The most satisfactory combination of characteristics for low-intercept communication systems remains to be chosen.

It is academically apparent that the two generic types of candidate systems (millimetre-wave and near-optical) can be made comparable in clear weather. Because the millimetre-wave technology is more mature, it has a present advantage. Technical problems involved in the computation of near-optical phenomena precluded full consideration of near-optical systems within the time limit of this study.

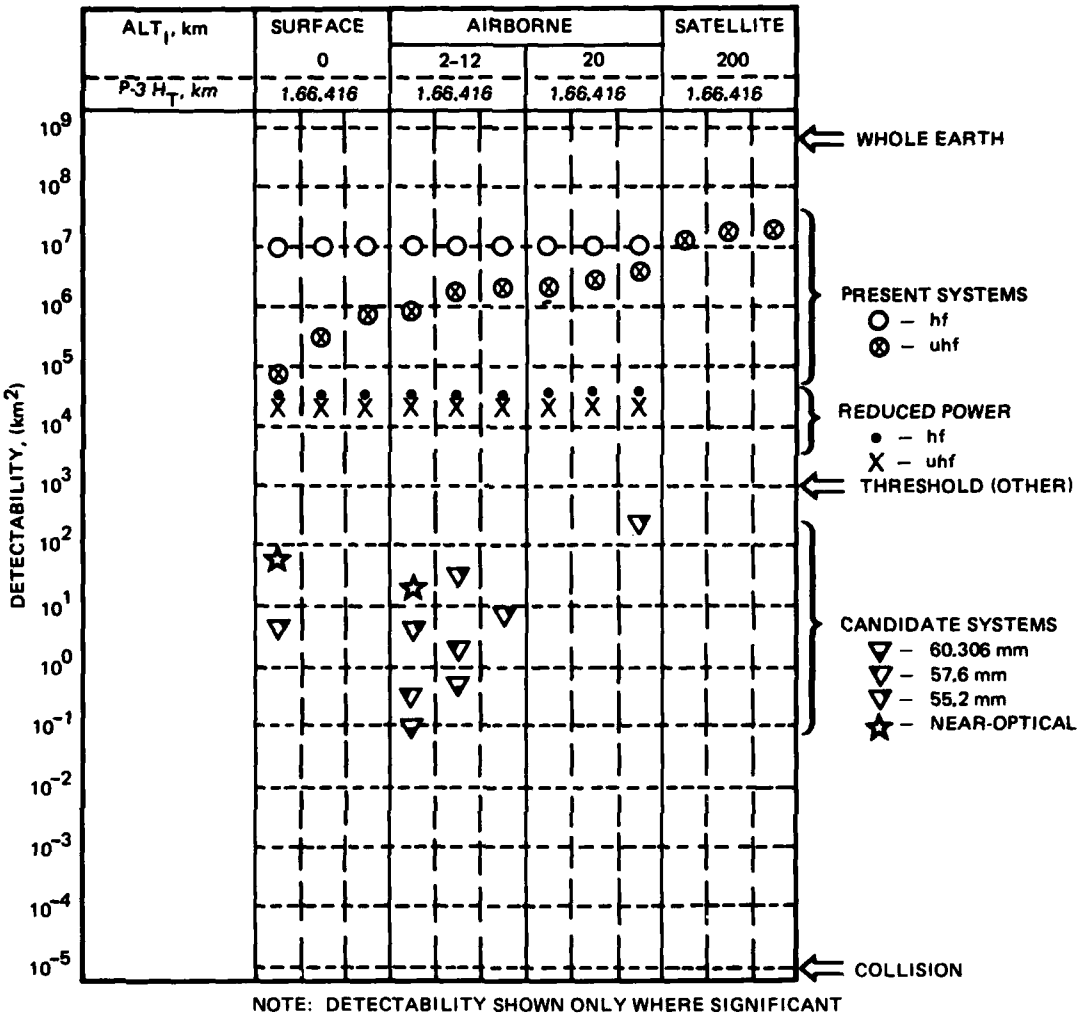

Figure G2. Graphical summary of detectability results. Geographical area of interceptor detection for millimetre-wave and near-optical communication systems is shown for a surface interceptor, an ensemble of airborne interceptors at 2-12 km altitudes, a 20 km altitude airborne interceptor, and a 200 km altitude satellite interceptor. Areas are averaged over an ensemble of beam elevation angles from -10 to +10 degrees. (Refer to table G3 for numerical values.) For context, present P-3C communication systems are also known along with such systems modified to transmit at reduced power. The area for whole-earth coverage, detection by collision, and the equivalent area for detection by other means are estimated for the purpose of giving scale to the detectability values.

A study of this nature involves the design of not only the communication system but also the interceptor system which will be used against it. This associated design problem involves a second set of operational problems. Whereas the detectability of long-range uhf communications by an interceptor on a satellite may be extremely high, none of the short-range communication systems appears to be susceptible to satellite interception. While both surface and airborne interceptors may be effective, the advantage generally lies with the airborne interceptor. For short-range communications in atmospheric absorption bands, the intercept range may be so short that surface interceptors or airborne interceptors at altitudes sufficiently different from the transmitter height may be ineffective. In this case the interceptor is forced to spread its activities over a range of altitudes. At some level of detectability, the yield of interceptor information will become too small for an enemy to justify the cost of interceptor operations.

RECOMMENDATIONS

1. The operational utility of short-range (meaning low-intercept) communications for P-3 to P-3 information transfer should be evaluated. This would probably require investigation of sensitive information considered beyond the scope of this study.

2. If there is adequate need for it, the scoring system devised in this study should be reconsidered and made into a more usable evaluation tool by fully coding it for digital computer.

3. The scoring system requires consistent interceptor design, a knowledge of practical interceptor operational problems, and further studies in this area are needed to support the scoring system.

4. Studies should be made to optimize communication system design for this purpose.

5. With the background of these scoring studies, some experimental data on the operational utility of available short-range communications systems should be acquired.

6. It is recommended that no present decision between millimetre-wave and near-optical frequencies be made for this application. Both technologies should continue to be developed.

DETECTABILITY SCORING

In this section the scoring procedure of detectability for the several communication systems is discussed. The score is intended to be widely applicable and defined well enough to be programmed for digital computer, with the characteristics of the communication/interception system used as parameters. The score has a physical meaning as a descriptor of the probability of detection by the interceptor, and it is usable in planning the operations of the P-3 aircraft in antisubmarine warfare. Approximate scores for a number of systems (other than the ones under consideration) are estimated in order to form a context for the judgment of the several systems.

MILITARY OPERATIONAL CONSIDERATIONS

The goal of the hand-over operation is to pass necessary messages (Teletype, voice, computer data, etc) from one P-3 to another while passing as little usable sensitive information

as possible from the P-3 to the enemy interceptor. Usable information may be the timing and location of P-3 antisubmarine operations. The mode of information transfer under consideration is the interception of communication signals by an enemy intercept receiver. It is assumed that if the enemy interceptor can conclude that the observed signal is a message signal (rather than noise) with an acceptable false-alarm rate, the direction of the signal and other of its characteristics are also available to him. He need not be able to read the message to gain useful information. The region of space within which he can do this is the region in which the communication signal intensity is above an intercept detection threshold.

If the detection threshold is examined in great detail, the probability of detection grades continuously from highly unlikely to highly likely, but this obscures the fact that the transition layer bounding the region of detection is fairly thin. It is a tremendous convenience in the following discussion to consider the detection region to have sharp boundaries.

The probability that the message signal will be detected is the probability that the interceptor is within the region of detection during the transmission of the message. It is assumed that the interceptor is completely ignorant of the location of the P-3 and of the time of its transmissions, and he is assigned to patrol some large geographical area (much larger than the extent of the detection region) for some fraction of the day. Actually, total ignorance is somewhat unrealistic, and both sides will attempt to exploit any regularities or constraints it perceives; however, proper operational control can conceal such regularities and constraints so that the advantage to the interceptor is minimized. For our purposes the interceptor is considered to be uniformly distributed geographically (though constrained in altitude) and uniformly distributed in time.

The probability of detection is proportional to the geographical area of the intersection of the detection region with a constant altitude surface (at the constrained altitude of the interceptor) as shown in figure G1. (We follow the convention of measuring distances and altitudes in kilometres and will refer to the altitude of the transmitting P-3 as "height" and the altitude of the interceptor as "altitude.") This area (in km^2) is to be called "detectability." The probability of detection during a communication interlude is the product of the ratio of the detectability area to the total area under patrol by the interceptor and the ratio of the transmitter-on time to the search time of the interceptor.

If the region of detection reaches neither the Earth's surface nor the altitude limit of the interceptor, the interceptor can totally miss detecting the signal by flying either too high or too low. This is a typical situation for the short-range communications equipment considered here, and it can force the interceptor to distribute his activities in altitude also, which further reduces the probability of detection.

Operationally, interceptor detection can be controlled by assigning each mission a budget of detectability times transmission time (say in $km^2 \cdot s$). If the missions are sufficiently infrequent and the detectability budgets sufficiently small, the enemy will find interception activities not worth his cost and will abandon them.

Detectability should be one criterion by which a communication system is chosen for the P-3 aircraft. Detectability has been of small concern in selecting the communication systems now on board the P-3C aircraft, and they are grossly unsuitable for low-intercept communications. The enemy probably has other means of detecting the P-3 than by its communication signals (by visual or acoustic detection, thermal (infrared) detection, etc). If the "other means" detection range is of the order of 10 miles, the equivalent detectability is about 1000 km^2. If the communications detectability is much less than this, there is little benefit to the enemy and the system is satisfactory for low-intercept communications. It appears that a large number of possible systems may have "satisfactory" detectability, and the choice among them may rest on other operational criteria.

There are obvious extremes of the detectability score. Whole Earth coverage (5.1×10^8 km^2) is an upper limit. A lower limit for consideration is the detectability by collision (about 10^{-5} km^2). The graph, figure G2, spans this range.

P-3 OPERATIONS

P-3 operations prepares flight plans and has responsibility for aircraft safety. The short-range communications (less than about 10 km) studied here will require some rendezvous procedure for both P-3 planes involved. This procedure will take fuel and time and will contribute some hazard, depending on visibility, altitude, etc. The shorter the range of the communications, the more severe these problems become.

The required on-time of the communications transmitter will depend on the message length and usable bit rate. In principle, very much larger bit rates than now in use can be sent over either millimetre-wave or near-optical systems. If the communication system is to feed into systems presently on board the P-3, the bit rate will be limited by those systems.

The typical detection budget for the mission, supplied by headquarters, will have subtracted from it the km^2·s communications required to establish the rendezvous. Depending on the size of the remainder and the necessary on-time, there will be some upper limit of detectability. This will translate to an upper limit on the communication range, for a given series of systems, and thus bounds the optimum performance from the standpoint of P-3 operations.

Under this scheme the communication range upper limit will be somewhat larger for systems operating in atmospheric-attenuation frequency bands. However, one of the prices to be paid for using atmospheric attenuation is that the detectability varies with the altitude of the transmitting aircraft.

TECHNICAL CONSIDERATIONS

Each frequency band has its own set of characteristics pertinent to the communication-interception function. In a small study both the communication and the interception system are designed by the same person without much review by independent experts. Valid comparisons should be limited to those systems that are comparable in cost; for novel hypothetical systems there may be no pertinent cost information. The pertinent costs would be those some 10 years in the future. We have attempted to follow certain rules for "fair" comparisons, but there are many pitfalls.

Once the communication and the interception system are fully defined, the performance is presumed to be calculable. For each direction from the transmitter, the distance to the detection region boundary set by the threshold radiation intensity is calculable as a technical problem. If the propagation medium (atmosphere) absorbs but does not scatter the radiation, the calculation may be simple; but if it scatters but does not absorb the radiation, the calculation may be very complex. One may find also that the basic information on atmospheric properties is not very reliable. The calculation is further complicated if there are strong natural sources of background radiation in the frequency band, such as the sun. In almost every consideration, the situation is worse for the near-optical systems than it is for the millimetre-wave systems.

COMMUNICATION SYSTEM PROPERTIES

We will consider primarily some relatively untried communication systems whose frequencies are located in regions of atmospheric absorption. Atmospheric absorption is an aid in preventing interception of messages by an enemy. Systems that exploit atmospheric absorption are necessarily limited to short range communications which require limitations on the operation of the aircraft (such as a rendezvous arrangement and parallel flight of the aircraft). It is only fair that they be compared with short-range communications at nonabsorbing frequencies which require similar limitations of aircraft operation. Using the detectability criterion, all of these should be compared with the communication systems that are now on board the P-3C aircraft. These systems will be considered in reverse order.

SYSTEMS ON BOARD THE P-3C

HF. This equipment has a frequency range of 2–30 MHz, with 100 Hz channels and a 1000 watt transmitter. At these frequencies the air offers no absorption and the radiation is trapped between the Earth's reflecting surface and reflecting ionospheric layers. Therefore propagation considerably beyond the horizon occurs, but propagation to satellite altitudes does not occur. Natural noise signals are also trapped and constitute the principal background noise which limits the range of communication and detection. The range of communication* (and of intercept detection) should be 1600 km. The surface and aircraft interceptor detectability is on the order of 10×10^6 km^2.

UHF. Uhf equipment has a frequency range of 225–400 MHz with 25-kHz channels and a 100 watt transmitter. At these frequencies the air offers no absorption and there is little ionospheric reflection, so that propagation is essentially line-of-sight. The principal background noise is receiver circuit noise. The range of communication works out to be 6000 km, which is well in excess of any horizon-limited distance considered here. Normally this excess communication range is used in overcoming nulls created by surface reflections and nulls in the antenna patterns to increase the reliability of communication. The line-of-sight interception range is larger still. The range of interception is limited by the horizon, and the computed line-of-sight detectability areas are given in table G1.

SYSTEMS WHICH COULD SOON BE ON BOARD THE P-3C

UHF SATELLITE. Satellite uhf communications for the P-3C have been demonstrated, but operational equipment is not yet available. The communication range is effectively worldwide. The detectability should be essentially the same as the present uhf communications (see table G7).

---

*$kT_oB = 4 \times 10^{-19}$ W. From the ITT handbook (Reference Data for Radio Engineers, Howard Sams and Co, Indianapolis, 1975), figures 2 and 3 of chap 29 show that a typical atmospheric noise factor, F_a, over the world and over the frequency range is 30 dB. For average transmitter power of 500 watts, the largest basic transmission loss for a 15 dB S/N is -166 dB which from figure 4 of chap 28 corresponds to a range of 1000 statute miles (1600 km) at 2 MHz. This will be taken as the interception range also.

Table G1. Uhf detectability.

Line-of-sight geographical area coverage for various transmitter heights (H_T) and interceptor altitudes (ALT_I).

H_T, km	ALT_I, km	Detectability, km^2
1.6	0	85 323
	2	382 868
	12	1 192 096
	2-12 avg	787 482
	20	1 753 506
	200	12 442 271
6.4	0	341 290
	2	829 673
	12	1 915 268
	2-12 avg	1 372 470
	20	2 612 428
	200	14 588 281
16.0	0	852 430
	2	1 562 336
	12	2 968 737
	2-12 avg	2 265 536
	20	3 823 476
	200	17 293 382

REDUCED-POWER SHORT-RANGE HF. The presently installed hf communication system on the P-3C is essentially designed for maximum range of communication and maximum likelihood of communication. It therefore has vastly more transmitter power than necessary for short-range communication comparable to ranges available in the atmospheric absorption frequencies. If the transmitter power were reduced from 1 kW to 2.5 μW, the communication range (and intercept detection range) would drop to about 100 km and the aircraft detectability would drop to 31 400 km^2. Satellite detectability should be zero.

REDUCED-POWER SHORT-RANGE UHF. Similarly if the transmitter power of the present uhf communication system were reduced from 100 W to 26 μW, the intercept range would be 91 km and the aircraft detectability would be 26 000 km^2. The satellite detectability would be zero.

CANDIDATE SYSTEMS.

The reader should be aware that the following systems have not been fully optimized for either minimum detectability or maximum utility.

MILLIMETRE-WAVE SYSTEMS. In concept, millimetre-wave systems are portable and will be installed temporarily, in pairs, in the P-3 aircraft that will be exchanging information. Several such systems have been proposed and/or demonstrated at a variety of frequencies in the 10–100 GHz band. The aircraft will rendezvous and fly side by side at an appropriate separation distance (say 1 km). The antenna will be hand-held and pointed out a window at the other plane during communication. With a moderately broad antenna beam and the low relative motion of the planes there should be no problem in tracking the antenna of the other unit for as long as communication is desired. The communication units will tie into the existing voice, data, and other lines of the P-3 aircraft.

Three closely related hypothetical millimetre-wave systems are possible, associated with the three frequencies, 60.306, 57.6, and 55.2 GHz. The 60.306 GHz frequency is precisely at an oxygen resonant line (one of many that widen at normal atmospheric pressures to form a broad absorption peak near 60 GHz). Possibly, the same hardware could cover all three frequencies.

The transmitter power for all three systems is 60 mW. A 25 dB gain horn antenna is used on the transmitter (see figure G3). An identical horn is assumed for the communication receiver. The maximum communication range (in vacuum) is 68.9 km. The vertical cross section of the communication volume (in atmosphere) is shown in figures G4 to G6.

The boxed parameters in both the communication and detection profile figures are defined as follows:

ELEVDEG = Transmitter beam elevation angle in degrees

BMVRKM = Beam vacuum range in km

SLDBKM = Sea-level atmospheric attenuation in dB/km

RNDB = Rain attenuation in dB

EANT = Antenna Pattern table number

HTKM = Transmitter height in km

The maximum communication range for these conditions is listed in the table G2. Note that the fractional change of range with height is less for this line resonant frequency (60.306 GHz).

The interceptor detection range (in vacuum) is 1730 km for each of these systems.

NEAR-OPTICAL SYSTEMS. A hypothetical near-infrared system at 319 000 GHz (0.94 μm) has been considered. The daylight communication range is 1.5 km at sea level. The antenna pattern is flat out to θ = 11.5 degrees, as shown in figure G7. The vertical cross section of the communication volume (range 1.5 km) is shown in figure G8.

Table G2. Communication range of millimetre-wave systems.

Frequency, GHz	Sea-level Atten, dB/km	Communication Range, km		
		H_T = 1.6 km	H_T = 6.4 km	H_T = 16 km
60.306	15.156	1.94	2.13	3.45
57.6	11.265	2.77	3.48	5.53
55.2	4.53	5.76	8.57	17.77

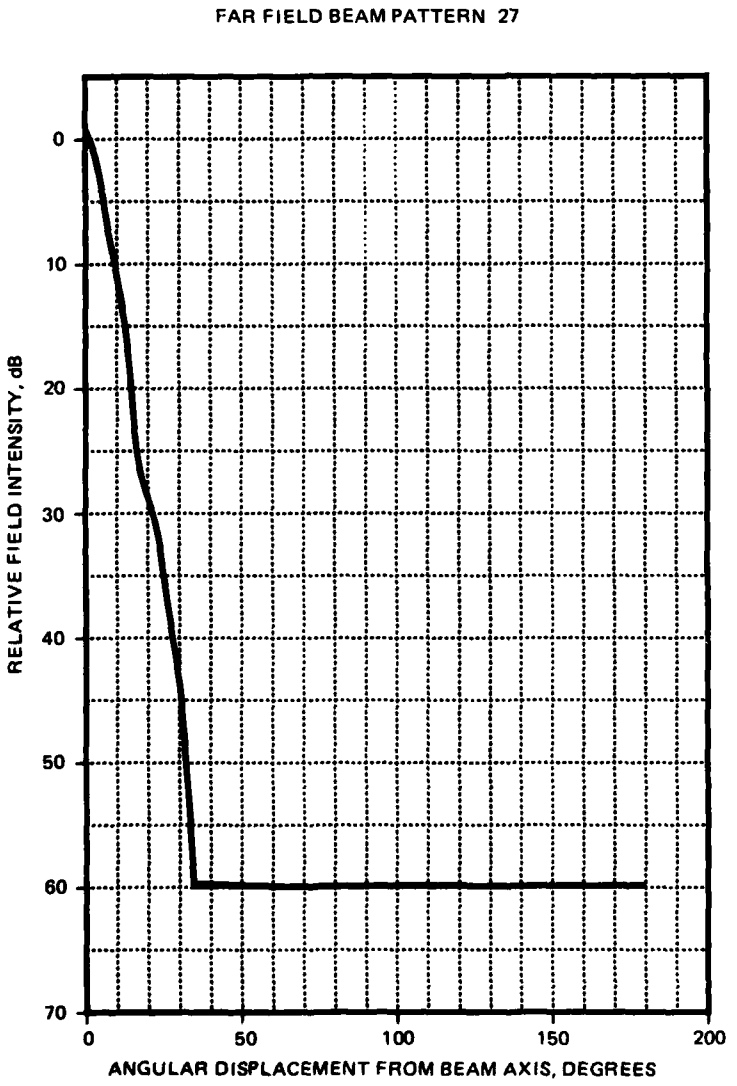

Figure G3. Axially symmetric antenna beam pattern for the millimetre-wave systems (adapted experimental data). The -60 dB tail is at the measurement threshold.

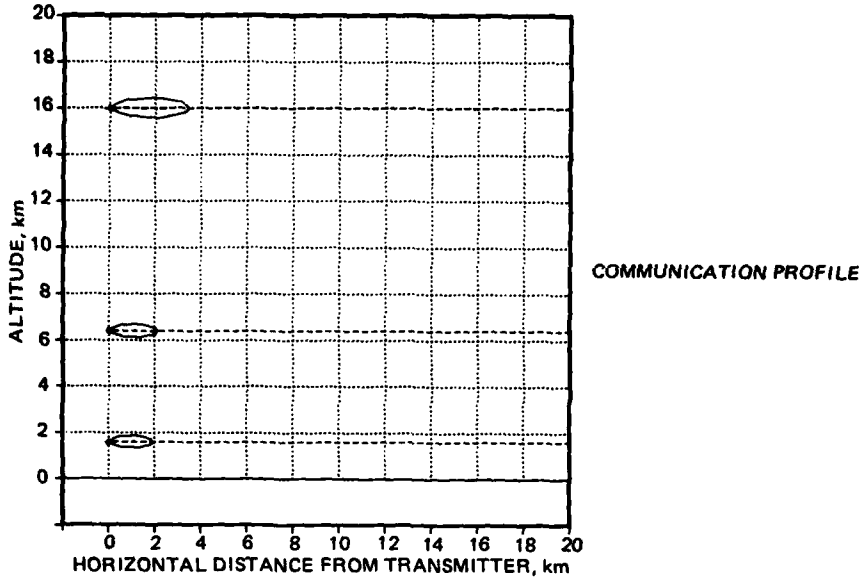

ELEVDEG	BMVRKM	SLDBKM	RNDB
0.0	69.	16.16	0.00
EANT	HTKM-1-2-3		
27	1.60 6.40	16.00	

Figure G4. Vertical profiles of the communication regions for a 60.306 GHz, shown for three transmitter heights. This frequency is exactly on an oxygen resonance line. Because of line-broadening, the absorption does not increase linearly with atmospheric density.

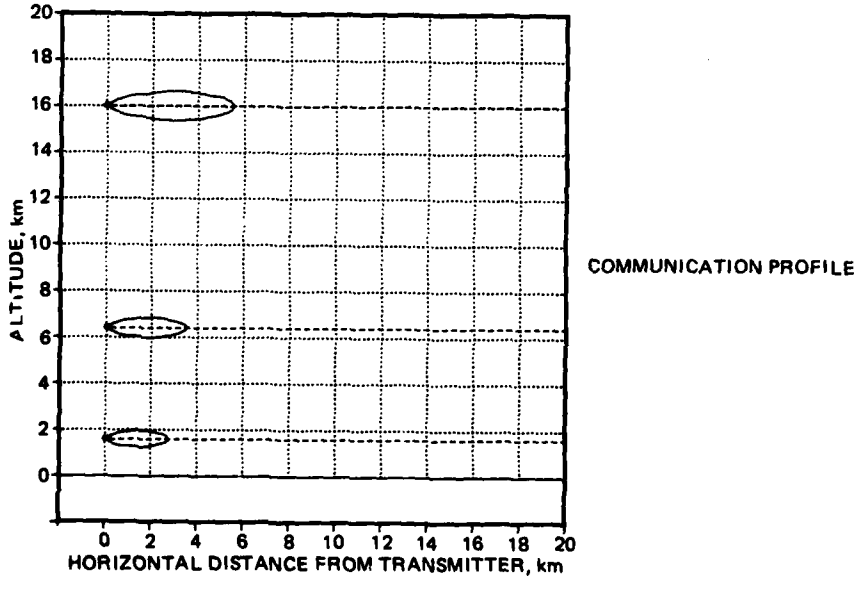

ELEVDEG	BMVRKM	SLDBKM	RNDB
0.0	69.	11.26	0.00
EANT	HTKM-1-2-3		
27	1.60 6.40	16.00	

Figure G5. Vertical profile of the communication region for 57.6 GHz.

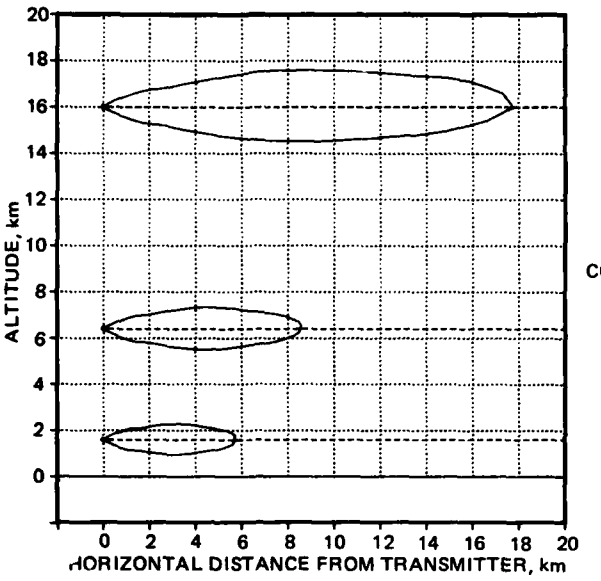

ELEVDEG	BMVRKM	SLDBKM	RNDB
0.0	69.	4.53	0.00
EANT	HTKM-1-2-3		
27	1.60 6.40	16.00	

Figure G6. Vertical profile of the communication region for 55.2 GHz.

The computational problems of S/N have been severe. The detectability in most instances has been unrepresentatively large due to factors which were not apparent at the time the hypothetical systems were set. The background noise is largely from scattered sunlight and proportional to the solid angle of reception by the receiver. In the present system the communications receiver has a much larger (perhaps unnecessarily larger) solid angle of reception than the intercept receiver; therefore the intercept range is much larger than the communications range. Since the transmitter power remains constant, the intercept range becomes very large in the absence of sunlight (ie at night) or when the transmitter height exceeds that of the layer of scattering haze near the Earth's surface.

With the transmitter at a height of 1.6 km, the intercept range has been calculated to be 23 km for the 319 000 GHz system in sunlight, and this range has been used to estimate detectability. Many of the other situations appear to give intercept ranges of hundreds of km, which would give detectabilities so large that revision of the communication system design might be considered.

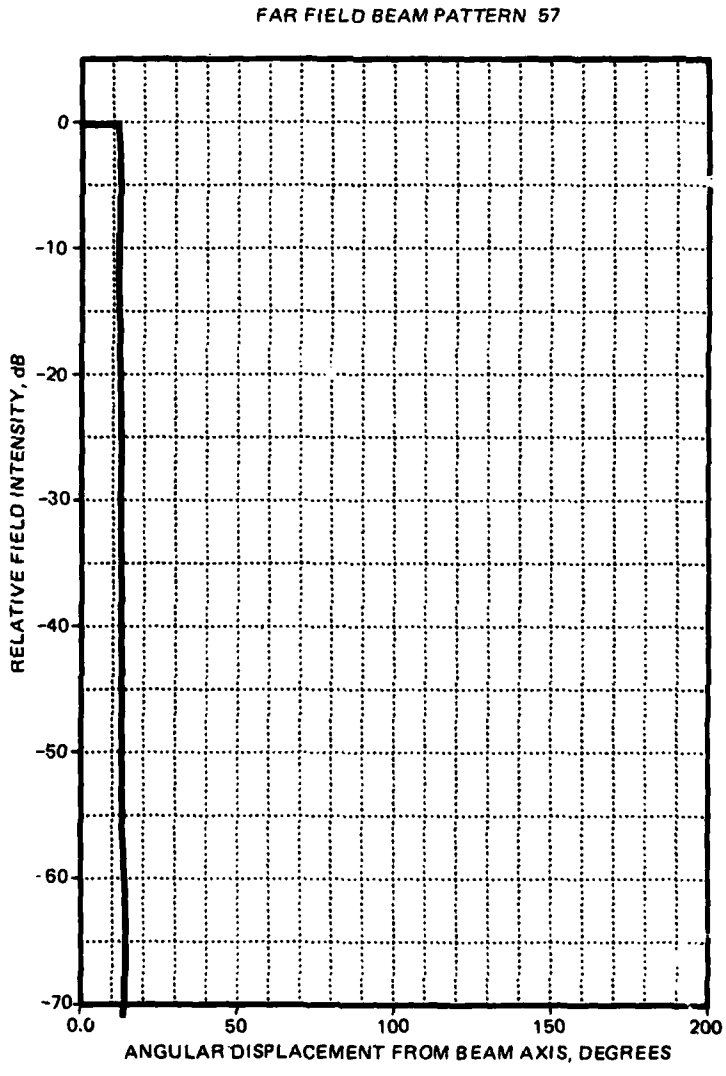

Figure G7. Hypothetical beam pattern for a near-optical system.

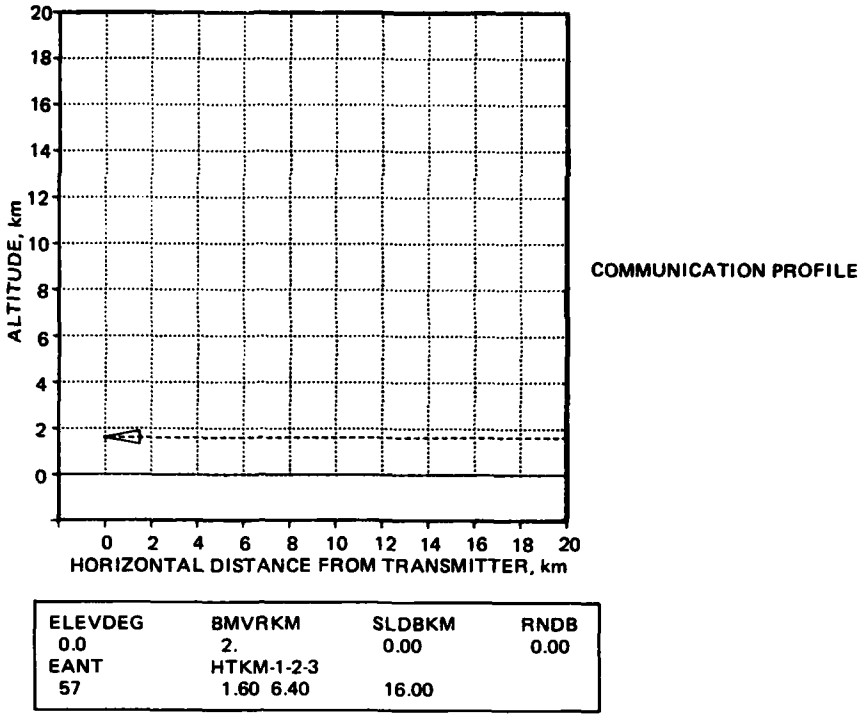

Figure G8. Vertical profile of the communication region for a near-optical system. The communication range is 1.5 km. Only the 1.6 km height is shown.

INTERCEPTION PROPERTIES

ACADEMIC CONSIDERATIONS

Let us consider more rigorously what defines the boundary of the detection region shown in Fig G1. Consider the interceptor to be located at point A. The interceptor is assumed to have a high gain antenna (40 dB or 1.5° beamwidth) which scans in direction (or has many simultaneous beams) and which at the time of detection is pointed at the transmitter, T. At that time the intercept receiver has an effective noise power level, N, and a received signal power, S, referred to the receiver output. The detection threshold has to be set sufficiently above N so that the false-alarm rate from the noise is sufficiently low.* The

*Blake's section 2.4 of the commonly available Radar Handbook by Merrill Skolnik reviews this problem. In common with many other treatments, that review uses thermal noise as a model. The signal pulse passes through one frequency filter system before rectification and a second filter after rectification. These stages affect the S/N ratio differently since it is assumed that the noise is continuous and that in the final output it is only the statistical fluctuations in the noise power that get confused with the signal pulse. Whereas at hf and below, the noise at the receiver output is principally the amplified, naturally generated atmospheric static captured by the antenna, the noise figure at uhf and millimetre-wave frequencies is commonly more than 3 dB, which indicates that most of the noise is circuit rather than thermal noise. At near-optical frequencies signal rectification is by photoemission, which is subject to quantum noise, particularly at low light levels. Thus some adjustment of the equivalent thermal noise level for the model is needed for the various frequency bands.

value of S is well above this threshold close to the transmitter and since it decreases continuously with the range, R, there is some range at which it drops below this threshold value. The locus of this maximum range as a function of angular displacement, θ, of TA from the beam axis defines the boundary of the detection region.

In brief, the appropriate method of calculating S/N as a function of range and direction depends on the frequency. It is useful to start with the "academic" method of calculation even though it is not fully appropriate for the instances here.

In the academic method, N is independent of range and direction. This is generally true for frequencies from millimetre-wave down through uhf because at these frequencies, most of the effective noise is generated by the intercept receiver itself and is usually calculated as a noise factor (measured for specific circuitry) times the basic Johnson noise power for 290 Kelvins of the receiver front end. This is not true at near-optical frequencies because much of the effective noise level comes from scattered sunlight.

The signal power, S, contains a factor called the antenna pattern, which is a property of the transmitter (including in this case the effects of aircraft structure etc) and a function of direction. The present calculations have restricted this function to one that is symmetrical about the beam axis and is thus a function of θ only (see figure G3 and G7). An antenna pattern factor has been used in all the present calculations.

The signal intensity is attenuated by the atmosphere, with an attenuation constant proportional to the density of the atmosphere. The attenuation constant in dB/km is shown for sea level density as a function of frequency in figure G9. The atmospheric density varies as a function of height, H km, above sea level by the factor exp(H/6.95). Since H varies along the path to the interceptor, the calculation of attenuation has to include this variation. The attenuation factor applies in addition to the geometrical spreading factor, $1/R^2$.

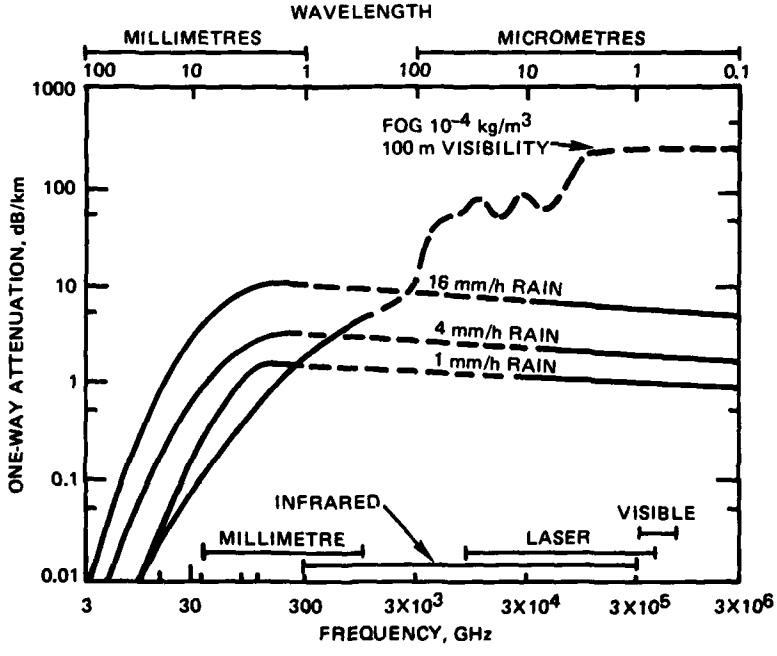

Figure G9. Sea-level atmospheric attenuation as a function of frequency. From BRL Report 1838, Rain Backscatter Measurements and Theory at Millimeter Wavelengths, by VW Richard and JE Kammerer, US Army Ballistic Research Laboratories, Aberdeen Proving Ground, Maryland, October 1975 (AD B008173L).

At the millimetre-wave frequencies considered here, the atmospheric attenuation constant is not proportional to atmospheric density because of intermolecular interactions and the height function used is an empirical one.* For near-optical frequencies, scattering is the dominant radiation absorption factor, and S is a complicated (and not easily calculated) function.

It should be noted in figure G9 that comparable attenuation constants are obtainable in both the millimetre-wave and near-optical frequency region. Thus one expects that comparable communication systems (from the detectability standpoint) can be designed on an academic basis.

In figure G10 the attenuation constant of rain and fog is shown as a function of frequency. Comparison with the atmospheric attenuation in figure G9 shows that both millimetre-wave and near-optical communications will be affected by rain heavier than "very light." Near-optical communications are far more affected by fog than are millimetre-wave communications. Scattering is the primary mechanism of both rain and fog attenuation. No calculations of detectability including rain or fog were made in this study.

The signal intensity, S, is also taken to be proportional to the radiated transmitter power. For maximally covert communication systems, this power would be adjusted to the minimum needed for communications under any specific conditions. The systems considered here do not include this complication; the power is kept constant. Consequently the communication and detection ranges vary with conditions. This has been a severe handicap to the near-optical systems, wherein the noise level depends so greatly both on sunlight conditions and, because haze scattering is concentrated at low altitudes, on transmitter altitude.

*EE Reber, RL Mitchell, CJ Carter, Oxygen Absorption in the Earth's Atmosphere, The Microwave Journal, November 1969

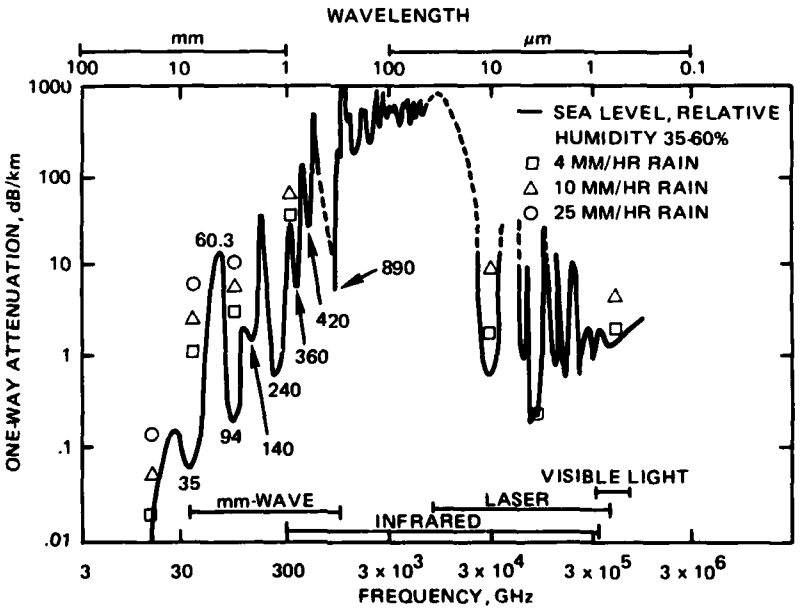

Figure G10. Sea-level attenuation by fog and rain as a function of frequency. (Same source as preceding figure.)

The definition of detectability described in figure G1 assumes an interceptor located randomly on a surface of fixed altitude. In that geometry, detectability is a function of the interceptor altitude, the transmitter altitude, the elevation angle of the transmitter beam, the antenna pattern, and the atmospheric propagation at the operating frequency. This function is often surprisingly complex.

It was mentioned that for intercept ranges less than the height of the atmosphere, an airborne interceptor may fly at altitudes above or below the region of detection. If the interceptor flies at an ensemble of altitudes (say a continuous ensemble from 2 to 12 km), it is very likely that the detection region will be intersected. If the detection region falls entirely within the range of the altitude ensemble, the detectability becomes the volume (km^3) of the detection region divided by the range of altitudes assumed for the interceptor (say 10 km). The ensemble-averaged detectability is less sensitive to some parameters than is the straight (discrete interceptor altitude) detectability.

The detectability at a given altitude is a function of the elevation angle of the beam. In a hand-directed device aimed at the companion airplane there will be a normal range of elevation angles produced both by errors in aiming and deviations in relative altitudes of the aircraft. In consequence, detectability should also be averaged over an ensemble of beam-elevation angles. This has been done here by estimation from calculations for two angles, +10° and -10°.

COMPUTER CALCULATIONS FOR CANDIDATE SYSTEMS

The vertical cross-section of the detection volume (titled detection profile to distinguish it from the communication profile shown in figures G4–G6) for the three millimetre-wave systems, the three representative transmitter heights of 1.6 km (5250 feet), 6.4 km (21 000 feet), and 16 km (52 500 feet), and the two beam elevation angles, +10° and -10°, are shown in figures G11–G16. The interception range in vacuum for all three systems is 1730 km. The parameters of the computer calculations are shown below the profiles. The three system frequencies (60.306, 57.6, and 55.2 GHz) are identified by their respective sea-level atmospheric attenuations in dB/km (16.16, 11.26, and 4.53). The attenuation as a function of altitude is the empirical function mentioned previously.

A similar detection profile for the single near-optical instance is shown in figure G17. The detection range is 23 km (just off the limits of the figure).

A summary of numerical values from these computations is given in table G3. (These numerical values are summarized graphically in figure G2.)

It will be noted that neither the 60.306 GHz nor the 57.6 GHz system has a detection region that intersects either the Earth's surface or the 20 km (65 600-foot) altitude surface in the examples shown. The 55.2 GHz system does have one example (H_t 1.6 km, EL -10°) in which the region intersects the ground. The 55.2 GHz system also has one example (H_T 16 km, EL 10°) in which the region intersects the 20 km altitude surface. The near-optical system instance shown does intersect the earth surface and it also reaches into the 2–12 km altitude region. None of these examples show a detection region which intersects the 200 km altitude surface; therefore satellite detection of these systems is ruled out for these examples.

It might not be expected from the preceding examples, but if the beam elevation is increased for the 55.2 GHz system at the 16 km height, the detection region does extend to satellite altitudes. An example of 45° elevation angle is shown in figure G18, which shows an intersection with the 200 km altitude surface. (Note change of scale from the preceding graphs.) The maximum altitude for the detection region is 511 km for this example.

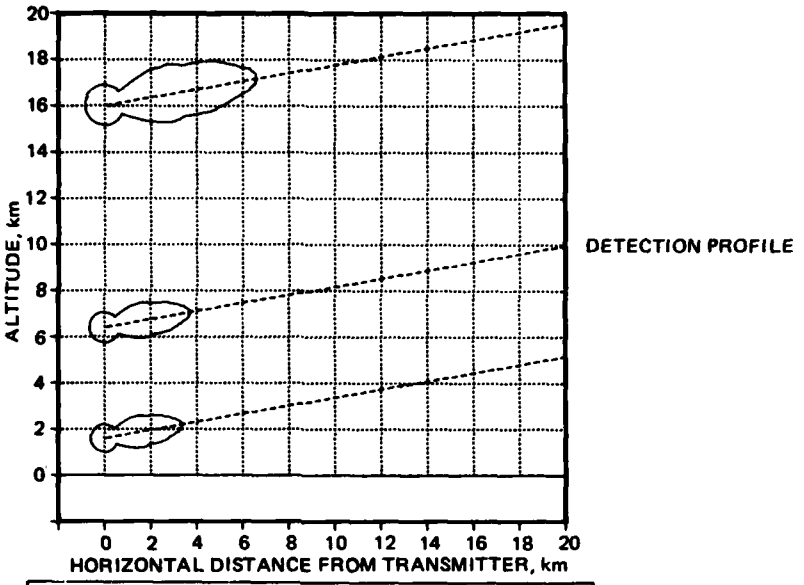

ELEVDEG	BMVRKM	SLDBKM	RNDB
10.0	1730.	16.16	0.00
EANT	HTKM-1-2-3		
27	1.60 6.40	16.00	

Figure G11. Vertical cross-section of the detection volume. Millimetre-wave system. Transmitter heights of 1.6, 6.4, and 16 km. Maximum detection range in vacuum 1730 km. Frequency 60.306 GHz; attenuation 16.16 dB/km at sea level. Elevation angle +10°.

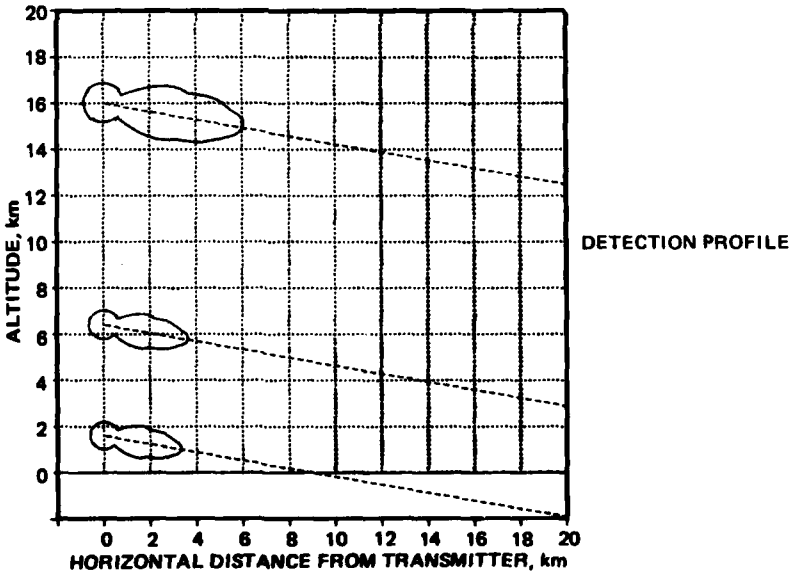

ELEVDEG	BMVRKM	SLDBKM	RNDB
-10.0	1730.	16.16	0.00
EANT	HTKM-1-2-3		
27	1.60 6.40	16.00	

Figure G12. Vertical cross-section of the detection volume. Millimetre-wave system. Transmitter heights of 1.6, 6.4, and 16 km. Maximum detection range in vacuum 1730 km. Frequency 60.306 GHz; attenuation 16.16 at sea level. Elevation angle -10°.

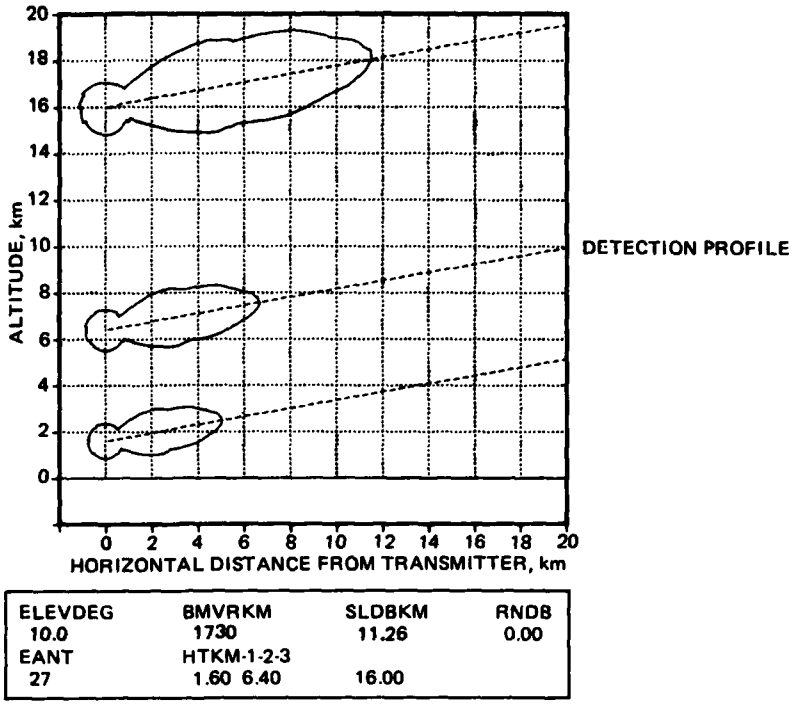

Figure G13. Vertical cross-section of the detection volume. Millimetre-wave system. Transmitter heights of 1.6, 6.4, and 16 km. Maximum detection range in vacuum 1730 km. Frequency 57.6 GHz; attenuation 11.26 dB/km at sea level. Elevation angle +10°.

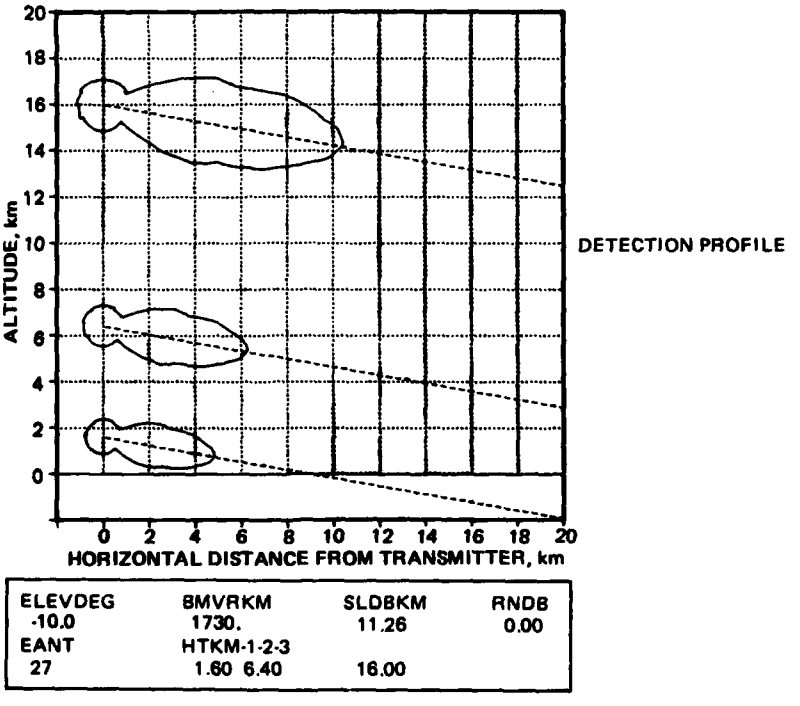

Figure G14. Vertical cross-section of the detection volume. Millimetre-wave system. Transmitter heights of 1.6, 6.4, and 16 km. Maximum detection range in vacuum 1730 km. Frequency 57.6 GHz; attenuation 11.26 dB/km at sea level. Elevation angle -10°.

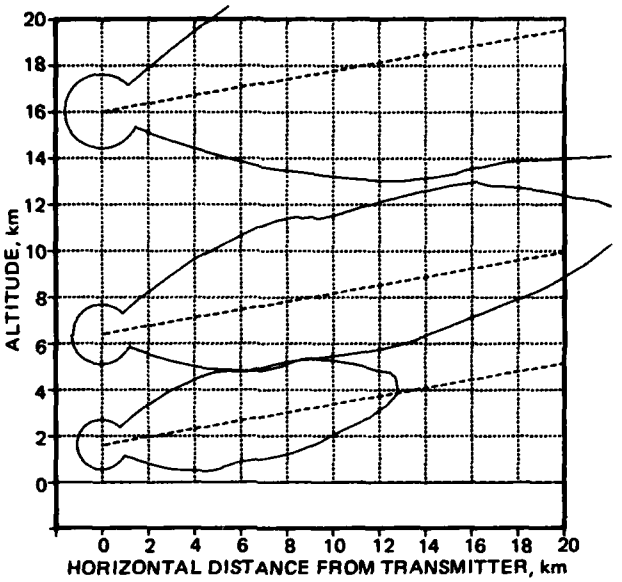

ELEVDEG	BMVRKM	SLDBKM	RNDB
10.0	1730.	4.53	0.00
EANT	HTKM-1-2-3		
27	1.60 6.40	16.00	

Figure G15. Vertical cross-section of the detection volume. Millimetre-wave system. Transmitter heights of 1.6, 6.4, and 16 km. Maximum detection range in vacuum 1730 km. Frequency 55.2 GHz; attenuation 4.53 dB/km at sea level. Elevation angle +10°.

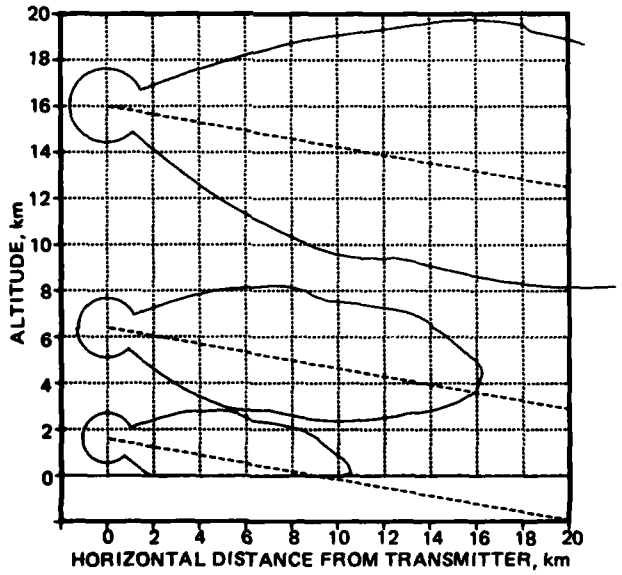

ELEVDEG	BMVRKM	SLDBKM	RNDB
-10.0	1730.	4.53	0.00
EANT	HTKM-1-2-3		
27	1.60 6.40	16.00	

Figure G16. Vertical cross-section of the detection volume. Millimetre-wave system. Transmitter heights of 1.6, 6.4, and 16 km. Maximum detection range in vacuum 1730 km. Frequency 55.2 GHz; attenuation 4.53 dB/km at sea level. Elevation angle -10°.

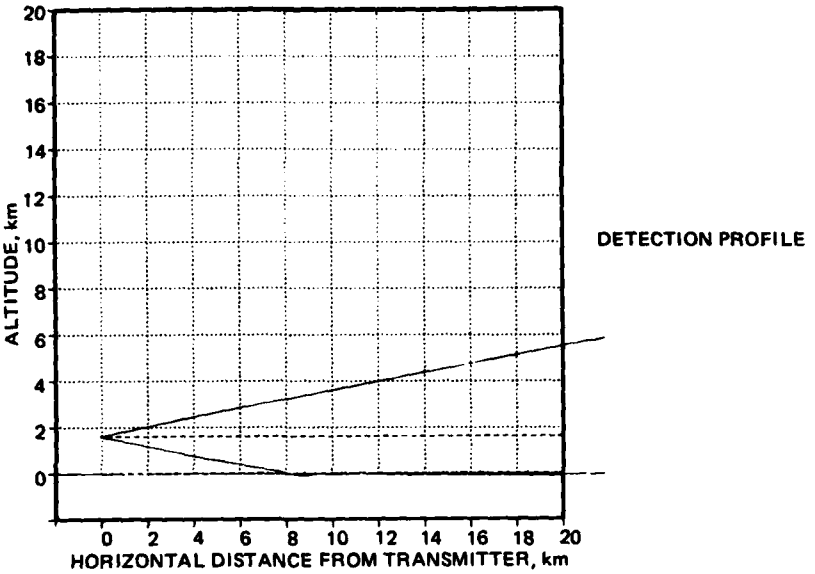

ELEVDEG	BMVRKM	SLOBKM	RNDB
0.0	23.	0.00	0.00
EANT	HTKM-1-2-3		
57	1.60 6.40	16.00	

Figure G17. Vertical cross-section of the detection volume. Near-optical system. Transmitter height 1.6 km. Maximum detection range in air 23 km. Elevation angle 0°.

How serious a problem does this last example represent? To evaluate the detectability at 200 km altitude, let us return to our definition shown in figure G1. In that figure the intersection of the constant-altitude surface with the detection region projected on the Earth's surface constitutes a "footprint" which is shown in the inset. The area of the footprint is defined as the detectability. There is a local computer program which draws this footprint and computes the area. The footprint for this particular case is shown in figure G19 (disregard some of the parameter numbers). The area of the footprint is 5120 km^2. The detectability is therefore somewhat above the nominal 1000 km^2 which we have taken to represent the detectability by other methods. Several things keep this higher value from being serious. An elevation angle of 45 degrees seems rather extreme in normal use. A height of 16 km (52 500 ft) for a P3 seems rather extreme. For this application, the 55.2 GHz system probably would be redesigned before production to have less transmitter power. While this example may not represent a serious problem, it is an example of the sort of system study by this means of scoring which should be investigated for proposed systems.

A second footprint example is shown in figure G20 for the 20 km altitude interceptor and the example (hgt = 16, el = 10°) whose detection profile is shown in figure G15. The waist on the footprint is due to the inflection in the antenna pattern (fig G3). The detectability area is 491 km^2. This value is included in table G3.

A third application of footprints is in calculating the ensemble averages. The most general method for doing numerical ensemble averages would be to make a weighted sum of a number of individual footprint areas. The number needed would depend on how complicated the area function is and the needed accuracy; typically it might be 50. As an example (and a rather simple one) let us take the uniform 2–12 km altitude ensemble for the 60.306

Table G3. Detectability results.

System and freq, GHz	H_T, km	EL, °	Detection		Detectability, km^2			
			Range, km	Volume, km^3	ALT_I = 0 km	ALT_I = 2-12 km	ALT_I = 20 km	ALT_I = 200 km
mm-wave								
60.306	1.6	+10	3.38.	3.6	–	0.15	–	–
		-10	3.39	3.5	–	0.01	–	–
		**				0.10		
	6.4	+10	3.79	4.7	–	0.47	–	–
		-10	3.69	4.4	–	0.44	–	–
		**				0.46		
	16.0	+10	6.70	19.9	–	–	–	–
		-10	6.15	17.1	–	–	–	–
		**				–		
57.6	1.6	+10	5.11	10.1	–	0.50	–	–
		-10	4.91	9.3	–	0.05	–	–
		**				0.30		
	6.4	+10	6.79	20.5	–	2.05	–	–
		-10	6.35	18.5	–	1.85	–	–
		**				1.95		
	16.0	+10	11.73	86.7	–	–	–	–
		-10	10.55	71.7	–	–	–	–
		**				–		
55.2	1.6	+10	13.03	109.6	–	6	–	–
		-10	10.66	70	19	1	–	–
		**			5	4		
	6.4	+10	23.03	469.8	–	47.0	–	–
		-10	16.36	246.5	–	24.7	–	–
		**				35		
	16.0	+10	105.15	***	–	–	491	–
		-10	36.51	2361	–	30	–	–
		**				8	250	
Near-optical								
319 000	1.6	0	23	500	70	23	–	–

*Detectability averaged over interceptor altitude 2-12 km
**Detectability averaged over beam elevation -10° to +10°
***Greater than 9999.

GHz system with beam elevation angle of 10° and transmitter height of 6.4 km, an example shown in profile in figure G11. Since we have an alternate method of calculating the volume of the detection region (4.7 km^3) and we know that the volume is totally contained in the 2-12 km altitude range, we know the ensemble average is 0.47 km^2. The footprints for altitudes of 6.6, 7.0, and 7.4 km are shown in figures G21, G22, and G23 (areas: 4.28, 3.26, 0.88 km^2). It should be noted that the footprint divides into two areas at 7.0 km altitude: one from the main beam and one from the -60 dB far-sidelobe region in the

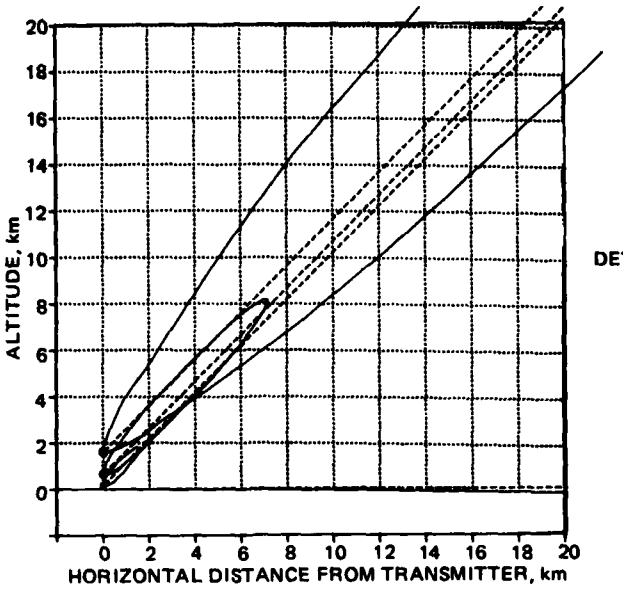

Figure G18. Vertical cross-section of the detection volume. Special case of 45° elevation angle for 55.2 GHz millimetre-wave system. Detection volume reaches satellite altitudes for 16 km transmitter height. Note change of scale from preceding figures.

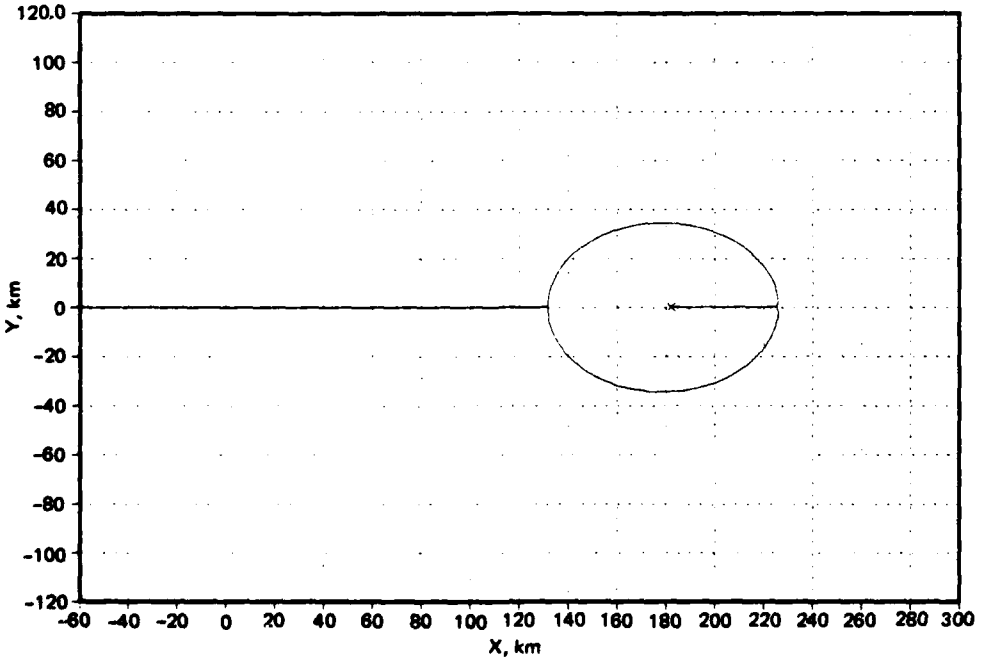

Figure G19. Detection footprint at 200 km interceptor altitude. Transmitter height is 16 km. Detectability (ie footprint area) is 5120 km^2. Compare with figure G18.

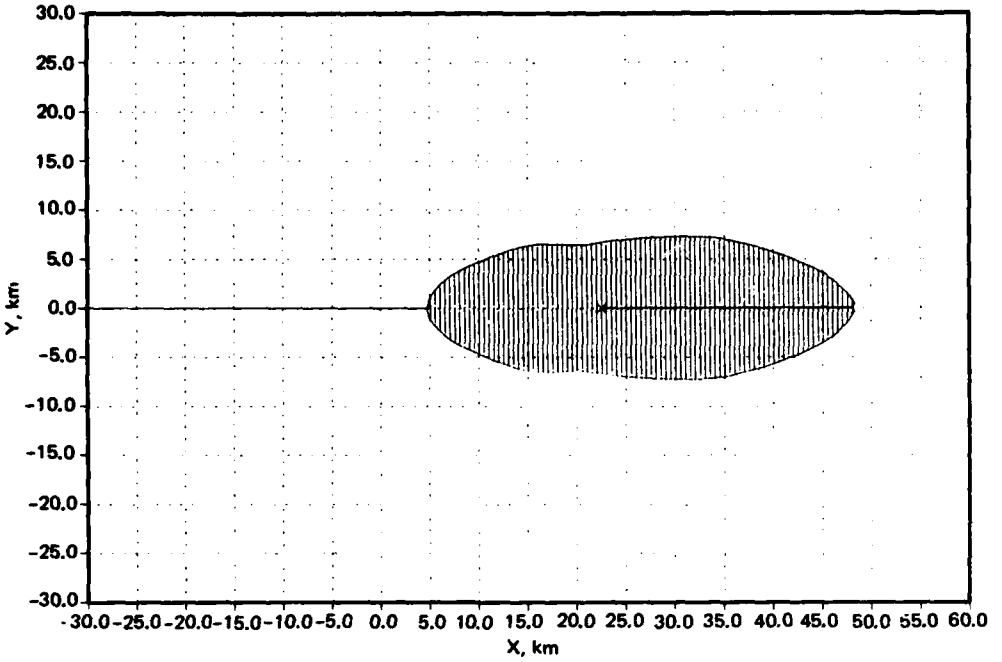

Figure G20. Detection footprint at 20 km interceptor altitude. Transmitter height 16 km. Detectability (ie footprint area) is 491 km^2. Compare figure G15.

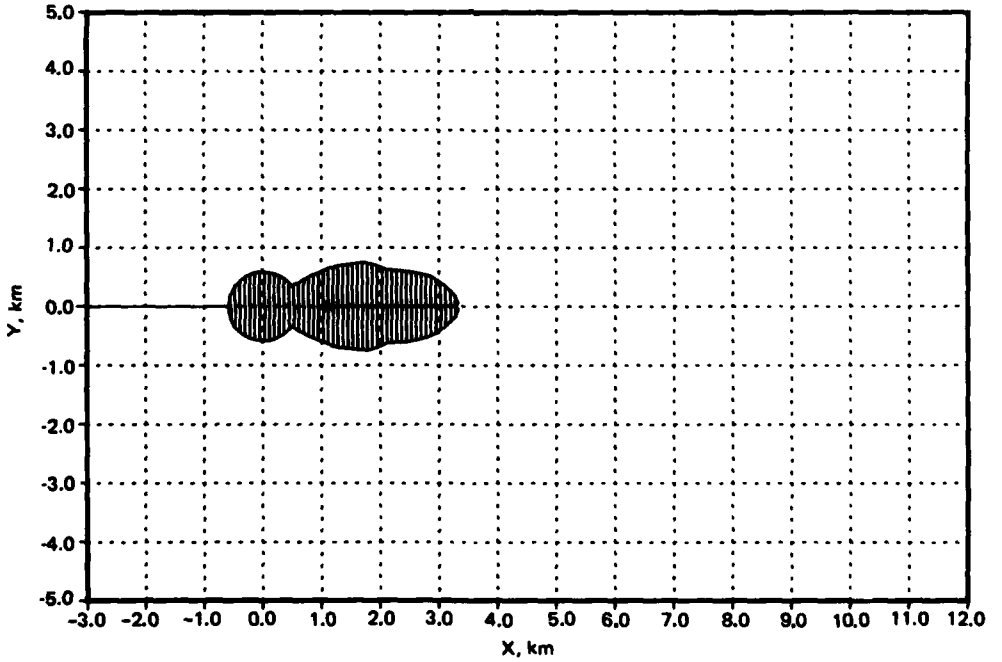

Figure G21. Detection footprint at 6.6 km interceptor altitude. Transmitter height 6.4 km. Compare against vertical cross-section of detection region in figure G11 (60.306 GHz and 10° elevation angle). Footprint area is 4.28 km^2. Data can be used to calculate an altitude ensemble average (data plotted in figure G24).

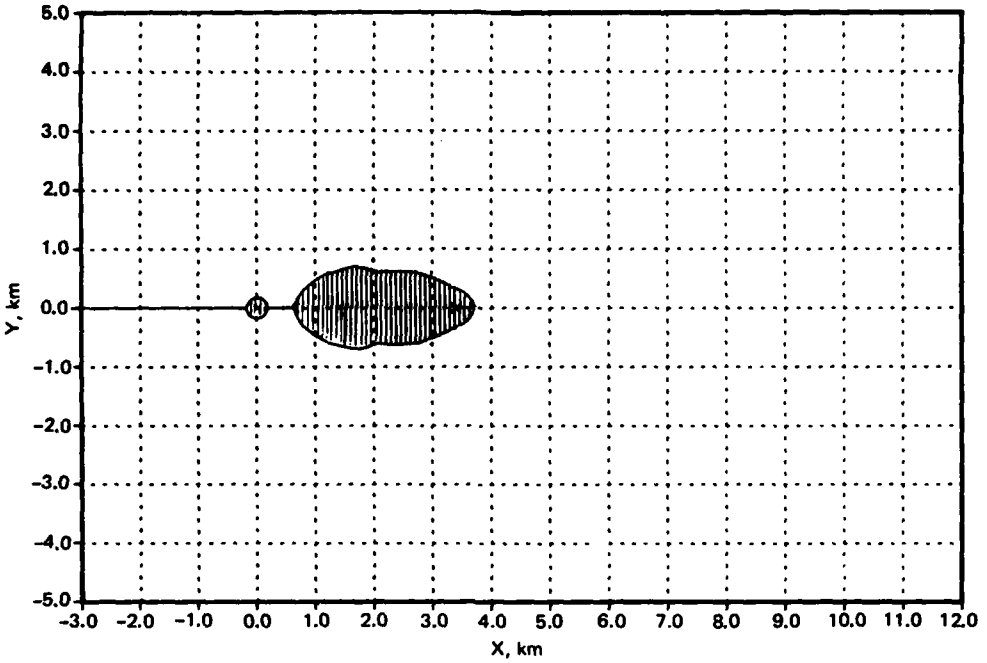

Figure G22. Detection footprint at 7.0 km interceptor altitude. Transmitter height 6.4 km. Compare against vertical cross-section of detection region in figure G11 (60.306 GHz and 10° elevation angle). Footprint area is 3.26 km^2. Data can be used to calculate an altitude ensemble average. Data plotted in figure G24.

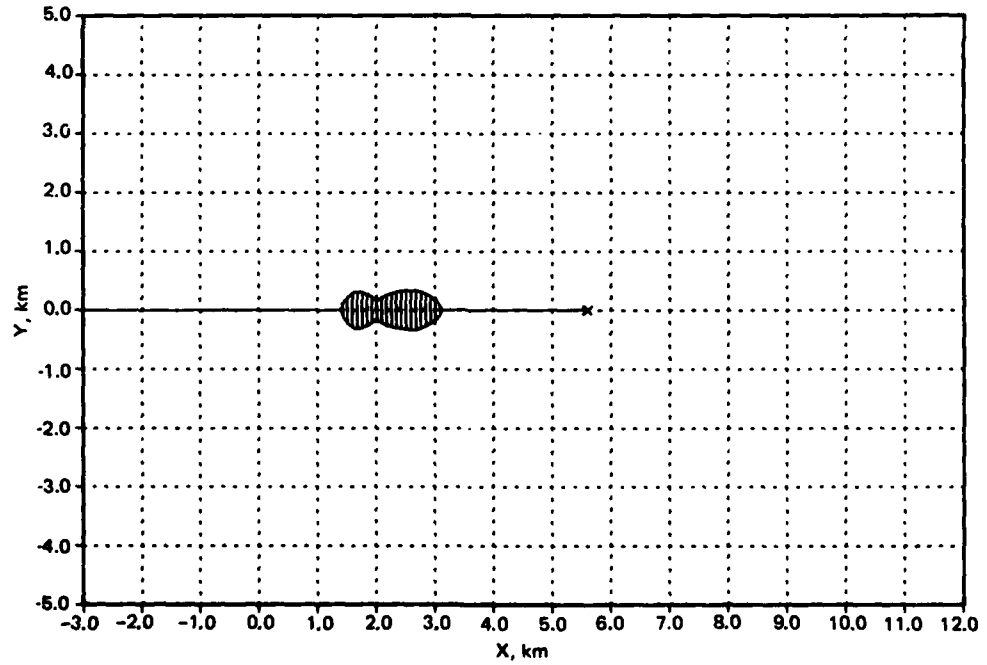

Figure G23. Detection footprint at 7.4 km interceptor altitude. Transmitter height 6.4 km. Compare against vertical cross-section of detection region in figure G11 (60.306 GHz and 10° elevation angle). Footprint area is 0.88 km^2. Data can be used to calculate an altitude ensemble average. Data plotted in figure G24.

antenna pattern (figure G3). The waist, mentioned earlier, also shows in all three footprints, with the 7.4 km example an extreme. The detectability vs altitude function is plotted in figure G24. The inflection at 6.0 km altitude is due to the onset of the main beam (see figure G11).

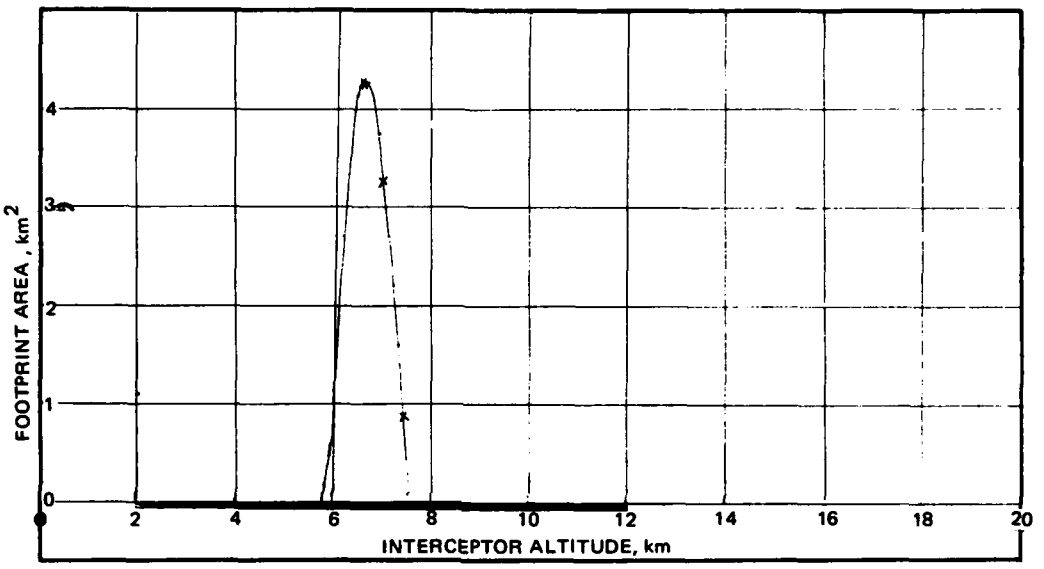

Figure G24. Detectability vs interceptor altitude. Compare figure G11 and figures G21, G22, and G23. The 2-12 km interceptor altitude average is proportional to the integral under this curve from 2-12 km.